Title
Ultrathin Wavy Nanowires as Highly Efficient Anode Electrocatalysts for Fuel Cell Applications

Author
Fu, Xiaoyang

Publication Date
2021

Peer reviewed|Thesis/dissertation

UNIVERSITY OF CALIFORNIA

Los Angeles

Ultrathin Wavy Nanowires as Highly Efficient Anode Electrocatalysts for Fuel Cell Applications

A dissertation submitted in partial satisfaction of the requirements for the degree Doctor of Philosophy in Chemistry

by

Xiaoyang Fu

2021

ABSTRACT OF THE DISSERTATION

Ultrathin Wavy Nanowires as Highly Efficient Anode

Electrocatalysts for Fuel Cell Applications

by

Xiaoyang Fu

Doctor of Philosophy in Chemistry

University of California, Los Angeles, 2021

Professor Xiangfeng Duan, Chair

Fuel cells that can directly convert the chemical energy stored in fuels to electricity are attracting increasing attention to enable a clean energy future. Compared with compressed hydrogen applied for industrialized hydrogen fuel cells, liquid fuels (*e.g.*, methanol, ethanol or hydrazine) feature higher volumetric energy density, more convenient storage and transport, and lower cost, making them attractive alternative candidates for fuel cells. However, the anode oxidation reactions for these fuel molecules usually show higher kinetic barriers compared with hydrogen and often require noble metal based electrocatalysts, which are costly and limits the widespread adoption of the relevant technologies. Therefore, an important challenge to develop fuel cells with low the overall cost is to develop highly effective electrocatalysts with high mass activity (MA), stability, faradaic efficiency (FE) and low overpotential, as well as long lifetime.

Methanol oxidation reaction (MOR) is the anode reaction of the direct methanol fuel cells. To facilitate MOR, I developed ultrathin Rh wavy nanowires with ultrahigh electrochemical surface area (ECSA ~144.2 m^2/g) as the highly effective electrocatalyst with nearly 3 times of MA (722 mA/mg) compared with the previously reported Rh-based nanomaterials. More importantly, the ultrathin Rh wavy nanowires retain the advantage of the Rh-based nanomaterials to exhibit a lower the overpotential for MOR with the current peak potential at 0.61 V Vs. RHE (compared with 0.8-0.9 V Vs. RHE for Pt-based nanomaterials), leading to very high MA compared with the previously reported Rh and Pt-based nanomaterials at 0.61 V vs. RHE for MOR.

Ethanol oxidation reaction (EOR) is also important for direct ethanol fuel cell application with even higher energy density, lower cost and lower toxicity compared with methanol. I designed and developed a facile solvothermal process for the synthesis of ultrathin alloy Pt_3Ag wavy nanowires as highly effective EOR electrocatalysts. The alloy Pt_3Ag (111) facet helps EOR by facilitating C-C bond cleavage as inspired by the previous theoretical prediction and thus contribute to higher specific activity (SA) and FE. The alloy of Ag with Pt also adjusts the electronic structure and enriches the electron density around Pt to lower the poisoning effect from carbonaceous species. Together, the resulting Pt_3Ag alloy wavy nanowires deliver an ultrahigh SA of 28.0 mA/cm^2 and an exceptional MA of 6.1 A/mg, far exceeding that of the benchmark commercial Pt/carbon black samples (1.1 A/mg) and higher than most of the previously reported state-of-the-art noble metal-based electrocatalysts.

Moving one step further, I designed and synthesized medium entropy Au-doped PtAgRhCu alloy wavy nanowire. By simultaneously employing ligand effect, strain effect and bifunctional

effect upon the introduction of Ag, Rh, Cu and Au elements, this strategy help alleviate the poisoning from the carbonaceous species. In addition, the introduction of these various elements may lead to unexpected synergistic effect (cocktail effect), resulting in further improved MA (8.43 ± 0.40 A/$mg_{noble\ metal}$) for EOR. Importantly, great long-term durability was also achieved for both MOR and EOR with excellent long-term durability, which may be further attributed to the sluggish diffusion effect due to the enhanced entropy of the system, and thus making it a highly promising anode electrocatalysts for the alkaline direct alcohol fuel cell applications.

Hydrazine also has high energy density and high potential output for fuel cell applications together with the advantage of zero carbon emission. I designed and synthesized $RhRu_{0.5}$ alloy wavy nanowires as highly effective electrocatalysts for hydrazine oxidation reaction (HzOR). In addition to the ultrahigh ECSA (>100 m^2/g) derived from the ultrathin wavy nanowire morphology, the alloying of Ru can greatly lower the overpotential compared with the Rh nanowires while retaining the capability to achieve the total electrooxidation of the hydrazine as confirmed from the rotating disk electrode (RDE) study, which can be attributed to the synergistic effect between Rh and Ru and the more facilitated removal of the surficial adsorbed hydrogen species. The resulting $RhRu_{0.5}$ alloy wavy nanowire catalysts deliver an ultrahigh mass activity of 60.4 ± 6.2 A/mg at 0.20 V vs. RHE along with high geometric current density and excellent long-term performances, demonstrating outstanding potential for alkaline direct hydrazine fuel cells.

The dissertation of Xiaoyang Fu is approved.

Yu Huang

Alexander Levine

Philippe Sautet

Xiangfeng Duan, Committee Chair

University of California, Los Angeles

Table of Contents

List of Figures and Table

Acknowledgements

Foremost, I would like to express my sincere gratitude to my advisor Prof. Xiangfeng Duan and Prof. Yu Huang for their patience, motivation, enthusiasm, and immense knowledge. Your guidance helped me in all the time of my research and writing of this thesis. I could not have imagined having a better advisor and mentor for my Ph.D study. Besides my advisors, I would like to thank the rest of my thesis committee: Prof. Alexander Levine and Prof. Philippe Sautet,

for their encouragement, talented comments, and insightful questions during my qualification exam and fourth year meeting.

I am also grateful to my lab mates from UCLA Chemistry department and MSE department: Aixin Zhang, Bocheng Cao, Chengzhang Wan, Frank Song, Hongtu Zhang, Mufan Li, Shuaijing Du, Wang Xue, Yiliu Wang, Zipeng Zhao and Zheng Fan, as well as my collaborator from UCI MSE department, Huaixun Huyan and Professor Xiaoqing Pan, for their help and assistance in experiments as well as their enlightening discussion and suggestions.

Finally, I want to thank my parents. Thank you for the continuous support you have given me throughout my time in graduate school. You selflessly encouraged me to explore new directions in life and seek my own destiny. This journey would not have been possible if not for you, and I dedicate this milestone to you.

Chapter 1 involves a summary version of Fu, X.; Wan, C.; Huang, Y; Duan, X., Noble metal based electrocatalysts for alcohol oxidation reactions in alkaline media. *Adv. Funct. Mater.* Submitted and under Revisions.

Chapter 2 is a version of Fu, X.; Zhao, Z.; Wan, C.; Wang, Y.; Fan, Z.; Song, F.; Cao, B.; Li, M.; Xue, W.; Huang, Y; Duan, X., Ultrathin wavy Rh nanowires as highly effective electrocatalysts for methanol oxidation reaction with ultrahigh ECSA. *Nano Res.* **2019,** *12* (1), 211-215.

Chapter 3 is a version of Fu, X.; Wan, C.; Zhang, A.; Zhao, Z.; Huyan, H.; Pan, X.; Du, S.; Duan, X.; Huang, Y., Pt_3Ag alloy wavy nanowires as highly effective electrocatalysts for ethanol oxidation reaction. *Nano Res.* **2020,** *13* (5), 1472-1478.

Chapter 4 is a version of Fu, X.; Wan, C.; Huaixun, H.; Zhang, H.; Pan, X.; Huang, Y;

Duan, X., Medium entropy Au-doped PtAgRhCu alloy wavy nanowire as highly effective and durable electrocatalysts for AOR. Manuscript in preparation.

Chapter 5 is a version of Fu, X.; Zhang, H.; Huaixun, H.; Wan, C.; Zhao, Z.; Pan, X.; Huang, Y; Duan, X., Ultrathin $RhRu_{0.5}$ alloy nanowire for as highly efficient hydrazine total electrooxidation with ultrahigh mass activity. Manuscript in preparation.

Biography

Xiaoyang Fu received his B.S. degree in Chemistry from Peking University, Beijing, China in 2015 and M.S. degree in Chemistry from University of California, San Diego in 2016. He joined Dr. Xiangfeng Duan's group in 2017 and conducted research of developing noble metal nanomaterials with wavy nanowire morphology for electrocatalysis and fuel cell related applications. He was awarded UCLA Dissertation Year Fellowship (DYF) in 2020 and Nano Research – UCLA Dissertation Award for Excellence in Inorganic Nanoscience in 2021.

Chapter 1. Background introduction

1.1 Alkaline direct alcohol fuel cell

Fuel cell represents an attractive option for mobile power supply by directly converting chemical energy stored in fuels to electricity. Although hydrogen (H_2) represents the most widely explored chemical fuel for fuel cell applications to date, liquid alcohols (*e.g.*, methanol and ethanol) are also attracting considerable interest for numerous reasons and Figure 1-1 (a) is a typical illustration of the alkaline direct methanol fuel cell (ADMFC). Importantly, alcohols typically have one magnitude higher volumetric energy density when compared with compressed H_2 (hydrogen: 0.18 kWh/L@1000 psi, 25^{o}C, methanol: 4.82 kWh/L, ethanol: 6.28 kWh/L)[1], indicating great potential to be employed as chemical fuel for fuel cells. Furthermore, when the weight of the hydrogen storage system (*e.g.*, gas tank and metal hydride with 4-5 wt% hydrogen) is also taken into account, alcohols will also exhibit more than five-fold higher gravimetric energy density compared with compressed hydrogen (hydrogen: 1.2 kWh/kg, methanol: 6.1 kWh/kg, ethanol: 8.0 kWh/kg) as shown in Figure 1-1 (b)[1]. Additionally, alcohols also have other fascinating features, such as lower cost, easier and intrinsically safer storage and transportation, to make them highly attractive fuel candidates for fuel cells.

In particular, the alkaline direct alcohol fuel cell (ADAFC) has been drawing considerable recent research interests along with the development of anion exchange membranes[2-6]. In the alkaline environment, the cathodic oxygen reduction reaction (ORR) has more favorable kinetics and the catalysis of ORR can be achieved by non-noble metal based electrocatalysts, such as AlN[7], ZrN[8], Fe SAs (single atoms)/NC[9-14], Co SAs/NC[9-11, 15], transition metal (*e.g.* Ni, Co, Cu, Mn, Zn, etc.) oxides[16], and carbon-based nanomaterials[17-20], etc. The low cost of these non-noble metal based electrocatalysts could greatly lower the overall cost of the fuel cells[21]. In

addition, the hydroxide anion transport from cathode to anode reverses electro-osmotic drag as illustrated in Figure 1-1 (a) and helps lower the alcohol crossover in the cell, thus reducing catalyst poisoning to the cathodic ORR catalysts and improving the efficiency[22, 23].

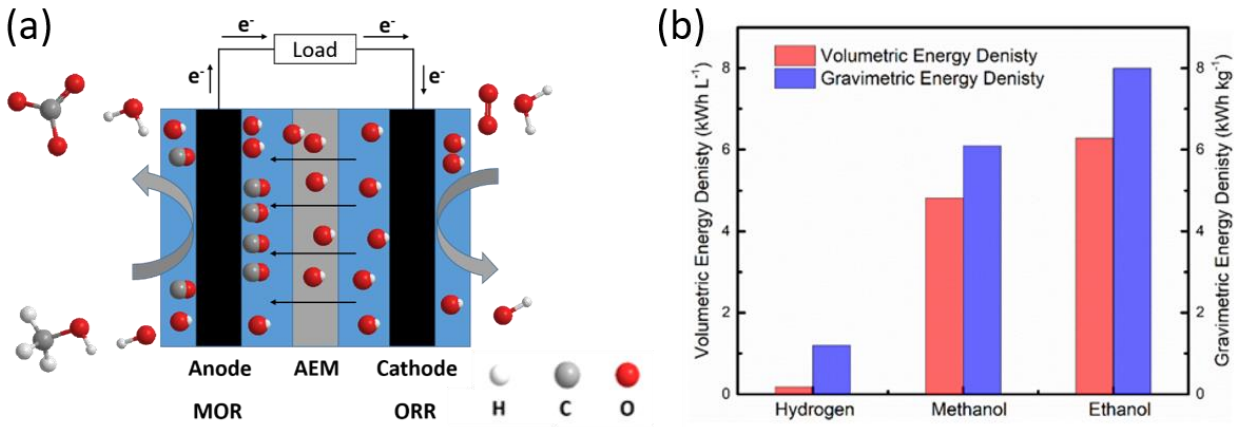

Figure 1-1. (a) Schematic illustration of alkaline direct methanol fuel cells. (b) Comparisons of the volumetric energy density and gravimetric energy density of hydrogen (@1000 psi, 25ºC, and with weight of the hydrogen storage system taken into consideration), methanol and ethanol.[1]

1.2 Alcohol oxidation reaction and electrocatalyst design criteria

However, the alcohol oxidation reactions (AOR) usually exhibit more sluggish kinetics and considerably higher overpotential when compared with the hydrogen oxidation reaction (HOR), and therefore results in lower operation voltage and typically requires noble metal based electrocatalysts (*e.g.*, Pt, Pd and Rh), which limits the widespread adoption and application of ADAFCs. Therefore, to develop highly effective noble metal based electrocatalysts that can minimize the required noble metal loading represents a central challenge in the field, and thus requires the electrocatalysts with high mass activity (MA) and good durability to lower the overall cost and improve the lifetime of the fuel cells. In addition, improving the faradaic

efficiency and lowering the overpotential of the electrocatalysts can also enhance the energy efficiency and power output of the fuel cells.

1.2.1 Mechanism of MOR and EOR in alkaline Media

For MOR in alkaline media (Figure 1-2), the chemisorption of methanol takes place in the initial stage, followed by consecutive dehydrogenation steps to produce the CHO_{ad} intermediate, which will either undergo a direct pathway to be directly oxidized to $COOH_{ad}$ or indirect pathway to CO intermediate that can be further oxidized into $COOH_{ad}$ with the help of hydroxyl group (-OH) adsorbed onto nearby sites[22], and finally oxidized to form carbonate in alkaline media. In addition, the one-step oxidation of CHO_{ad} and CO_{ad} into carbonate was also mentioned by some previous literature[24, 25]. Minor byproducts, such as formaldehyde and formate from partial oxidation, have also been reported in the process[26, 27]. Therefore, the facile removal of the CO species that can block the noble metal sites has been recognized as the most fundamental problem for MOR.

For EOR in alkaline media, the ethanol also starts with the chemisorption and consecutive dehydrogenation steps, followed by the production of CH_3CO_{ad}/CH_3CHO_{ad} intermediates[28-30]. They may either undergo the cleavage of C-C bond into C1 species (*e.g.* CH_x, CO) and can then be oxidized to form carbonate as the final product (C1 pathway) or may be directly oxidized to form acetate without further oxidation (C2 pathway)[28-30]. For EOR, a notable challenge is the C-C bond cleavage to facilitate C1 pathway, which is critical to achieve the conversion of the chemical energy from ethanol into electricity since the C2 pathway can only utilize ~36% of the chemical energy in ethanol (Figure 1-2)[31]. The CO intermediates are commonly involved in the C1 pathway, thus the design of catalysts that can facilitate rapid removal/oxidization of CO species is essential for boosting the C1 pathway and increasing the energy conversion efficiency,

which also helps prevent the poisoning of the noble metal based electrocatalysts in the same time.

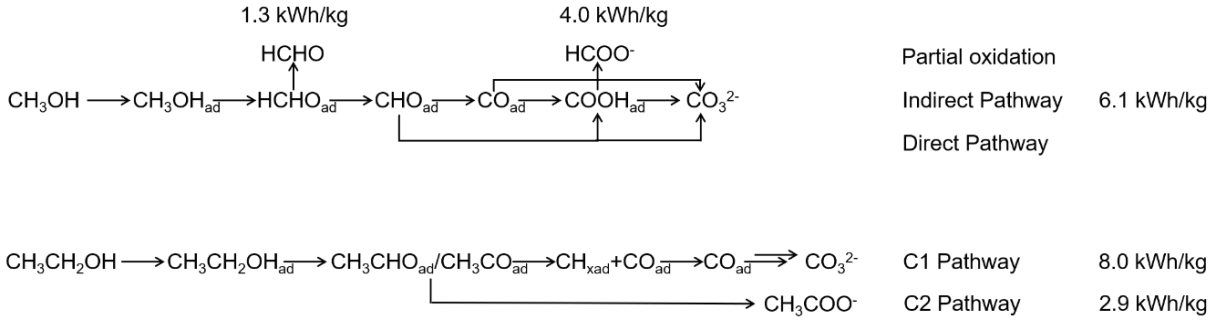

Figure 1-2. MOR and EOR mechanisms in alkaline media with energy density for different pathways. Adapted with permission[28]. Copyright 2014, American Chemical Society. Adapted with permission[29]. Copyright 2019, American Chemical Society. Adapted with permission[1]. Copyright 2015, Cambridge Core. Adapted with permission[25]. Copyright 2007, Royal Society of Chemistry. Adapted with permission[24]. Copyright 2003, Elsevier.

1.2.2 Design criteria for AOR electrocatalysts

The SA stands for the intrinsic catalytic activity of a given electrocatalyst and is fundamentally determined by the electronic structure and coordination environment of the surficial active sites. The design criteria for improving SA are briefly summarized in Figure 1-3. Facet effect involves the variation of the exposed crystal facets and thus changes the surface bonding configuration, electronic structure and d-band center[32-34] to alter the AOR performances, for example, Pt nanoparticles with (111) facet is reported to have more than 2-fold higher SA for MOR and EOR compared with their (100) facet exposed counterparts[35]. Ligand effect and strain effect can also tune the electronic structure and d-band center and thus the interactions with reactants and adsorbates[32, 36, 37] to potentially enhance the AOR performances. Bifunctional

effect aims to facilitate the removal of the poisonous CO species adsorbed on noble metal sites with the assistance of hydroxyl groups adsorbed on the nearby sites via the Langmuir–Hinshelwood (L-H) mechanism, which is commonly achieved by surface decoration with more oxophilic species[38, 39], in addition, the facile removal of the CO can also facilitate the C1 pathway selectivity for EOR since the product from C1 pathway can be facilely removed[38].

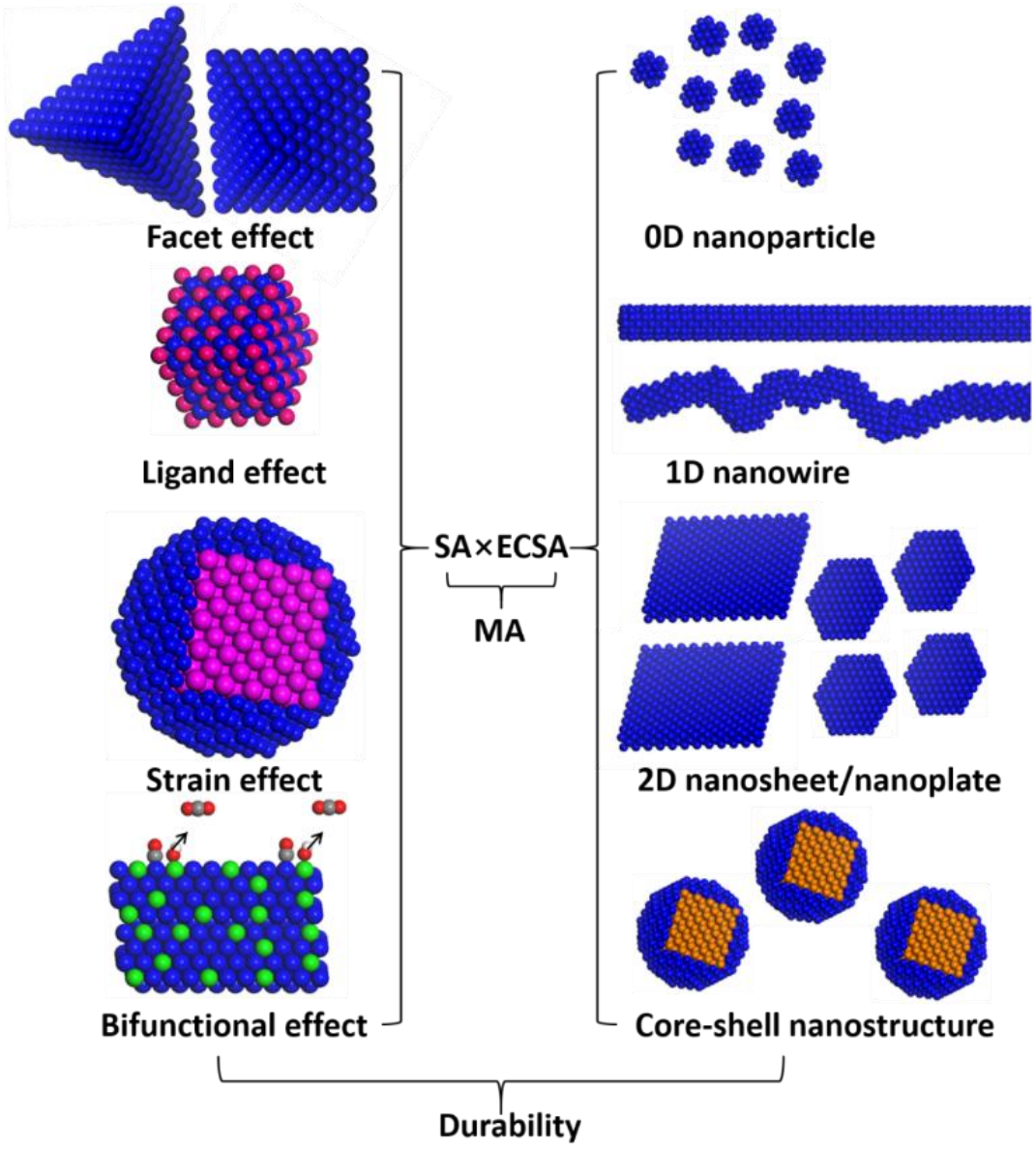

Figure 1-3. Schematic illustration of design criteria for noble metal based electrocatalysts for MOR and EOR.

The MA is defined as the oxidation current at the peak potential (or a certain potential such as 0.6 V vs. RHE[40]) normalized by the mass loading of noble metal on the electrode and is the most important factor for AOR electrocatalyst as it directly determines the amount of noble metal needed for a given power output in fuel cells. Since MA equals the product of SA and electrochemical active surface area (ECSA), ECSA represents another critical factor to improve MA. As shown in Figure 1-3, ultrafine nanostructures (*i.e.* ultrasmall nanoparticle, ultrathin nanowire, ultrathin nanoplate/nanosheet) with higher specific area and clean surface can generally lead to higher ECSA. Core-shell nanostructures with an ultrathin skin of active elements can also lead to higher ECSA and ensure more efficient utilization of noble metals.

The long-term performance is also crucial because it directly affects the lifetime of the electrocatalysts when applied for fuel cells. The core-shell nanostructures with noble metal shell can help protect the core of more reactive transition metals under longtime of harsh electrochemical conditions[41]. In addition, the 1D or 2D nanostructures often demonstrate less movement and aggregation, as well less Oswald ripening to ensure better stability while achieving improved ECSA from the ultrathin thickness[42-45]. For the 0D ultrasmall nanoparticles, carbon based supports[46-49] are often utilized to help spread the nanoparticles and reduce their agglomeration during long-term operation. In addition, the support material can also lower the charge transfer resistance to improve the electrocatalytic performance[50].

Apart from maintaining the structure integrity, the catalyst poisoning by the carbonaceous species (*e.g.* CO) is another critical factor that can hinder the long-term performance of the AOR electrocatalysts. In general, the design criteria mentioned above for improving SA can all help improve resistance against CO poisoning to some extent, either by adjusting the d-band

center to the interaction with CO or by facilitating -OH groups adsorption on nearby sites to facilitate CO removal via the L-H bifunctional mechanism.

In my research work, I first developed ultrathin Rh wavy nanowire as electrocatalysts for MOR with high MA of 722 mA/mg at 0.61 V vs. RHE, which is attributed to the ultrahigh ECSA of 144.2 m^2/g determined from CO-stripping[44]. I also designed Pt_3Ag alloy wavy nanowire with (111) facet exposed as inspired by the previous theoretical prediction[51], demonstrating ultrahigh MA of 6.1 A/mg for EOR as a result of ultrahigh SA (28.0 mA/cm^2) attributed to the ligand effect from Ag alloying[52]. In addition, I also designed and synthesized the medium entropy Au-doped PtAgRhCu alloy wavy nanowire, which not only demonstrated further improved MA of 8.43±0.40 $A/mg_{noble\ metal}$ as well as much improved durability for EOR and MOR.

1.3 Alkaline direct hydrazine fuel cell and hydrazine oxidation reaction

Hydrazine has high gravimetric energy density as well as high volumetric energy density, which is at similar level to those of methanol and ethanol[53]. The total oxidation of hydrazine only produces nitrogen gas and water without any carbon emission compared with alcohols, which is not only environmentally friendly, but also avoids carbonate formation so that the pH will not evidently change when applied for alkaline direct hydrazine fuel cells (ADHFCs). The alkaline fuel cells can also employ cheaper cathode electrocatalysts for ORR and have lower fuel crossover[23]. In addition, the aqueous solution of hydrazine has similar risk level of carcinogenicity as gasoline (class 2B)[54, 55]. Therefore, hydrazine also has the potential to serve as a chemical fuel for fuel cell applications.

For the hydrazine oxidation reaction (HzOR) on the anode side, the total electrooxidation of hydrazine leads to the products of nitrogen gas and water, with surficially adsorbed H atom considered as the intermediate[56], which may undergo recombination and lead to the products of

H_2[56]. In addition, the NH_3 generation was also proven as a possible byproduct from incomplete oxidation according to the differential electrochemical mass spectrometry (DEMS) results of the previous study of single atom catalyst-Ni, Fe, and Co[57]. Previous rotating disk electrode (RDE) study also revealed non-noble metals (*e.g.* Co, Ni and Ru) are unable to achieve the total electrooxidation of hydrazine[58] although there were also some previous reports about these non-noble metals[59-63]. The complete oxidation of hydrazine is also crucial for efficient utilization of energy and avoiding the generation of potentially harmful species, such as NH_3. Noble metals (*e.g.* Rh, Pd and Pt) are needed for total electrooxidation (n=4) of hydrazine based on previous RDE study[58], therefore, it is still an important challenge is to design highly efficient electrocatalysts with ultrahigh mass activity to lower the loading of the noble metal based electrocatalysts in order to reduce the overall cost of the fuel cells.

In my work, I designed and synthesized ultrathin $RhRu_{0.5}$ alloy wavy nanowire with ultrahigh MA of 60.4±6.2 A/mg at 0.20 V vs. RHE, lower overpotential and good durability as well as the ability to achieve the total electrooxidation of hydrazine from the RDE study, which could serve as highly efficient electrocatalysts when applied for fuel cell applications.

1.4 Reference

1. Joghee, P.; Malik, J. N.; Pylypenko, S.; O'Hayre, R., A review on direct methanol fuel cells–In the perspective of energy and sustainability. *MRS Energy Sustain* **2015,** *2*.

2. Bahrami, H.; Faghri, A., Multi-layer membrane model for mass transport in a direct ethanol fuel cell using an alkaline anion exchange membrane. *J. Power Sources* **2012,** *218*, 286-296.

3. Herranz, D.; Escudero-Cid, R.; Montiel, M.; Palacio, C.; Fatas, E.; Ocon, P., Poly (vinyl alcohol) and poly (benzimidazole) blend membranes for high performance alkaline direct ethanol fuel cells. *Renew. Energy* **2018,** *127*, 883-895.

4. Li, Y. S.; Zhao, T. S., A passive anion-exchange membrane direct ethanol fuel cell stack and its applications. *Int. J. Hydrogen Energy* **2016,** *41* (44), 20336-20342.

5. Wang, Y.; Li, L.; Hu, L.; Zhuang, L.; Lu, J.; Xu, B., A feasibility analysis for alkaline membrane direct methanol fuel cell: thermodynamic disadvantages versus kinetic advantages. *Electrochem. Commun.* **2003,** *5* (8), 662-666.

6. Zakaria, Z.; Kamarudin, S. K.; Timmiati, S. N., Membranes for direct ethanol fuel cells: An overview. *Appl. Energy* **2016,** *163*, 334-342.

7. Lei, M.; Wang, J.; Li, J.; Wang, Y.; Tang, H.; Wang, W., Emerging methanol-tolerant AlN nanowire oxygen reduction electrocatalyst for alkaline direct methanol fuel cell. *Sci. Rep.* **2014,** *4*, 6013.

8. Yuan, Y.; Wang, J.; Adimi, S.; Shen, H.; Thomas, T.; Ma, R.; Attfield, J. P.; Yang, M., Zirconium nitride catalysts surpass platinum for oxygen reduction. *Nat. Mater.* **2019**, 1-5.

9. Wan, C.; Duan, X.; Huang, Y., Molecular Design of Single-Atom Catalysts for Oxygen Reduction Reaction. *Adv. Energy Mater.* **2020,** *10* (14), 19.

10. Fei, H. L.; Dong, J. C.; Chen, D. L.; Hu, T. D.; Duan, X. D.; Shakir, I. R.; Huang, Y.; Duan, X. F., Single atom electrocatalysts supported on graphene or graphene-like carbons. *Chem. Soc. Rev.* **2019,** *48* (20), 5207-5241.

11. Fei, H. L.; Dong, J. C.; Feng, Y. X.; Allen, C. S.; Wan, C. Z.; Volosskiy, B.; Li, M. F.; Zhao, Z. P.; Wang, Y. L.; Sun, H. T.; An, P. F.; Chen, W. X.; Guo, Z. Y.; Lee, C.; Chen, D. L.; Shakir, I.; Liu, M. J.; Hu, T. D.; Li, Y. D.; Kirkland, A. I.; Duan, X. F.; Huang, Y., General synthesis and definitive structural identification of MN4C4 single-atom catalysts with tunable electrocatalytic activities. *Nat. Catalysis* **2018,** *1* (1), 63-72.

12. Liu, X.; Liu, H.; Chen, C.; Zou, L. L.; Li, Y.; Zhang, Q.; Yang, B.; Zou, Z. Q.; Yang, H., Fe2N nanoparticles boosting FeNx moieties for highly efficient oxygen reduction reaction in Fe-N-C porous catalyst. *Nano Res.* **2019,** *12* (7), 1651-1657.

13. Ding, R.; Liu, Y. D.; Rui, Z. Y.; Li, J.; Liu, J. G.; Zou, Z. G., Facile grafting strategy synthesis of single-atom electrocatalyst with enhanced ORR performance. *Nano Res.* **2020,** *13* (6), 1519-1526.

14. Su, P. P.; Huang, W. J.; Zhang, J. W.; Guharoy, U.; Du, Q. G.; Sun, Q.; Jiang, Q. K.; Cheng, Y.; Yang, J.; Zhang, X. L.; Liu, Y. S.; Jiang, S. P.; Liu, J., Fe atoms anchored on defective nitrogen doped hollow carbon spheres as efficient electrocatalysts for oxygen reduction reaction. *Nano Res.* **2021,** *14* (4), 1069-1077.

15. Fei, H. L.; Dong, J. C.; Wan, C. Z.; Zhao, Z. P.; Xu, X.; Lin, Z. Y.; Wang, Y. L.; Liu, H. T.; Zang, K. T.; Luo, J.; Zhao, S. L.; Hu, W.; Yan, W. S.; Shakir, I.; Huang, Y.; Duan, X. F., Microwave-Assisted Rapid Synthesis of Graphene-Supported Single Atomic Metals. *Adv. Mater.* **2018,** *30* (35), 8.

16. Wang, Y.; Li, J.; Wei, Z. D., Transition-metal-oxide-based catalysts for the oxygen reduction reaction. *J. Mater. Chem. A* **2018,** *6* (18), 8194-8209.

17. Wang, D.-W.; Su, D., Heterogeneous nanocarbon materials for oxygen reduction reaction. *Energy Environ. Sci.* **2014,** *7* (2), 576-591.

18. Jia, N.; Weng, Q.; Shi, Y. R.; Shi, X. Y.; Chen, X. B.; Chen, P.; An, Z. W.; Chen, Y., N-doped carbon nanocages: Bifunctional electrocatalysts for the oxygen reduction and evolution reactions. *Nano Res.* **2018,** *11* (4), 1905-1916.

19. Fu, S. F.; Zhu, C. Z.; Song, J. H.; Engelhard, M. H.; Li, X. L.; Zhang, P. N.; Xia, H. B.; Du, D.; Lin, Y. H., Template-directed synthesis of nitrogen-and sulfur-codoped carbon

nanowire aerogels with enhanced electrocatalytic performance for oxygen reduction. *Nano Res.* **2017,** *10* (6), 1888-1895.

20. Liu, Y. Y.; Wang, H. T.; Lin, D. C.; Zhao, J.; Liu, C.; Xie, J.; Cui, Y., A Prussian blue route to nitrogen-doped graphene aerogels as efficient electrocatalysts for oxygen reduction with enhanced active site accessibility. *Nano Res.* **2017,** *10* (4), 1213-1222.

21. Weng, M. M.; Liu, D. J.; He, X. Q.; Asefa, T., Fe3C nanoparticles-loaded 3D nanoporous N-doped carbon: A highly efficient electrocatalyst for oxygen reduction in alkaline media. *Int. J. Hydrogen Energy* **2019,** *44* (39), 21506-21517.

22. Yu, E. H.; Krewer, U.; Scott, K., Principles and materials aspects of direct alkaline alcohol fuel cells. *Energies* **2010,** *3* (8), 1499-1528.

23. Antolini, E.; Gonzalez, E. R., Alkaline direct alcohol fuel cells. *J. Power Sources* **2010,** *195* (11), 3431-3450.

24. Yu, E. H.; Scott, K.; Reeve, R. W., A study of the anodic oxidation of methanol on Pt in alkaline solutions. *J. Electroanal. Chem.* **2003,** *547* (1), 17-24.

25. Cohen, J. L.; Volpe, D. J.; Abruna, H. D., Electrochemical determination of activation energies for methanol oxidation on polycrystalline platinum in acidic and alkaline electrolytes. *Phys. Chem. Chem. Phys.* **2007,** *9* (1), 49-77.

26. Haisch, T.; Kubannek, F.; Haisch, C.; Bahnemann, D. W.; Krewer, U., Quantification of formaldehyde production during alkaline methanol electrooxidation. *Electrochem. Commun.* **2019,** *102*, 57-62.

27. Yang, Y. Y.; Ren, J.; Zhang, H. X.; Zhou, Z. Y.; Sun, S. G.; Cai, W. B., Infrared Spectroelectrochemical Study of Dissociation and Oxidation of Methanol at a Palladium Electrode in Alkaline Solution. *Langmuir* **2013,** *29* (5), 1709-1716.

28. Yang, Y.-Y.; Ren, J.; Li, Q.-X.; Zhou, Z.-Y.; Sun, S.-G.; Cai, W.-B., Electrocatalysis of ethanol on a Pd electrode in alkaline media: an in situ attenuated total reflection surface-enhanced infrared absorption spectroscopy study. *ACS Catal.* **2014,** *4* (3), 798-803.
29. Zhu, C.; Lan, B.; Wei, R.-L.; Wang, C.-N.; Yang, Y.-Y., Potential-Dependent Selectivity of Ethanol Complete Oxidation on Rh Electrode in Alkaline Media: A Synergistic Study of Electrochemical ATR-SEIRAS and IRAS. *ACS Catal.* **2019,** *9* (5), 4046-4053.
30. Kutz, R. B.; Braunschweig, B. r.; Mukherjee, P.; Dlott, D. D.; Wieckowski, A., Study of ethanol electrooxidation in alkaline electrolytes with isotope labels and sum-frequency generation. *J. Phys. Chem. Lett.* **2011,** *2* (17), 2236-2240.
31. Evans, F. W.; Skinner, H. A., THE HEAT OF COMBUSTION OF ACETIC ACID. *Transactions of the Faraday Society* **1959,** *55* (2), 260-261.
32. Hammer, B.; Norskov, J. K., Theoretical surface science and catalysis - Calculations and concepts. In *Advances in Catalysis, Vol 45: Impact of Surface Science on Catalysis*, Gates, B. C.; Knozinger, H., Eds. Elsevier Academic Press Inc: San Diego, 2000; Vol. 45, pp 71-129.
33. Huang, L.; Zheng, C. Y.; Shen, B.; Mirkin, C. A., High-Index-Facet Metal-Alloy Nanoparticles as Fuel Cell Electrocatalysts. *Adv. Mater.* **2020**, 2002849.
34. Yu, N. F.; Tian, N.; Zhou, Z. Y.; Sheng, T.; Lin, W. F.; Ye, J. Y.; Liu, S.; Ma, H. B.; Sun, S. G., Pd Nanocrystals with Continuously Tunable High-Index Facets as a Model Nanocatalyst. *ACS Catal.* **2019,** *9* (4), 3144-3152.
35. Hu, C.; Zhou, Y. N.; Xiao, M. F.; Yu, G., Precise size and dominant-facet control of ultra-small Pt nanoparticles for efficient ethylene glycol, methanol and ethanol oxidation electrocatalysts. *Int. J. Hydrogen Energy* **2020,** *45* (7), 4341-4354.

36. Bligaard, T.; Norskov, J. K., Ligand effects in heterogeneous catalysis and electrochemistry. *Electrochim. Acta* **2007,** *52* (18), 5512-5516.

37. Mavrikakis, M.; Hammer, B.; Norskov, J. K., Effect of strain on the reactivity of metal surfaces. *Phys. Rev. Lett.* **1998,** *81* (13), 2819-2822.

38. Huang, W.; Ma, X. Y.; Wang, H.; Feng, R.; Zhou, J.; Duchesne, P. N.; Zhang, P.; Chen, F.; Han, N.; Zhao, F.; Zhou, J.; Cai, W. B.; Li, Y., Promoting effect of Ni (OH) 2 on palladium nanocrystals leads to greatly improved operation durability for electrocatalytic ethanol oxidation in alkaline solution. *Adv. Mater.* **2017,** *29* (37), 1703057.

39. Huang, W.; Wang, H.; Zhou, J.; Wang, J.; Duchesne, P. N.; Muir, D.; Zhang, P.; Han, N.; Zhao, F.; Zeng, M., Highly active and durable methanol oxidation electrocatalyst based on the synergy of platinum–nickel hydroxide–graphene. *Nat. Commun.* **2015,** *6*.

40. Wu, D. S.; Kusada, K.; Yamamoto, T.; Toriyama, T.; Matsumura, S.; Kawaguchi, S.; Kubota, Y.; Kitagawa, H., Platinum-Group-Metal High-Entropy-Alloy Nanoparticles. *J. Am. Chem. Soc.* **2020,** *142* (32), 13833-13838.

41. Huang, J.; Liu, Y.; Xu, M.; Wan, C.; Liu, H.; Li, M.; Huang, Z.; Duan, X.; Pan, X.; Huang, Y., PtCuNi Tetrahedra Catalysts with Tailored Surfaces for Efficient Alcohol Oxidation. *Nano Lett.* **2019,** *19* (8), 5431-5436.

42. Li, M.; Zhao, Z.; Cheng, T.; Fortunelli, A.; Chen, C.; Yu, R.; Zhang, Q.; Gu, L.; Merinov, B. V.; Lin, Z.; Zhu, E.; Yu, T.; Jia, Q.; Guo, J.; Zhang, L.; Goddard, W. A.; Huang, Y.; Duan, X., Ultrafine jagged platinum nanowires enable ultrahigh mass activity for the oxygen reduction reaction. *Science* **2016,** *354* (6318), 1414-1419.

43. Fan, J.; Yu, S.; Qi, K.; Liu, C.; Zhang, L.; Zhang, H.; Cui, X.; Zheng, W., Synthesis of ultrathin wrinkle-free PdCu alloy nanosheets for modulating d-band electrons for efficient methanol oxidation. *J. Mater. Chem. A* **2018,** *6* (18), 8531-8536.

44. Fu, X.; Zhao, Z.; Wan, C.; Wang, Y.; Fan, Z.; Song, F.; Cao, B.; Li, M.; Xue, W.; Huang, Y.; Duan, X., Ultrathin wavy Rh nanowires as highly effective electrocatalysts for methanol oxidation reaction with ultrahigh ECSA. *Nano Res.* **2019,** *12* (1), 211-215.

45. Huang, X.; Zhao, Z.; Chen, Y.; Chiu, C.-Y.; Ruan, L.; Liu, Y.; Li, M.; Duan, X.; Huang, Y., High density catalytic hot spots in ultrafine wavy nanowires. *Nano Lett.* **2014,** *14* (7), 3887-3894.

46. Ali, A.; Shen, P. K., Recent advances in graphene-based platinum and palladium electrocatalysts for the methanol oxidation reaction. *J. Mater. Chem. A* **2019,** *7* (39), 22189-22217.

47. Fan, J. J.; Fan, Y. J.; Wang, R. X.; Xiang, S.; Tang, H. G.; Sun, S. G., A novel strategy for the synthesis of sulfur-doped carbon nanotubes as a highly efficient Pt catalyst support toward the methanol oxidation reaction. *J. Mater. Chem. A* **2017,** *5* (36), 19467-19475.

48. Hu, C.; Wang, X., Highly dispersed palladium nanoparticles on commercial carbon black with significantly high electro-catalytic activity for methanol and ethanol oxidation. *Int. J. Hydrogen Energy* **2015,** *40* (36), 12382-12391.

49. Yang, J.-M.; Wang, S.-A.; Sun, C.-L.; Ger, M.-D., Synthesis of size-selected Pt nanoparticles supported on sulfonated graphene with polyvinyl alcohol for methanol oxidation in alkaline solutions. *J. Power Sources* **2014,** *254*, 298-305.

50. Yu, M.; Wu, X. K.; Zhang, J. D.; Meng, Y. B.; Ma, Y. X.; Liu, J. H.; Li, S. M., Platinum nanoparticles-loaded holey reduced graphene oxide framework as freestanding

counter electrodes of dye sensitized solar cells and methanol oxidation catalysts. *Electrochim. Acta* **2017,** *258*, 485-494.

51. Monyoncho, E. A.; Steinmann, S. N.; Sautet, P.; Baranova, E. A.; Michel, C., Computational screening for selective catalysts: Cleaving the CC bond during ethanol electro-oxidation reaction. *Electrochim. Acta* **2018,** *274*, 274-278.

52. Fu, X.; Wan, C.; Zhang, A.; Zhao, Z.; Huyan, H.; Pan, X.; Du, S.; Duan, X.; Huang, Y., Pt3Ag alloy wavy nanowires as highly effective electrocatalysts for ethanol oxidation reaction. *Nano Res.* **2020,** *13* (5), 1472-1478.

53. Kobayashi, H.; Hayakawa, A.; Somarathne, K.; Okafor, E. C., Science and technology of ammonia combustion. *Proceedings of the Combustion Institute* **2019,** *37* (1), 109-133.

54. Sakamoto, T.; Serov, A.; Masuda, T.; Kamakura, M.; Yoshimoto, K.; Omata, T.; Kishi, H.; Yamaguchi, S.; Hori, A.; Horiuchi, Y.; Terada, T.; Artyushkova, K.; Atanassov, P.; Tanaka, H., Highly durable direct hydrazine hydrate anion exchange membrane fuel cell. *J. Power Sources* **2018,** *375*, 291-299.

55. Who In *IARC MONOGRAPHS ON THE EVALUATION OF CARCINOGENIC RISKS TO HUMANS*, Conference of the IARC Monographs on the Evaluation of Carcinogenic Risks to Humans, Lyon, FRANCE, Oct 10-17; Lyon, FRANCE, 2006; pp 9-38.

56. de Oliveira, D. C.; Silva, W. O.; Chatenet, M.; Lima, F. H. B., NiOX-Pt/C nanocomposites: Highly active electrocatalysts for the electrochemical oxidation of hydrazine. *Appl. Catal. B-Environ.* **2017,** *201*, 22-28.

57. Zhang, J.; Wang, Y. X.; Yang, C. J.; Chen, S.; Li, Z. J.; Cheng, Y.; Wang, H. N.; Xiang, Y.; Lu, S. F.; Wang, S. Y., Elucidating the electro-catalytic oxidation of hydrazine over carbon nanotube-based transition metal single atom catalysts. *Nano Res.* **2021**.

58. Finkelstein, D. A.; Imbeault, R.; Garbarino, S.; Roue, L.; Guay, D., Trends in Catalysis and Catalyst Cost Effectiveness for N2H4 Fuel Cells and Sensors: a Rotating Disk Electrode (RDE) Study. *Journal of Physical Chemistry C* **2016,** *120* (9), 4717-4738.

59. Tang, P. P.; Lin, X.; Yin, H.; Zhang, D. X.; Wen, H.; Wang, J. J.; Wang, P., Hierarchically Nanostructured Nickel-Cobalt Alloy Supported on Nickel Foam as a Highly Efficient Electrocatalyst for Hydrazine Oxidation. *Acs Sustainable Chemistry & Engineering* **2020,** *8* (44), 16583-16590.

60. Feng, G.; An, L.; Li, B.; Zuo, Y. X.; Song, J.; Ning, F. H.; Jiang, N.; Cheng, X. P.; Zhang, Y. F.; Xia, D. G., Atomically ordered non-precious Co3Ta intermetallic nanoparticles as high-performance catalysts for hydrazine electrooxidation. *Nat. Commun.* **2019,** *10*.

61. Liu, Y.; Zhang, J. H.; Li, Y. P.; Qian, Q. Z.; Li, Z. Y.; Zhu, Y.; Zhang, G. Q., Manipulating dehydrogenation kinetics through dual-doping Co3N electrode enables highly efficient hydrazine oxidation assisting self-powered H-2 production. *Nat. Commun.* **2020,** *11* (1).

62. Li, Y. P.; Zhang, J. H.; Liu, Y.; Qian, Q. Z.; Li, Z. Y.; Zhu, Y.; Zhang, G. Q., Partially exposed RuP2 surface in hybrid structure endows its bifunctionality for hydrazine oxidation and hydrogen evolution catalysis. *Sci. Adv.* **2020,** *6* (44).

63. He, F.; Xia, N. N.; Zheng, Y.; Zhang, Y. X.; Fan, H. L.; Ma, D. L.; Liu, Q. H.; Hu, X., In Situ Electrochemical Fabrication of Ultrasmall Ru-Based Nanoparticles for Robust N2H4 Oxidation. *ACS Appl. Mater. Interfaces* **2021,** *13* (7), 8488-8496.

Chapter 2. Ultrathin wavy Rh nanowires as highly effective electrocatalysts for methanol oxidation reaction with ultrahigh ECSA

2.1 Introduction

Compared with the industrialized hydrogen fuel cells, direct methanol fuel cell (DMFC) has received tremendous research interests because the storage of methanol is much cheaper and safer compared with that of hydrogen. Additionally, methanol also has a higher volumetric energy density than liquid hydrogen[1]. In particular, the alkaline direct methanol fuel cell (ADMFC) is attracting increasing research interests recently[2]. In alkaline environment, the kinetics of ORR becomes more favorable, which enables the choice of cheaper ORR electrocatalyst[2], such as AlN[3] and many carbon-based nanomaterials[4]. The reversed direction of the electro-osmotic drag also lowers the methanol crossover in the cell, leading to higher efficiency[2]. Unlike the hydrogen fuel cells in which the anode hydrogen oxidation reaction is highly kinetically favorable, the anode methanol oxidation reaction (MOR) in DMFCs is much more difficult and typically requires specific electrocatalysts. For example, nanostructured platinum has been widely studied as anode electrocatalysts for MOR in both alkaline and acidic environments with high mass activity (MA) and specific activity (SA) at the current peak (1236 mA/mg_{Pt} and 1.93 mA/cm^2 for $Pt/Ni(OH)_2$/graphene (alkaline environment)[5], 2260 mA/mg_{Pt} and 18.2 mA/cm^2 for PtCu nanoframework (alkaline environment)[6], 1261.5 mA/mg_{Pt} and 2.96 mA/cm^2 for PtPdRuTe (acidic environment)[7], 2252 mA/mg_{Pt} and 6.09 mA/cm^2 for PtCu nanotube (acidic environment)[8]). However, these current peaks typically appear at very high overpotential like ~0.8-0.9V vs. reversible hydrogen electrode (RHE)[5-8], which is undesirable for practical fuel cell applications since even the most effective cathode ORR electrocatalysts requires ~0.9 V vs. RHE to obtain a considerable reducing current for ORR[9]. Therefore, beyond

the peak current density, it is essential to develop a catalyst system that can considerably reduce the overpotential. Rhodium as a noble metal, has received tremendous research interests in the field of catalysis, such as hydrogenation[10], hydroformylation[10], hydrodechlorination[11], ammonia-borane hydrolysis[12, 13], CO oxidation[14], NOx remediation[14, 15], etc. It is also widely involved in the electrocatalysis of many reactions. Specifically, for MOR, the rhodium is often involved as one component of a binary or ternary electrocatalysts, such as PtRh[16-18], PdRh[19], PtRhRu[20], PtSnRh[21], and other noble metals like Pt, Pd are also involved because it is generally believed that the oxophilic nature of Rh is helpful for –OH adsorption, which further helps with the removal of the adsorbed CO[17]. However, it has been challenging to significantly lower the over potential of MOR in order to achieve a high oxidation current at lower potential[16-21]. Various monometallic Rh nanostructures, such as nanodendrites[22], mesoporous nanoparticles[15] and nanosheets/RGO[23] have been recently explored as electrocatalysts for MOR with respectable performances in alkaline media. Compared with the CV curves of MOR carried out on Pt, those Rh electrocatalysts can significantly lower the overpotential of MOR in terms of the peak current potential (~0.6 V vs. RHE compared with ~0.8-0.9 V for Pt), which is important for a higher voltage operation to improve the power output in ADMFCs[15, 22, 23]. However, the mass activity and the specific activity of these electrocatalysts are usually rather low (MA < 300 mA/mg)[15, 22, 23] compared with those of Pt based nanomaterials[5-8] (MA >1000 mA/mg), which negates their advantage of lower over potential for MOR because high mass activity is essential for reducing the usage of noble metal catalysts and therefore minimizing the costs for practical applications. In general, the mass activity of an electrocatalyst is determined by the specific activity and electrochemical active surface area (ECSA). The Rh-based MOR electrocatalysts typically exhibit a rather low ECSA (~43 m^2/g for Rh nanodendrites[22], Rh ~49 m^2/g for nanosheets/RGO[23],

and 50 m^2/g for Rh mesoporous nanoparticle[15]) due to their relatively large size. Therefore, a straightforward way to improve the mass activity is to increase the ECSA by using ultrafine nanostructures. However, ultrafine nanoparticles (*e.g.*, 2 nm) are typically not stable under relatively aggressive electrochemical conditions due to the physical movement/aggregation and Oswald ripening processes. We have recently reported that ultrafine Pt nanowires are highly stable under oxygen reduction conditions and are exhibiting an extraordinarily high ECSA up to 118 m^2/g[9]. Previously, our group have synthesized ultrathin wavy Rh nanowires that show excellent performances for the selective oxidation of benzyl alcohol to benzaldehyde[24]. Here we report the exploration of ultrafine wavy Rh nanowires as a highly effective MOR catalysts with ultrahigh ECSA. We propose that the high specific surface area and the rich surface defects[24] of the ultrathin wavy nanowires may promise increased ECSA and thus higher MA in electrocatalysis. Furthermore, the one-dimensional nanowire geometry is also considered to have an intrinsic advantage in charge transport, which is also beneficial to more efficient utilization of the noble metal nanostructures for electrocatalysis. Herein we successfully synthesized the ultrathin (2-3 nm) wavy Rh nanowires and demonstrated that they can work as excellent MOR electrocatalysts in alkaline media. Significantly, with ultrasmall diameter, the Rh NWs exhibit an ultrahigh $ECSA_{CO}$ of 144.2 m^2/g and more than 2.5-fold higher mass activity (722 mA/mg at 0.61V vs. RHE) compared with the previously reported Rh nanomaterials[15, 22, 23].

2.2 Experimental

2.2.1 Chemicals

Sodium hexachlororhodate (III) (Na_3RhCl_6, analytical grade), potassium iodide (KI, ACS reagent, ≥99.5%), polyvinylpyrrolidone (PVP, MW. ~55000), sodium ascorbate (NaAA, crystalline, ≥98%) and ethylene glycol (EG, anhydrous, 99.8%) were all purchased from

Sigma-Aldrich. The commercial Rh black (>99.9%) was purchased from Alfa Aesar. All the chemicals were used as received without further purification.

2.2.2 Synthesis of ultrathin Rh nanowires

The synthesis was following the previous research[24]. Briefly, 10 mg of Na_3RhCl_6, 40 mg NaAA, 160 mg PVP and 85 mg KI were dissolved in 1 mL DI water after ultra-sonication. Then 5 mL of ethylene glycol was added and mixed as a homogenous mixture. Then the vial is heated at 170 ^oC for 2h. After cooling under room temperature, the products were collected via centrifugation after the addition of acetone. The products were then washed via ultra-sonication/centrifugation in the solvent combination of ethanol/acetone for 1 time and ethanol/hexane for 2 times. The final products were dispersed in ethanol for further study after ultra-sonication.

2.2.3 Structural characterizations

The X-ray diffraction (XRD) was tested on a Panalytical X'Pert Pro X-ray Powder Diffractometer with Cu-Kα radiation after drop-casting the ethanol dispersion of ultrathin Rh wavy nanowires onto the glass substrate and drying under room temperature. X-ray photoelectron spectroscopy (XPS) tests were carried out with Kratos AXIS Ultra DLD spectrometer after drying the ethanol dispersion of the sample on the silicon substrate. Transmission electron microscopy (TEM) images were carried out on a FEI T12 transmission electron microscope operated at 120 kV. High resolution TEM images (HRTEM) was taken on FEI TITAN transmission electron microscope operated at 300 kV. The TEM samples were prepared by dropping ethanol dispersion of the sample onto the carbon-coated copper TEM grids. The loading of ultrathin Rh wavy nanowires on the GCE was determined by the inductively coupled plasma-atomic emission spectroscopy (ICP-AES).

2.2.4 Electrochemical measurements

All the electrochemical tests were carried out via a three-electrode cell system. The working electrode was a glassy carbon electrode (GCE) with a geometry area of 0.196 cm^2 and the counter electrode was a Pt wire. The reference electrode was Hg/HgO (1 M KOH) purchased from CHI152 and all the potential are converted against RHE after the calibration of the reference electrode in H_2-saturated 1 M KOH aqueous solution. In order to fabrication the working electrode, the Rh wavy nanowires were homogeneously dispersed in EtOH after sonication and 10 μL of the ink was drop casted onto the surface of the electrode surface. After drying under room temperature, 10 μL Nafion (0.05 wt ‰) was added and wait till dried under room temperature again. To activate the Rh electrocatalysts, cyclic voltammetry (CV) was performed in Ar-saturated 1M KOH electrolyte with a scan rate of 50 mV/s for 50 segments ranging from 0.05 V to 1.1 V vs. RHE. The electrochemical active surface area determined from hydrogen under potential deposition ($ECSA_{HUPD}$) was calculated from integrating hydrogen desorption charge from the last cycle of the CV curve using the constant of 220 μC/cm^2 for the hydrogen monolayer. Methanol oxidation reaction (MOR) tests were carried out in Ar-saturated 1 M KOH, 1 M MeOH electrolyte with potential scan rate of 50 mV/s. The chronoamperometry tests were carried out at 0.52 V vs. RHE for 6000s. The CO-stripping tests were also carried out to determine the $ECSA_{CO}$. After activation in Ar-saturated 1 M KOH via CV, the GCE was dipped into CO-saturated 1 M KOH electrolyte for allowing the CO to be adsorbed onto the Rh as monolayer. The electrolyte was then changed to Ar-saturated 1 M KOH and CO-stripping test was carried out with potential scan rate of 50 mV/s. The metal loading of Rh nanowires on the electrode determined from ICP-AES was 0.880 μg (4.49 μg/cm^2 normalized over the geometric area of the GCE) and the value of currents were normalized by the mass of the Rh loading on the

electrode. The commercial Rh black was also tested as control under the same conditions with a mass loading of 1.0 μg (5.1μg/cm^2).

2.3 Results and discussion

2.3.1 Characterizations of ultrathin Rh nanowires

The morphologies of the ultrafine wavy Rh nanowires were studied by transmission electron microscope (TEM) studies. TEM image clearly demonstrates ultrafine wavy nanowire geometry with diameters of about 2-3 nm and lengths exceeding 200 nm (Figure 2-1 (a)), which agrees well with the previous literature[24]. The high-resolution TEM (HRTEM) image shows clearly resolved lattice fringes with a lattice spacing of 0.22 nm (Figure 2-1 (b) and inset), corresponding to the (111) lattice planes of the FCC Rh, which is also consistent with previous literatures[15, 22, 23]. There are also apparently many surface defects as observed in previous literature, which represents the catalytic active sites for selective oxidation of benzyl alcohol to benzyl aldehyde[24]. The ultrafine size and rich surface defects may potentially contribute to the electrocatalysis of MOR as well.

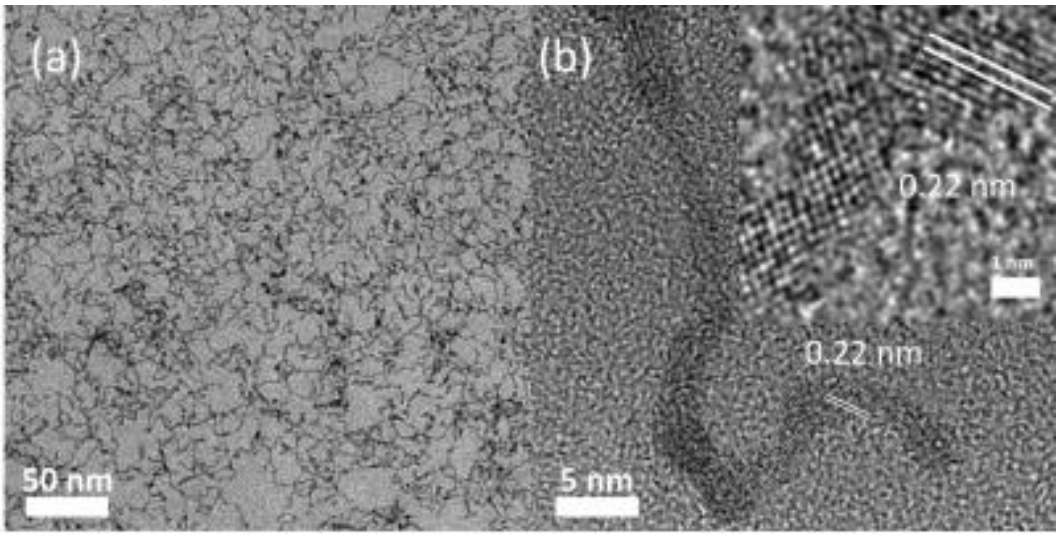

Figure 2-1. Morphology of the ultrathin wavy nanowires. (a) Representative TEM picture. (b) HRTEM picture.

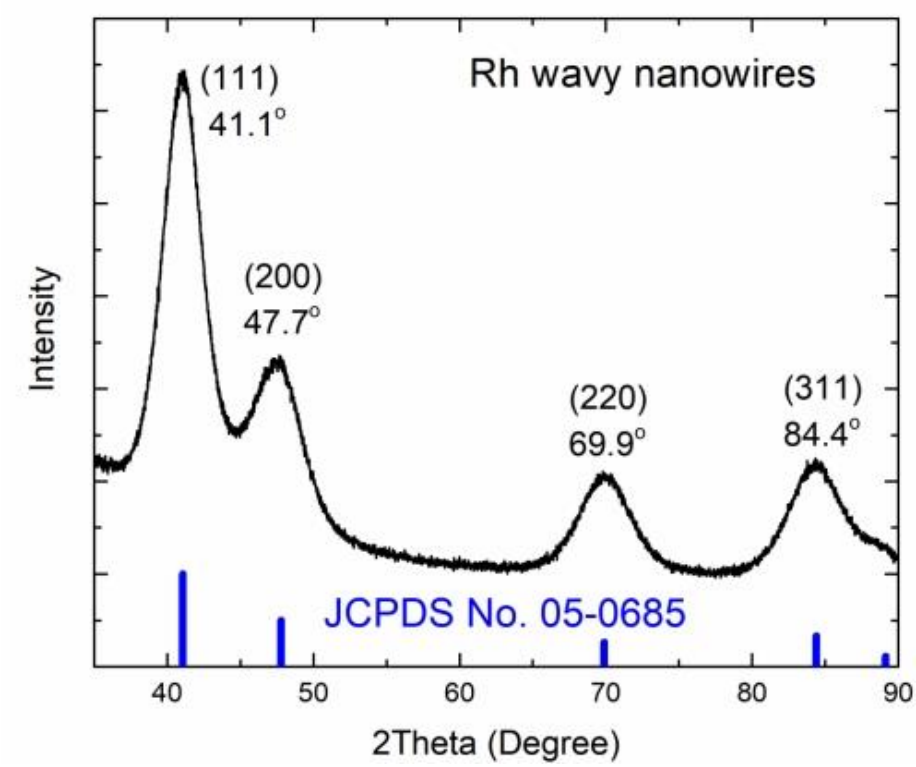

Figure 2-2. XRD characterization of the ultrathin Rh wavy nanowires.

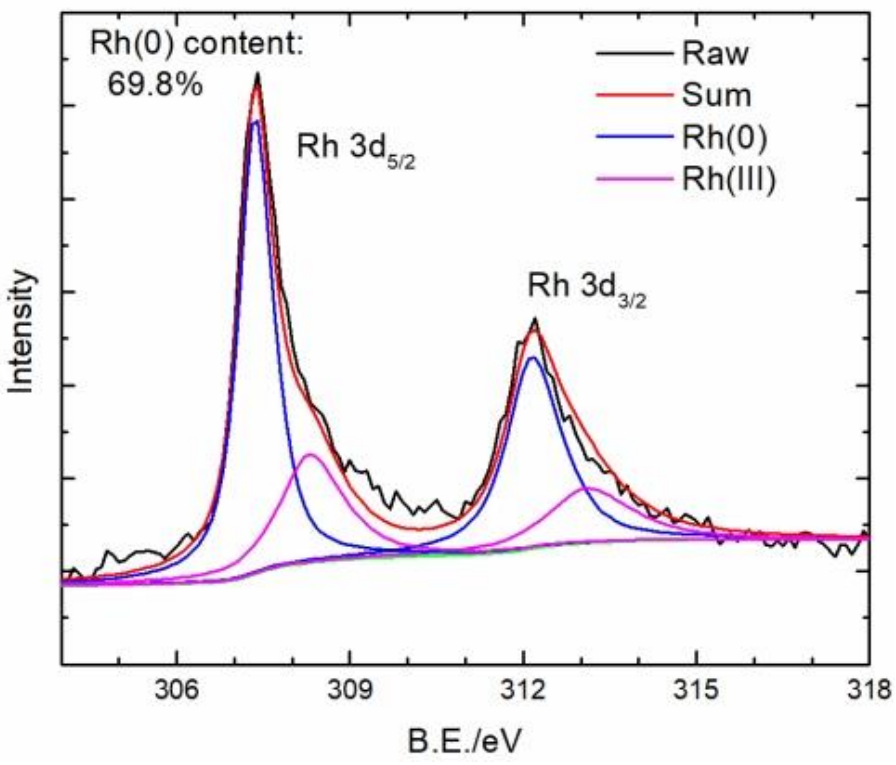

Figure 2-3. XPS characterization of the ultrathin Rh wavy nanowires.

Figure 2-2 shows the XRD pattern of the ultrathin wavy rhodium nanowire sample, the peaks at 41.1°, 47.7°, 69.9° and 84.4° are corresponding to the (111), (200), (220) and (311) crystal planes of the FCC Rh (JCPDS No. 05-0685), which also agree with the previous[15, 22, 23]. In Figure 2-3, the XPS shows the composition and valence of the surficial rhodium species. The peaks at the binding energies of 307.3 and 312.1 eV correspond to the $3d_{5/2}$ and $3d_{3/2}$ of the metallic Rh (0)[15, 22, 23], respectively. The peaks at the binding energies of 308.3 eV and 313.1 eV correspond to the $3d_{5/2}$ and $3d_{3/2}$ of the Rh (III)[15, 22, 23] which may result from the oxidized surficial Rh in air and the unreacted residue precursor. Peak area ratio of $3d_{5/2}$ and $3d_{3/2}$ follows the theoretical value of 3:2 for both Rh (0) and Rh (III) and the content of the Rh (0) is calculated as 69.8% from the peak area.

2.3.2 Electrocatalytic methanol oxidation reaction

The electrochemical performances of the Rh nanowire catalysts were first studied via CV to determine the $ECSA_{HUPD}$ (Figure 2-4 (a) dotted line). In the 1 M KOH electrolyte without methanol, the forward scan demonstrates two primary peaks corresponding to hydrogen desorption at 0.06-0.35 V[22, 23] and oxygen adsorption at >0.4 V[22, 24]. The reverse scan also exhibits two primary peaks corresponding to hydrogen adsorption at 0.05-0.27 V[22, 23] and oxygen desorption at 0.43 V[22, 24]. The $ECSA_{HUPD}$ was calculated to be 105.3 m^2/g by using the constant of 220 $\mu C/cm^2$ for the hydrogen monolayer[23, 25] after integration, which is more than 2-fold higher than the $ECSA_{HUPD}$ of Rh electrocatalysts reported previously (Rh nanodendrites: ~43 m^2/g, Rh nanosheets/RGO: ~49 m^2/g)[22, 23]. The $ECSA_{CO}$ of the Rh nanowires determined from CO-stripping (Figure 2-4 (a) solid line) by using the constant of 440 $\mu C/cm^2$ for the CO monolayer[25] is 144.2 m^2/g and is 7.2-fold higher than that of the commercial Rh black (20 m^2/g) (Figure 2-4 (b) solid line). The ultrahigh ECSA mostly likely arises from the high surface to volume ratio and rich surface defects of the ultrathin wavy nanowire[24]. Additionally, the favorable charge transport in the 1D geometry is also beneficial for maximizing the utilization efficiency of the active sites in electrocatalysis. Together, the ultrahigh ECSA suggests excellent potential of the Rh nanowires as highly effective electrocatalysts.

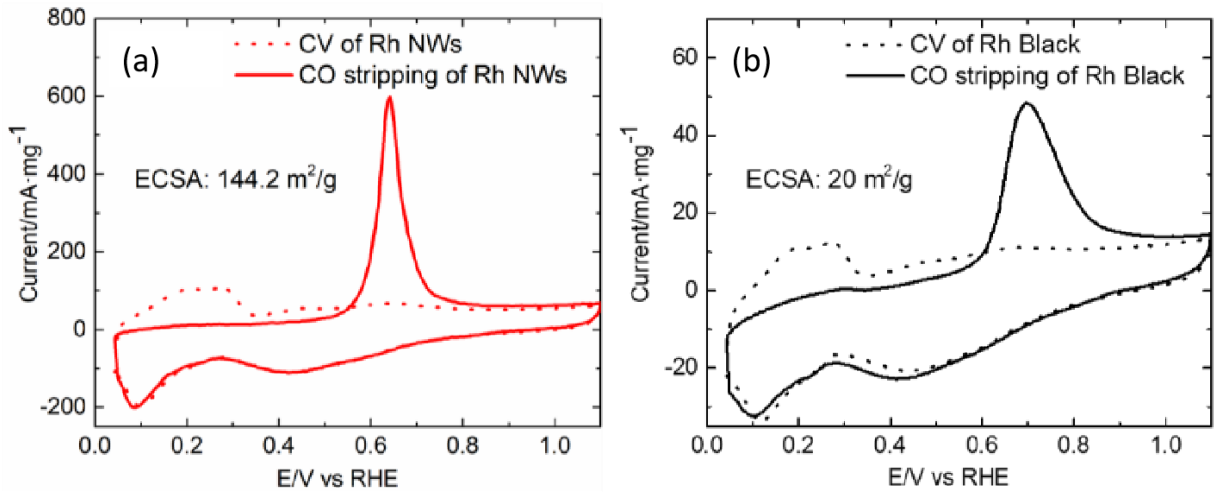

Figure 2-4. ECSA measurements of the Rh electrocatalysts. (a) Mass-normalized CV and CO-stripping curves of the ultrathin Rh wavy nanowires in 1 M KOH electrolyte at scan rate of 50 mV/s. (b) Mass-normalized CV and CO-stripping curves of the commercial Rh black in 1 M KOH electrolyte at scan rate of 50 mV/s.

The catalytic activity of the Rh nanowires for MOR was carried out in the electrolyte of 1 M KOH and 1 M methanol as shown in Figure 2-5 (a). The forward scan demonstrates a strong current peak at the potential of 0.61 V vs. RHE, corresponding to the oxidation of methanol with a peak mass activity of 722 mA/mg. This mass activity represents the highest value among all the previously reported monometallic Rh electrocatalysts tested at room temperature, including Rh mesoporous nanoparticle (288 mA/mg), Rh nanosheets/RGO (264 mA/mg), Rh nanodendrites (255.6 mA/mg) and is 7.7-fold higher than the commercial Rh black (93.6 mA/mg), and is also higher than many MOR catalysts reported to date at 0.61 V vs. RHE, indicating great utilization efficiency of the noble metal. The peak potential at 0.61 V also generally agrees well with the corresponding values from the previous literature and may be tentatively attributed to the intrinsic properties of Rh nanomaterials (with a lower the peak potential compared with those of

Pt-based nanomaterials)[15, 22, 23]. The specific activity is calculated as 0.686 mA/cm^2 based on the $ECSA_{HUPD}$ and this value is slightly higher compared with the previous literature[22, 23] (Rh nanodendrites: 0.590 mA/cm^2 based on the $ECSA_{HUPD}$, Rh nanosheets: 0.543 mA/cm^2 based on the on the $ECSA_{HUPD}$), which may be attributed to the low coordination number of Rh in the ultrathin wavy nanowires and the intrinsic advantage of charge transport of the nanowires[9, 24]. We can tentatively conclude that the high mass activity of the Rh wavy nanowires largely arises from the ultrahigh ECSA since the specific activity is not greatly improved.

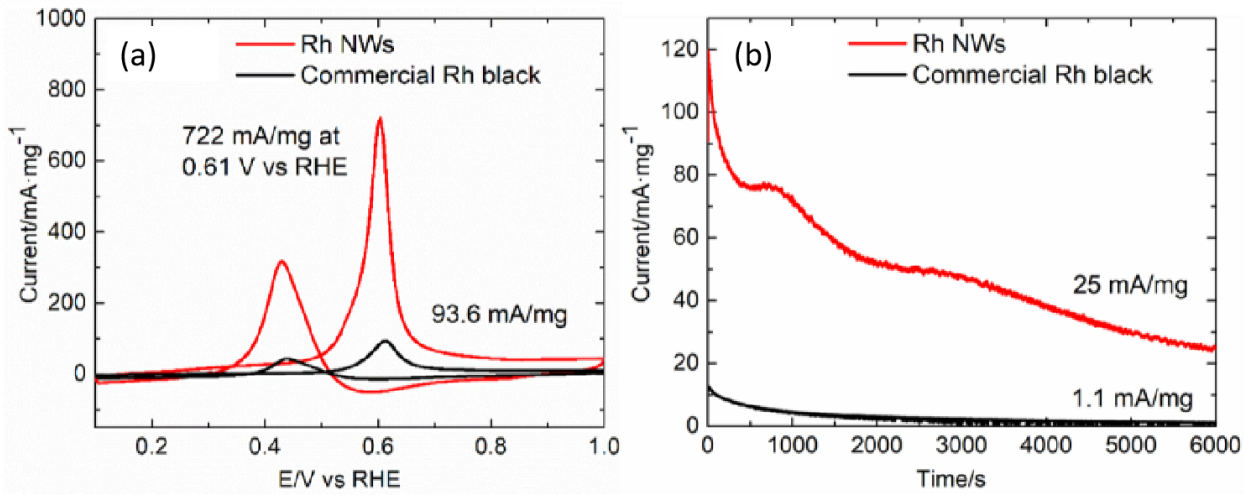

Figure 2-5. MOR performances of the Rh electrocatalysts. (a) Mass-normalized CV curves of the ultrathin Rh wavy nanowires and commercial Rh black in 1 M KOH + 1 M MeOH electrolyte at scan rate of 50 mV/s. (b) Chronoamperometry results of the ultrathin Rh wavy nanowires and commercial Rh black in 1 M KOH + 1 M MeOH electrolyte at 0.52 V vs. RHE

In the reverse scan the anodic peak has a negative potential shift and lower current compared with those in the forward scan, this phenomenon has also been widely observed with Pt-based nanomaterials during MOR. According to the most recent literatures, this hysteresis phenomenon on the Pt-based nanomaterials during MOR is explained as the change of rate-determining-step from water dissociation step to methanol dehydrogenation step during the reverse scan since the

oxygenated species are adsorbed onto the Pt surface after the forward scan, which makes the current peak potential and peak current different in the reverse scan[26, 27]. The I_F/I_R demonstrates the oxophilicity of the catalyst and lower I_R indicates the electrocatalysts surface are occupied by more oxygenated species which demonstrates higher oxophilicity[26, 27]. The I_F/I_R of the ultrathin Rh wavy nanowires is ~2.3, which is higher compared with some of the previously reported Pt-based nanomaterials with $I_F/I_R < 2$[5, 6, 28], indicating comparably higher oxophilicity. This also agrees with the volcano plot, in which Rh binds more easily to OH and oxygen[19, 29], which also indicates that Rh is considered to be more oxophilic than Pt. The chronoamperometry tests (Figure 2-5 (b)) were carried out to demonstrate the stability of the Rh nanowire electrocatalyst during long time of operation. The ultrathin wavy Rh nanowire is able to retain a current of 25 mA/mg at 0.52 V vs. RHE after 6,000 s. This value is much higher than commercial Rh black and generally comparable with the previous literatures[15, 22], which indicates acceptable stability and CO-tolerance.

2.3.3 Comparison with previously reported Pt-based electrocatalysts

For the Pt-based nanomaterials, despite of the ultrahigh mass activity, the current peak appears at much higher potential[5-8] (~0.8-0.9 V vs. RHE.), which may not be really applicable for DMFCs since it is close to the half-wave potential of the cathode ORR eletrocatalysts[9]. The comparison in Figure 2-6 (a) clearly demonstrates that Rh nanowires exhibit a favorable combination of high mass activity and lower overpotential, furthermore, the mass activity of Rh wavy nanowires at 0.61 V vs. RHE is also higher than many previously reported Pt-based nanomaterials as shown in Figure 2-6 (b)[5, 6, 15, 22, 23, 30].

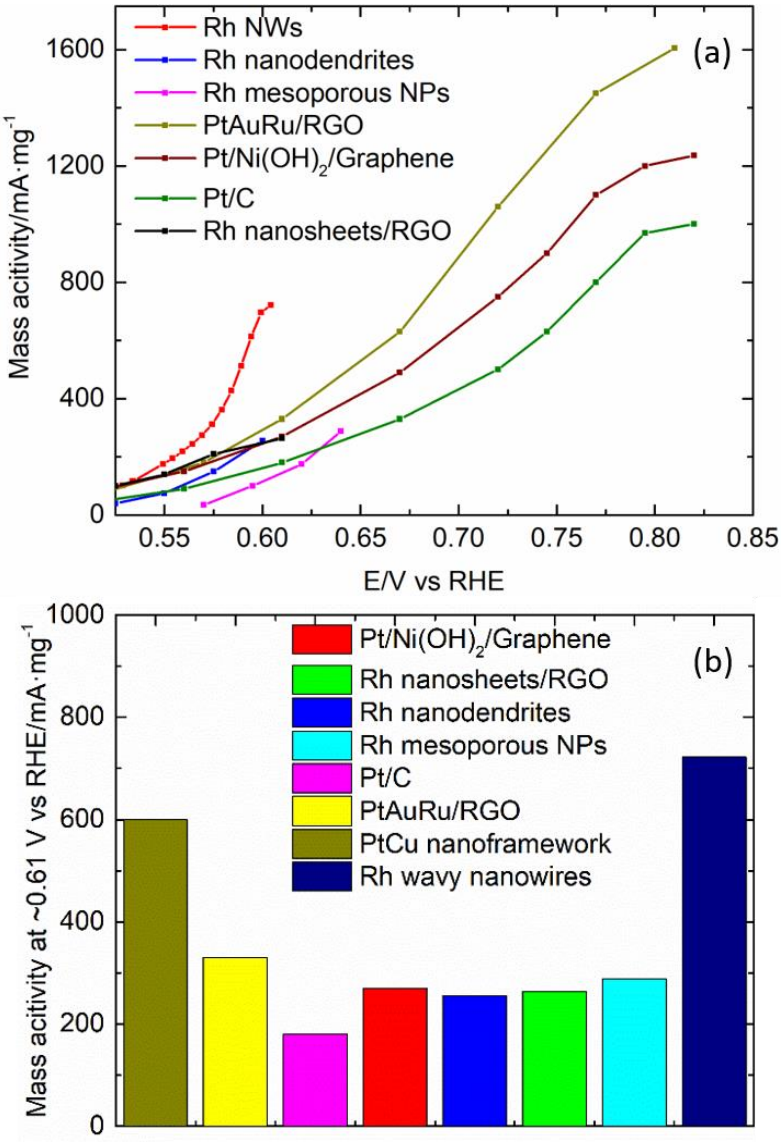

Figure 2-6. Comparison with previously reported electrocatalysts. (a) Summary of Rh and Pt-based electrocatalysts tested in the electrolyte of 1M MeOH + 1M KOH regarding their mass activities at different potentials. (b) The MOR mass activity at ~ 0.61 V vs. RHE of the Rh and Pt-based electrocatalysts tested in alkaline media.

2.4 Conclusion

In summary, we have shown that ultrathin rhodium wavy nanowires can function as highly effective MOR catalysts with low overpotential and ultrahigh ECSA, together delivering a mass

activity of 722 mA/mg at 0.61 V vs. RHE, which is higher than most of the previously reported electrocatalyst at the same potential. Therefore, we believe the ultrathin wavy Rh nanowires may represent a highly promising electrocatalyst for MOR.

2.5 Reference

1. Joghee, P.; Malik, J. N.; Pylypenko, S.; O'Hayre, R., A review on direct methanol fuel cells–In the perspective of energy and sustainability. *MRS Energy Sustain* **2015,** *2*.

2. Antolini, E.; Gonzalez, E. R., Alkaline direct alcohol fuel cells. *J. Power Sources* **2010,** *195* (11), 3431-3450.

3. Lei, M.; Wang, J.; Li, J.; Wang, Y.; Tang, H.; Wang, W., Emerging methanol-tolerant AlN nanowire oxygen reduction electrocatalyst for alkaline direct methanol fuel cell. *Sci. Rep.* **2014,** *4*, 6013.

4. Wang, D.-W.; Su, D., Heterogeneous nanocarbon materials for oxygen reduction reaction. *Energy Environ. Sci.* **2014,** *7* (2), 576-591.

5. Huang, W.; Wang, H.; Zhou, J.; Wang, J.; Duchesne, P. N.; Muir, D.; Zhang, P.; Han, N.; Zhao, F.; Zeng, M., Highly active and durable methanol oxidation electrocatalyst based on the synergy of platinum–nickel hydroxide–graphene. *Nat. Commun.* **2015,** *6*.

6. Zhang, Z.; Luo, Z.; Chen, B.; Wei, C.; Zhao, J.; Chen, J.; Zhang, X.; Lai, Z.; Fan, Z.; Tan, C., One-Pot Synthesis of Highly Anisotropic Five-Fold-Twinned PtCu Nanoframes Used as a Bifunctional Electrocatalyst for Oxygen Reduction and Methanol Oxidation. *Adv. Mater.* **2016,** *28* (39), 8712-8717.

7. Ma, S.-Y.; Li, H.-H.; Hu, B.-C.; Cheng, X.; Fu, Q.-Q.; Yu, S.-H., Synthesis of Low Pt-Based Quaternary PtPdRuTe Nanotubes with Optimized Incorporation of Pd for Enhanced Electrocatalytic Activity. *J. Am. Chem. Soc.* **2017,** *139* (16), 5890-5895.

8. Li, H.-H.; Fu, Q.-Q.; Xu, L.; Ma, S.-Y.; Zheng, Y.-R.; Liu, X.-J.; Yu, S.-H., Highly crystalline PtCu nanotubes with three dimensional molecular accessible and restructured surface for efficient catalysis. *Energy Environ. Sci.* **2017**.

9. Li, M.; Zhao, Z.; Cheng, T.; Fortunelli, A.; Chen, C.-Y.; Yu, R.; Zhang, Q.; Gu, L.; Merinov, B. V.; Lin, Z., Ultrafine jagged platinum nanowires enable ultrahigh mass activity for the oxygen reduction reaction. *Science* **2016,** *354* (6318), 1414-1419.

10. Guerrero, M.; Chau, N. T. T.; Noel, S.; Denicourt-Nowicki, A.; Hapiot, F.; Roucoux, A.; Monflier, E.; Philippot, K., About the Use of Rhodium Nanoparticles in Hydrogenation and Hydroformylation Reactions. *Curr. Org. Chem.* **2013,** *17* (4), 364-399.

11. Cobo, M.; Becerra, J.; Castelblanco, M.; Cifuentes, B.; Conesa, J. A., Catalytic hydrodechlorination of trichloroethylene in a novel NaOH/2-propanol/methanol/water system on ceria-supported Pd and Rh catalysts. *Journal of Environmental Management* **2015,** *158*, 1-10.

12. Akbayrak, S.; Tonbul, Y.; Ozkar, S., Ceria supported rhodium nanoparticles: Superb catalytic activity in hydrogen generation from the hydrolysis of ammonia borane. *Appl. Catal. B-Environ.* **2016,** *198*, 162-170.

13. Wang, L. B.; Li, H. L.; Zhang, W. B.; Zhao, X.; Qiu, J. X.; Li, A. W.; Zheng, X. S.; Hu, Z. P.; Si, R.; Zeng, J., Supported Rhodium Catalysts for Ammonia-Borane Hydrolysis: Dependence of the Catalytic Activity on the Highest Occupied State of the Single Rhodium Atoms. *Angew. Chem.-Int. Edit.* **2017,** *56* (17), 4712-4718.

14. Parry, I. S.; Kartouzian, A.; Hamilton, S. M.; Balaj, O. P.; Beyer, M. K.; Mackenzie, S. R., Collisional Activation of N2O Decomposition and CO Oxidation Reactions on Isolated Rhodium Clusters. *J. Phys. Chem. A* **2013,** *117* (36), 8855-8863.

15. Jiang, B.; Li, C.; Dag, Ö.; Abe, H.; Takei, T.; Imai, T.; Hossain, M. S. A.; Islam, M. T.; Wood, K.; Henzie, J., Mesoporous metallic rhodium nanoparticles. *Nat. Commun.* **2017,** *8*, 15581.

16. Li, L.; Tian, C.; Yang, J.; Zhang, X.; Chen, J., One-pot synthesis of PtRh/β-CD-CNTs for methanol oxidation. *Int. J. Hydrogen Energy* **2015,** *40* (43), 14866-14874.

17. Lee, Y.-W.; Park, K.-W., Pt–Rh alloy nanodendrites for improved electrocatalytic activity and stability in methanol electrooxidation reaction. *Catal. Commun.* **2014,** *55*, 24-28.

18. Wu, T.-Y.; Kuo, Z.-Y.; Jow, J.-J.; Kuo, C.-W.; Tsai, C.-J.; Chen, P.-R.; Chen, H.-R., Co-electrodeposition of platinum and rhodium in poly (3, 4-ethylenedioxythiophene)-poly (styrene sulfonic acid) as electrocatalyst for methanol oxidation. *Int. J. Electrochem. Sci.* **2012,** *7*, 8076-8090.

19. Jurzinsky, T.; Bär, R.; Cremers, C.; Tübke, J.; Elsner, P., Highly active carbon supported palladium-rhodium Pd X Rh/C catalysts for methanol electrooxidation in alkaline media and their performance in anion exchange direct methanol fuel cells (AEM-DMFCs). *Electrochim. Acta* **2015,** *176*, 1191-1201.

20. Kawaguchi, T.; Rachi, Y.; Sugimoto, W.; Murakami, Y.; Takasu, Y., Performance of ternary PtRuRh/C electrocatalyst with varying Pt: Ru: Rh ratio for methanol electro-oxidation. *J. Appl. Electrochem.* **2006,** *36* (10), 1117-1125.

21. Jiang, K.; Bu, L.; Wang, P.; Guo, S.; Huang, X., Trimetallic PtSnRh wavy nanowires as efficient nanoelectrocatalysts for alcohol electrooxidation. *ACS Appl. Mater. Interfaces* **2015,** *7* (27), 15061-15067.

22. Kang, Y.; Li, F.; Li, S.; Ji, P.; Zeng, J.; Jiang, J.; Chen, Y., Unexpected catalytic activity of rhodium nanodendrites with nanosheet subunits for methanol electrooxidation in an alkaline medium. *Nano Res.* **2016,** *9* (12), 3893-3902.

23. Kang, Y.; Xue, Q.; Jin, P.; Jiang, J.; Zeng, J.; Chen, Y., Rhodium Nanosheets–Reduced Graphene Oxide Hybrids: A Highly Active Platinum-Alternative Electrocatalyst for the Methanol Oxidation Reaction in Alkaline Media. *ACS Sustain. Chem. Eng.* **2017,** *5* (11), 10156-10162.

24. Huang, X.; Zhao, Z.; Chen, Y.; Chiu, C.-Y.; Ruan, L.; Liu, Y.; Li, M.; Duan, X.; Huang, Y., High density catalytic hot spots in ultrafine wavy nanowires. *Nano Lett.* **2014,** *14* (7), 3887-3894.

25. Durst, J.; Simon, C.; Hasché, F.; Gasteiger, H. A., Hydrogen oxidation and evolution reaction kinetics on carbon supported Pt, Ir, Rh, and Pd electrocatalysts in acidic media. *J. Electrochem. Soc.* **2015,** *162* (1), F190-F203.

26. Hofstead-Duffy, A. M.; Chen, D.-J.; Sun, S.-G.; Tong, Y. J., Origin of the current peak of negative scan in the cyclic voltammetry of methanol electro-oxidation on Pt-based electrocatalysts: a revisit to the current ratio criterion. *J. Mater. Chem.* **2012,** *22* (11), 5205-5208.

27. Zhao, Y.; Li, X.; Schechter, J. M.; Yang, Y., Revisiting the oxidation peak in the cathodic scan of the cyclic voltammogram of alcohol oxidation on noble metal electrodes. *RSC Adv.* **2016,** *6* (7), 5384-5390.

28. Mikkelsen, K.; Cassidy, B.; Hofstetter, N.; Bergquist, L.; Taylor, A.; Rider, D. A., Block Copolymer Templated Synthesis of Core–Shell PtAu Bimetallic Nanocatalysts for the Methanol Oxidation Reaction. *Chem. Mater.* **2014,** *26* (24), 6928-6940.

29.Nørskov, J. K.; Rossmeisl, J.; Logadottir, A.; Lindqvist, L.; Kitchin, J. R.; Bligaard, T.; Jonsson, H., Origin of the overpotential for oxygen reduction at a fuel-cell cathode. *J. Phys. Chem. B* **2004,** *108* (46), 17886-17892.

30. Ren, F.; Wang, C.; Zhai, C.; Jiang, F.; Yue, R.; Du, Y.; Yang, P.; Xu, J., One-pot synthesis of a RGO-supported ultrafine ternary PtAuRu catalyst with high electrocatalytic activity towards methanol oxidation in alkaline medium. *J. Mater. Chem. A* **2013,** *1* (24), 7255-7261.

Chapter 3. Pt_3Ag alloy wavy nanowires as highly effective electrocatalysts for ethanol oxidation reaction

3.1 Introduction

Compared with compressed hydrogen, alcohols have higher volumetric energy density and gravimetric energy density (by considering the weight of the hydrogen tank)[1]. In addition, they are also easier and intrinsically safer for storage and transport, making them attractive candidates for fuel cells[1]. Among the various candidate alcohol fuels, ethanol has even higher volumetric energy and gravimetric energy density than methanol, as well as the advantage for being much less toxic and produced renewably at lower cost[1]. Specifically, the alkaline direct ethanol fuel cell (ADEFC) is attracting research interests[2] since the alkaline environment enables the choice for non-noble metal based cathode oxygen reduction reaction (ORR) electrocatalysts[3-7] to lower the overall cost of the fuel cells. Additionally, the direction of the electro-osmotic drag is reversed due to the reverse direction of hydroxide anion transport, which could also help lower the alcohol crossover in the cell, leading to less cathode catalyst poisoning as well as higher efficiency[2, 8]. The disadvantage of voltage drop caused by the carbonate formation can be alleviated by changing electrolyte periodically or increasing operation temperature[9, 10]. However, the ethanol oxidation reaction (EOR) is kinetically much more difficult compared with the hydrogen oxidation reaction (HOR), and often requires noble metal-based electrocatalysts, such as Pt[11] and Pd[12] that are limited by relatively high overpotential, poisoning and low mass activity. Therefore, developing noble metal based electrocatalysts with high mass activities (defined as electrocatalytic performance normalized by the mass loading of the noble metal) is of great importance for cost-effective direct ethanol fuel cells.

In general, the mass activity of an electrocatalyst is determined by the product of the specific

activity (SA) and electrochemical active surface area (ECSA). To enhance the specific activities, the surface modification remains to be the most common way, including creating alloys and hybrids materials. For example, Ru[13-15], Ni[16, 17] or $Ni(OH)_2$[18, 19] have been employed as highly oxophilic components to modify Pt or Pd and facilitate the formation of surficial -OH group, which is beneficial for the removal of the carbonaceous species on the nearby noble metal sites via the Langmuir−Hinshelwood mechanism through a bifunctional effect.

Ag has also been suggested as a beneficial component to modify Pt via the ligand effect and has received tremendous research interests. Ag itself has the highest specific conductivity among all metals, which is intrinsically beneficial for electrocatalysis since charge transport is essential for electrocatalysis[20]. Additionally, Ag not only intrinsically binds weakly to CO as shown from the volcano plot (like Cu and Au from the same group)[21], but also helps adjust the d-band structure and enrich the local electron density around Pt upon alloying, which lowers the electron donation from CO to Pt and thus potentially weakens CO chemisorption and mitigates undesirable poisoning effect[22, 23]. Very recently, theoretical study suggested that the Pt_3Ag alloy with (111) crystal surface exposed can facilitate the C-C bond cleavage during ethanol oxidation reaction[24], thus delivering a higher efficiency of utilizing ethanol as a fuel. Therefore, it is expected the Pt_3Ag alloy may be a good candidate for electrocatalytic ethanol oxidation reaction with improved SA.

Apart from increasing the SA, the enhancement of ECSA is also essential for enhancing the overall MA. To this end, the use of ultrafine nanostructures is important. However, ultrafine nanoparticles are usually not very stable under aggressive electrochemical reaction conditions due to the physical movement/aggregation and Oswald ripening processes. The one-dimensional (1D) nanowires is less mobile, more stable and less subjected to these drawbacks[25]. Thus,

ultrathin nanowires represent an attractive class of electrocatalysts that can deliver ultrahigh ECSA[17, 25]. For the nanowires with wavy morphologies (wavy nanowires), the wavy surface with rich surface defects may also provide additional catalytic hotspots for further improved activity[26, 27]. Lastly, the 1D structure is also believed to have an intrinsic advantage to facilitate charge transport for more efficient utilization all available catalytic sites.

Here we report the synthesis of the Pt_3Ag wavy nanowires through a particle attachment mechanism in a facile solvothermal process. Transmission microscopy studies and elemental analyses reveal highly wavy nanowire structure with an average diameter of 4.6±1.0 nm and uniform Pt_3Ag alloy formation. Electrocatalytic studies demonstrate that the alloy wavy nanowires may function as high effective electrocatalysts for ethanol oxidation reactions (EOR) with an ultrahigh SA (28.0 mA/cm^2) and a highest mass activity of 6.1 A/mg, far exceeding that of the commercial Pt/carbon samples (1.10 A/mg).

3.2 Experimental

3.2.1 Chemicals

Potassium tetrachloroplatinate (IV) (K_2PtCl_4, 98%), silver nitrate ($AgNO_3$, analytical grade), polyvinylpyrrolidone (PVP, MW. ~55000), concentrated ammonium hydroxide ($NH_3 \cdot H_2O$, 28.0%-30.0%), sodium borohydride ($NaBH_4$), were purchased from Sigma-Aldrich and the commercial platinum on carbon black (commercial Pt/C, 20%) were purchased from Alfa Aesar and the chemicals were used as received.

3.2.2 Synthesis of Pt_3Ag wavy nanowires

160 mg PVP were dissolved into 4mL of EG after ultrasonication at first. And 0.018 mmol of K_2PtCl_4 and 0.006 mmol $AgNO_3$ were dissolved in 1.0 mL and 0.25 mL DI water, respectively. Then we uniformly mixed the aqueous solution of the Pt and Ag precursors with the EG solution

of PVP in turn. The vial was then heated at 210 ^{o}C for 4h. After cooling to room temperature, we added 0.7 mL concentrated ammonia water and 2 mL of aqueous solution of $NaBH_4$ (5.0 mg) for cleaning. After 1 hour, the products were collected via centrifugation after the addition of acetone and then washed with water for 2 times and ethanol for 2 times. Finally, they were re-dispersed in ethanol for further study.

3.2.3 Structural characterizations

The X-ray diffraction (XRD) was tested on a Panalytical X'Pert Pro X-ray Powder Diffractometer with Cu-Kα radiation after drop-casting the ethanol dispersion of Pt_3Ag wavy nanowires onto the glassy substrate and dried under room temperature. X-ray photoelectron spectroscopy (XPS) tests were carried out with Kratos AXIS Ultra DLD spectrometer after drop-casting ethanol dispersion of the sample on the silicon substrate and then dried. Transmission electron microscopy (TEM) images were carried out on FEI T12 transmission electron microscope operated at 120 kV. High resolution TEM images (HRTEM) were taken on FEI Titan transmission electron microscope operated at 300 kV. The STEM image and EDX (energy dispersive x-ray spectroscopy) mapping were carried out on Joel Jem-300CF (Grand Arm) operated at 300 kV. The samples were prepared by dropping ethanol dispersion of the sample onto the carbon-coated copper TEM grids. The Pt loading of Pt_3Ag wavy nanowires on the GCE was determined by the inductively coupled plasma-atomic emission spectroscopy (ICP-AES).

3.2.4 Electrochemical measurements

All the electrochemical studies were carried out via a three-electrode cell system. The working electrode was a glassy carbon electrode (GCE) with a geometry area of 0.196 cm^2 and the counter electrode was a Pt wire. We used Hg/HgO (1 M KOH) as the reference electrode for electrochemical test in alkaline media and Ag/AgCl as the reference electrode in acidic media.

All potentials are converted against RHE. In order to fabrication the working electrode, the Pt_3Ag wavy nanowires were homogeneously dispersed in EtOH after sonication and 10.0 μL of the ink was drop-cast onto the surface of the electrode surface and dried at room temperature. The Pt loading of our nanowires on the electrode determined from ICP-AES was 2.10 μg (10.7 $\mu g/cm^2$ as normalized by the geometric area of the GCE).

To activate the electrocatalysts, cyclic voltammetry (CV) tests were performed in Ar-saturated 0.5 M H_2SO_4 electrolyte with a scan rate of 50 mV/s ranging from 0.05 V to 1.0 V vs. RHE. The electrochemical active surface area determined from hydrogen under potential deposition ($ECSA_{HUPD}$) was calculated by integrating hydrogen desorption charge using the constant of 210 $\mu C/cm^2$ for the hydrogen monolayer on platinum. The electrocatalytic ethanol oxidation reaction (EOR) tests were carried out in Ar-saturated 1 M KOH + 1 M EtOH electrolyte with potential scan rate of 50 mV/s in the range from 0.05 V to 1.1 V vs. RHE. To test the long-term performance of the electrocatalysts, the chronoamperometry (CA) tests were carried out at 0.72 V vs. RHE for 6000s. Commercial platinum carbon was used as control and 1.00 mg commercial Pt/C (20%) was mixed with 0.99 mL ethanol and 10.0 μL of Nafion (5 wt%) to prepare the ink after ultrasonication. And 5.0 μL of the Pt/C catalyst ink was drop-cast onto the GCE and dried to ensure a platinum loading of 1.0 μg (5.1 $\mu g/cm^2$) on the working electrode to ensure similar background current during CV scan. For the CA tests, the Pt-loading of Pt/C is 2.0 μg (10.2 $\mu g/cm^2$) by drop casting 10.0 μL of the Pt/C catalyst ink. All the electrochemical tests were carried out under the same conditions for the controlled sample of commercial Pt/C (20%).

3.3 Results and discussion

3.3.1 Characterizations of Pt_3Ag wavy nanowires

The morphologies of the wavy Pt_3Ag nanowires were studied by transmission electron

microscope (TEM). TEM image clearly demonstrates ultrafine wavy nanowire geometry with diameters mainly in the range of ~3-6 nm and lengths exceeding 300 nm (Figure 3-1 (a)). The high-resolution TEM shows clearly resolved lattice fringes with a lattice spacing of 0.231 nm (Figure 3-1 (b) and inset). This value falls between the lattice spacing of the (111) crystal planes of FCC Pt (0.227 nm) and FCC Ag (0.236 nm), indicating the formation of FCC alloys between Pt and Ag, which is also generally consistent with previous reports about the alloys between platinum and silver[28, 29]. Like the previously reported wavy nanowires, there are also apparently many surface defects, which may function as the catalytic active sites and contribute to the electrocatalytic performances according to the previous reports about wavy nanowires[26, 27]. More importantly, the exposed (111) crystal plane of Pt_3Ag is also believed to help with C-C bond cleavage during EOR based on the previous theoretical study[24]. A statistical analysis of the diameters of the wavy nanowires reveal an average diameter of 4.6±1.0 nm (Figure 3-1 (c)). Such small diameter is beneficial for boosting the ECSA.

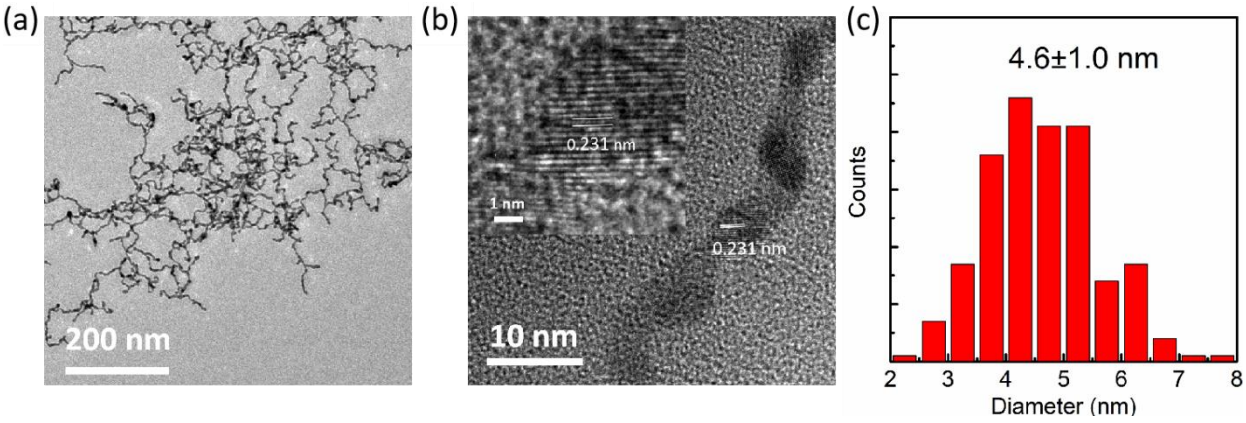

Figure 3-1. Morphology of the ultrathin wavy Pt_3Ag alloy nanowires: (a) TEM image. (b) HRTEM image. (c) Diameter-distribution of nanowires.

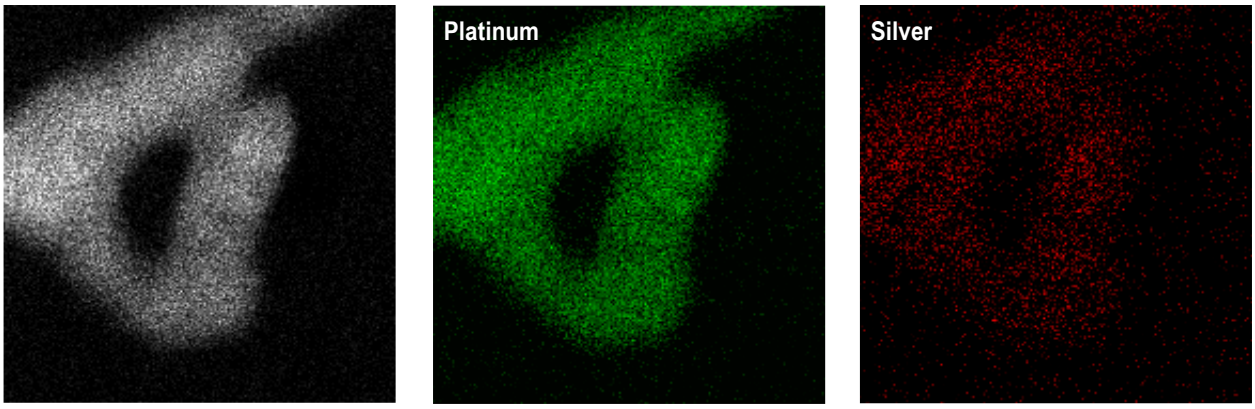

Figure 3-2. EDX mapping of the ultrathin wavy Pt_3Ag alloy nanowires regarding Pt and Ag element.

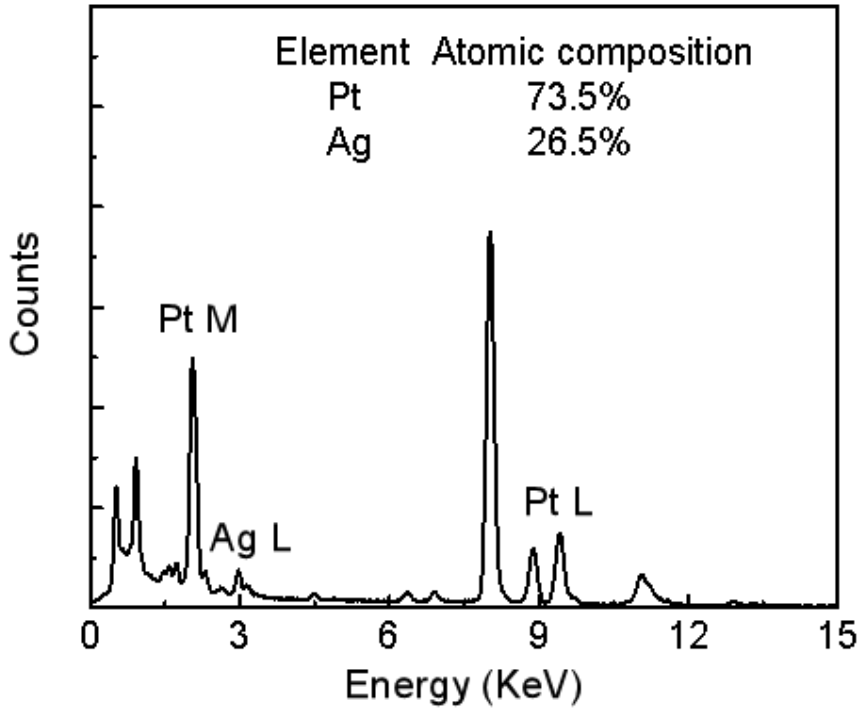

Figure 3-3. EDX spectrum and elemental composition of the ultrathin wavy Pt_3Ag alloy nanowires.

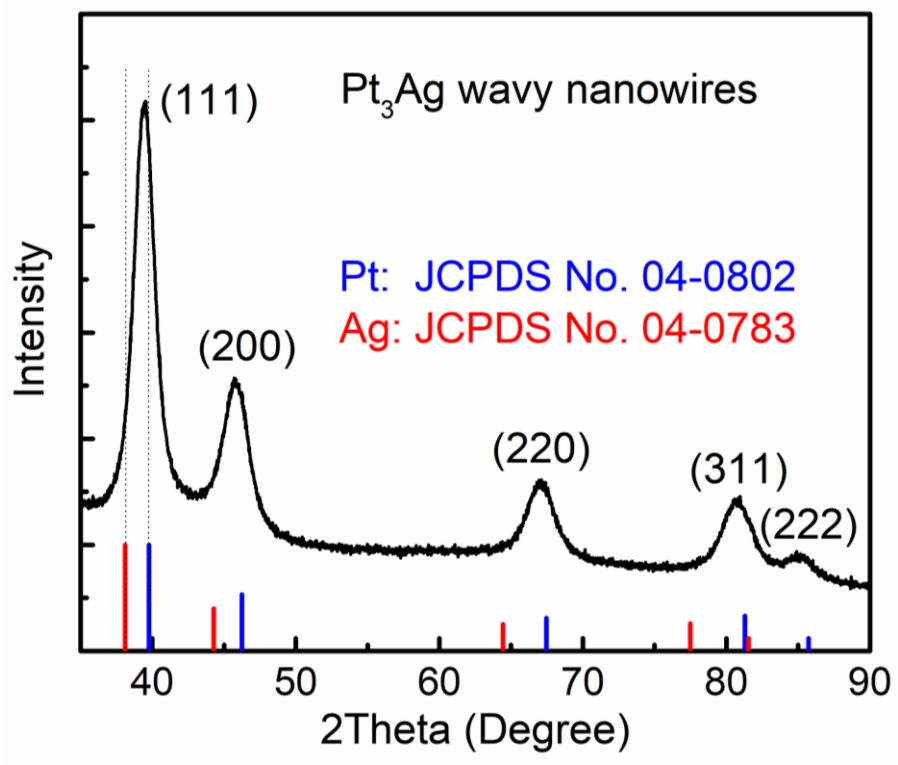

Figure 3-4. XRD pattern of the ultrathin wavy Pt_3Ag alloy nanowires.

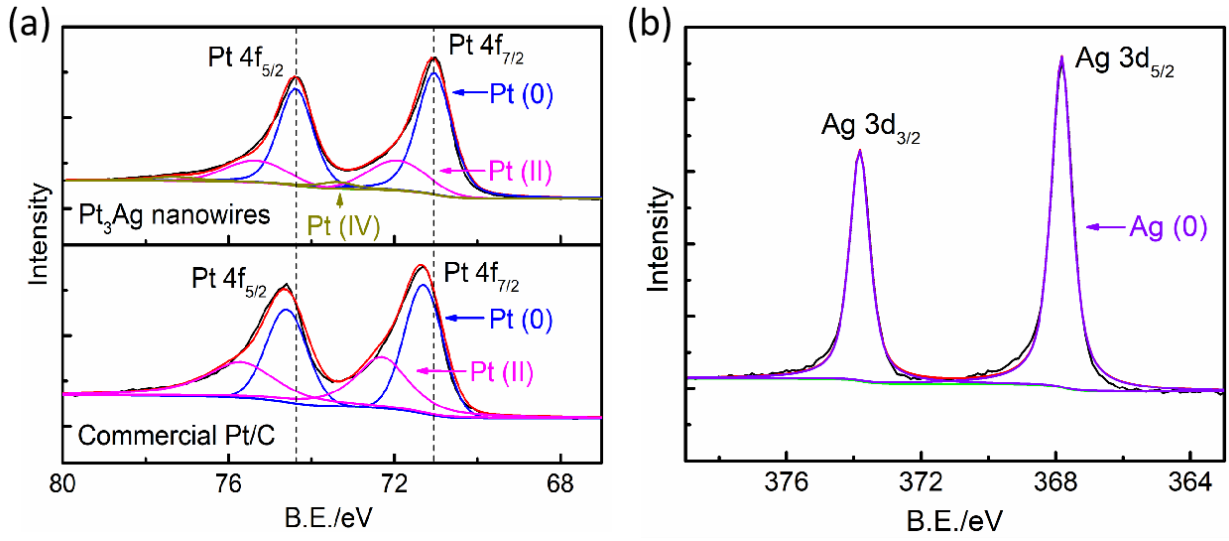

Figure 3-5. XPS characterization. (a) XPS for Pt element and the comparison between ultrathin wavy Pt_3Ag alloy nanowires and commercial Pt/C. (b) XPS for Ag element for ultrathin wavy Pt_3Ag alloy nanowires

To evaluate the alloy formation and elemental distribution within the wavy nanowires, we have conducted scanning transmission electron microscopy (STEM) studies and elemental mapping statues using energy dispersive X-ray spectroscopy (EDX) (Figure 3-2). The EDX mapping demonstrates that uniform distributions of platinum and silver throughout the wavy nanowires, confirming the formation of uniform alloy. The ratio of Pt: Ag determined from EDX analysis is 2.76:1 as shown in Figure 3-3, which also agrees well with the results from ICP-AES (2.83:1) and the feed ratio of the precursors (3:1), further confirming the composition of the alloy wavy nanowires. Figure 3-4 shows the XRD pattern of the Pt_3Ag wavy nanowires sample. Compared with the standard XRD pattern of the FCC silver (JCPDS No. 04-0783) and FCC platinum (JCPDS No. 04-0802) whose characteristic peaks are attributed to the (111), (200), (220), (311) and (222) crystal planes, the Pt_3Ag nanowires also show the same set of peaks attributed to (111), (200), (220), (311) and (222) crystal plane positioned exactly between those of Pt and Ag, further confirming the formation of uniform alloys, which is also consistent with the observations from HRTEM and EDX mapping. By applying Scherrer's equation for these peaks, the size of the crystallites was estimated to be 4.3 nm, which generally agrees with the observations from TEM. In Figure 3-5, the XPS results demonstrates the composition and valence of the surface platinum and silver species in Pt_3Ag nanowires. The peaks at the binding energies (BE) of 71.0 and 74.4 eV correspond to the $4f_{7/2}$ and $4f_{5/2}$ of the Pt (0), respectively[28, 29]. The peaks at the BE of 71.9 eV and 75.3 eV correspond to the $4f_{7/2}$ and $4f_{5/2}$ of the Pt (II)[28, 29] while the peaks at the 73.4 eV and 77.3 eV correspond to the $4f_{7/2}$ and $4f_{5/2}$ of the Pt (IV) species[30]. These oxidized Pt species might be attributed to the oxidized surficial Pt in air or the unreacted precursor. The peak area ratio of $4f_{7/2}$ and $4f_{5/2}$ follows the theoretical value of 4:3 for all split peaks of Pt (0), Pt (II) and Pt (IV) and the content of Pt (0) is calculated as 70.2% based on the peak area. For silver, the peaks at the

BE of 367.8 and 373.8 eV correspond to the $3d_{5/2}$ and $3d_{3/2}$ of the Ag (0) following the theoretical value of 3:2, The absence of other split peaks indicates that the silver exists predominately as metallic Ag (0). We also find that the BE for the Pt 4f orbits are comparably lower than those of commercial Pt/C as shown in Figure 3-5 (a) with Pt (0) $4f_{7/2}$ shifted from 71.3 eV to 71.0 eV and Pt (0) $4f_{5/2}$ shifted from 74.6 eV to 74.4 eV upon alloying with silver, indicating the electronic states of Pt are adjusted due to the electron donation from silver (electronegativity: 1.93) to platinum (electronegativity: 2.28). It has been proposed that the negatively shifted BE indicates enriched electron density of Pt, which could weaken the interaction with lone electron pair of CO and other carbonaceous species, and thus lowers the binding and poisoning effect[23, 31]. Accordingly, silver also has higher BE when compared with pure Ag NWs with Ag (0) $3d_{5/2}$ shifted from 367.4 eV to 367.8 eV and Ag (0) $3d_{3/2}$ shifted from 373.4 eV to 373.8 eV, which further confirms the electron transfer from Ag to Pt[32].

In our synthesis of the Pt_3Ag wavy nanowires, EG works as the reducing agent under high temperature while PVP works as the template agent to help forming wavy nanowires via the particle attachment mechanism. Similar synthetic system for wavy nanowire growth has also been reported with PVP as the template agent previously[26]. In addition, PVP will also help with the exposure of the (111) crystal plane of the noble metals, which is important for many catalytic reactions[33, 34], including EOR[24].

To further reveal the growth mechanism, we have also taken TEM pictures of the products collected at the different reaction intervals as depicted in Figure 3-6. At t=1 min, there are lots of tiny crystallites (~2 nm) formation. As the reaction time goes, there are short nanorods beginning to form (t= 5 and 10 min), followed by the formation of longer nanowires (t=20, 30 and 60 min). This observation also agrees with the previous literature about the particle attachment mechanism

for wavy nanowire growths[26, 28].

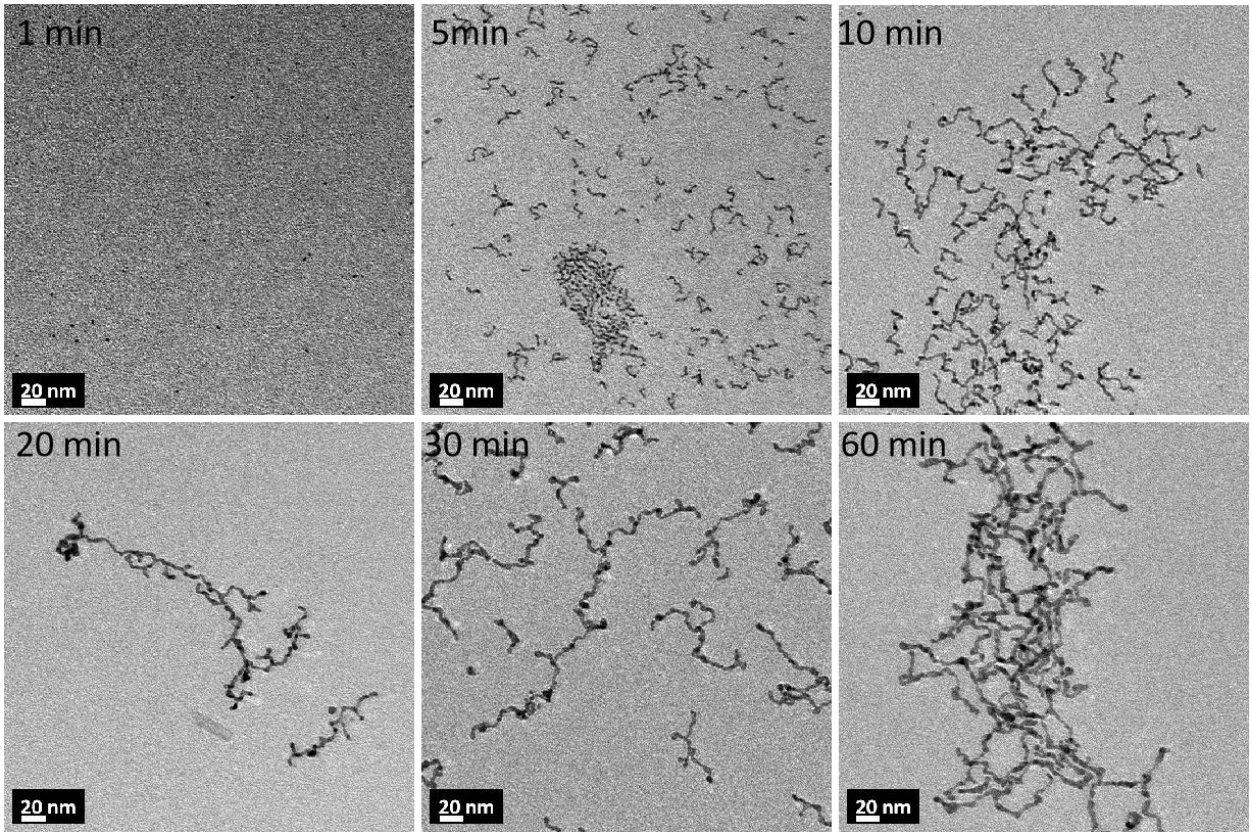

Figure 3-6. TEM pictures of reaction intermediates collected at different time intervals from 1 to 60 min.

3.3.2 Electrocatalytic ethanol oxidation reaction

We have first conducted electrochemical cyclic voltammetry (CV) to determine the $ECSA_{HUPD}$ of the Pt_3Ag wavy nanowire catalysts (Figure 3-7 (a)). In the 0.5 M H_2SO_4 electrolyte, the forward scan demonstrates the characteristic hydrogen desorption region while the reverse scan exhibits the characteristic hydrogen adsorption region. The $ECSA_{HUPD}$ was calculated to be 21.8 m^2/g by using the constant of 210 $\mu C/cm^2$ for the hydrogen monolayer. While the $ECSA_{HUPD}$ of commercial platinum carbon was calculated as 37.5 m^2/g. The regions corresponding to oxygen desorption and adsorption were very weak since it is not a highly favorable process in acidic

media compared with alkaline media.

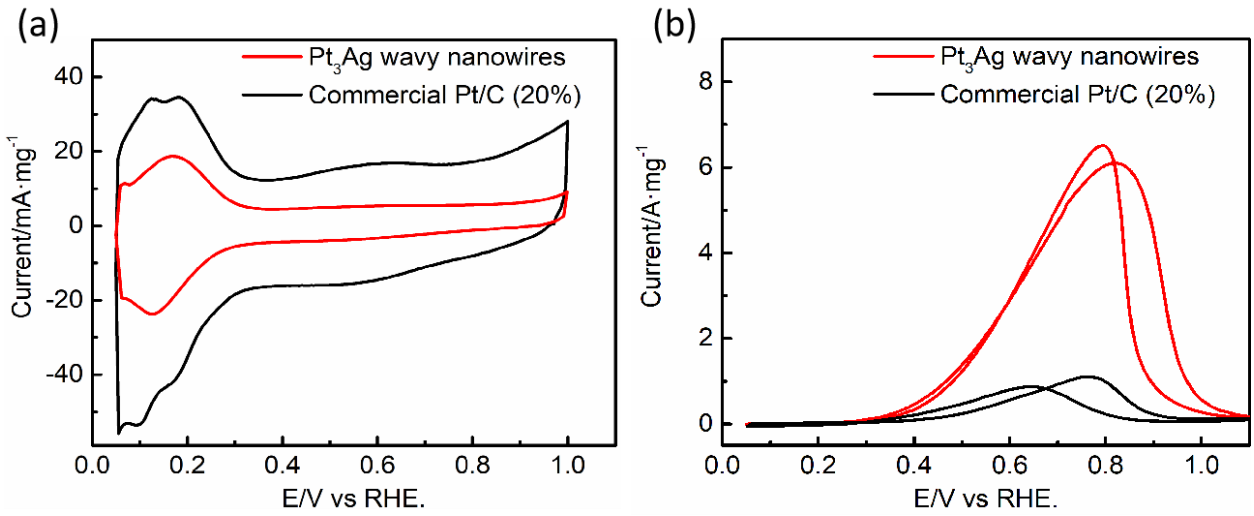

Figure 3-7. Electrochemistry study of the electrocatalysts. (a) Mass-normalized CV curves of the ultrathin wavy Pt_3Ag alloy nanowires (Pt loading: 10.7 μg/cm^2) and commercial Pt/C (Pt loading: 5.1 μg/cm^2) electrocatalysts in 0.5 M H_2SO_4 electrolyte at scan rate of 50 mV/s. (b) Corresponding mass-normalized CV curves of the ultrathin wavy Pt_3Ag alloy nanowires and commercial Pt/C electrocatalysts in 1 M KOH + 1 M EtOH electrolyte at scan rate of 50 mV/s.

The theoretical surface area ($ECSA_{GEO}$) for 1D Pt nanowires with average diameter of 4.6 nm is expected to be ~40.5 m^2/g by using the geometrical model of thin and long circular cylinder with only lateral area taken into consideration. The smaller ECSA observed in experiments might be attributed to the introduction of Ag on the surface, which is inactive towards the hydrogen underpotential deposition and may partially block the Pt sites[28].

The catalytic activity of the Pt_3Ag nanowires for EOR was carried out in the electrolyte of 1 M KOH and 1 M ethanol (Figure 3-7 (b)). The forward scan demonstrates a strong current peak at the potential of 0.81 V vs. RHE, corresponding to the oxidation of ethanol with a peak mass activity of 6.1 A/mg. This mass activity is not only 5.5-fold higher than the commercial Pt/C

(20%) (1.10 A/mg), but also higher than those of the most previously reported Pt and Pd-based electrocatalysts as shown in Figure 3-8 (a) (Single atom Ni-Pt NWs[17], Core-shell $Pt_{56}Cu_{28}Ni_{16}$ tetrahedra[35], $Pt_{75.4}Cu_{24.6}$/RGO[36], $PtPd_3$/rGO/GC[37], $Pd/Ni(OH)_2$/RGO[19] and Pd Aerogel[38]), indicating a great utilization efficiency of the noble metal. In addition, the Pt_3Ag wavy nanowire electrocatalysts also have a more negative shifted onset over-potential (defined as the over-potential required to reach a MA of 0.1 A/mg according to the previous literature[17]) at 0.30 V when compared with the commercial Pt/C (20%) at 0.41 V, suggesting our alloy nanowires also have lower activation barrier for ethanol oxidation reaction.

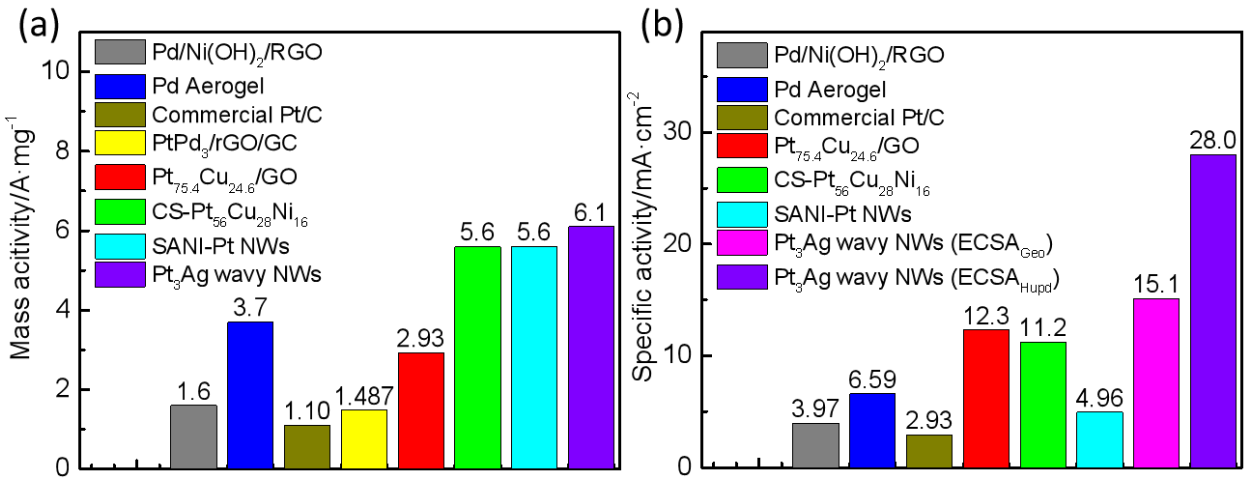

Figure 3-8. The comparisons of EOR performances of our thin Pt_3Ag alloy wavy nanowires with the previously reported Pt and Pd-based electrocatalysts tested in alkaline media in terms of: (a) Mass activity. (b) Specific activity.

The specific activity is calculated as 28.0 mA/cm^2 based on the $ECSA_{HUPD}$. Considering that the $ECSA_{HUPD}$ may be underestimated, we may recalculate the SA as 15.1 mA/cm^2 by using the geometrical surface area ($ECSA_{GEO}$ ~40.5 m^2/g), which is still much higher than most of the previous literatures as shown in Figure 3-8 (b) (Single atom Ni-Pt NWs[17], Core-shell Core-shell $Pt_{56}Cu_{28}Ni_{16}$ tetrahedra[35], $Pt_{75.4}Cu_{24.6}$/RGO[36], $Pd/Ni(OH)_2$/RGO[19] and Pd Aerogel[38]). Such high

SA might be attributed to the formation of the Pt_3Ag alloy since the introduction of silver alters the band structure of platinum and lowers the electron donation with CO and other carbonaceous species thus mitigates the binding and the poisoning effect[22], in addition to that Ag also binds very weakly towards CO. Finally, according to the recent theoretical studies, the (111) crystal plane of Pt_3Ag alloy can also help cleaving the C-C bond during ethanol oxidation reaction[24], to ensure a more efficient utilization the energy in ethanol. Therefore, we can tentatively conclude that the ultrahigh mass activity of the Pt_3Ag wavy nanowires largely arise from the ultrahigh SA since the ECSA of the wavy nanowire is moderate due to the relatively thick diameter compared with the previously reported ultrathin nanowires.

In the reverse scan, the anodic peak has a negative potential shift and slightly higher peak current compared with those in the forward scan. However, this reverse scan peak should be no longer attributed to the oxidation of the residue carbonaceous species[39, 40] after the previous forward scan and the I_F/I_R ratio should not be a criterion to evaluate the CO-tolerance ability of the electrocatalyst[41]. Instead, according to the most recent literature about Pt electrocatalyst, during the forward scan, the rate-determining-step (RDS) is the water dissociation step and after the forward scan the Pt will be oxidized at high potential, causing a change in the surface and covered with the oxygenated species. Then during the reverse scan, the RDS will be changed to the alcohol dehydrogenation step due to oxygenated Pt surface, leading to different peak potential and peak current in the reverse scan[39, 41].

For our electrocatalyst, it is noted that during the CVs in alkaline electrolyte (without ethanol), our Pt_3Ag nanowires have much less reactivity to oxygen adsorption and desorption compared with the commercial Pt/C (Figure 3-9), indicating that it is comparably less susceptible to surface oxide formation during the forward scan and more easily to recover during the backward scan. As

a result, the backward scan would be less impacted by oxygenated Pt surfaces after the forward scan. Therefore, the backward scan exhibits a more similarly high current and more similar peak position to those of the forward scan (I_F/I_R=0.94, ΔE_P=0.02 V). In comparison, commercial Pt/C has much higher tendency to form a layer of surficial oxide, as indicated by CV in alkaline media, causing the backward scan to go into the alternate pathways and a more evident change in the peak potential and peak current during the backward scan (I_F/I_R=1.26, ΔE_P=0.13 V). This similar phenomena and explanations have also been reported with PtNi electrocatalysts before[42].

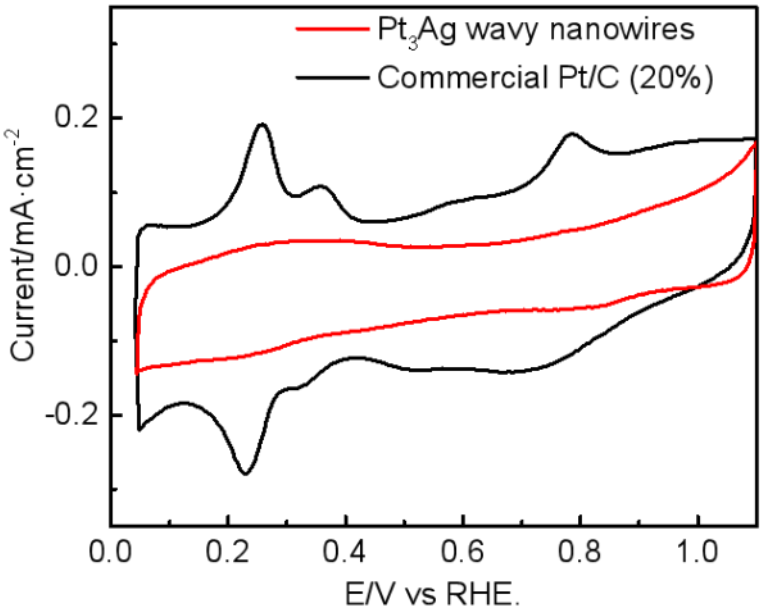

Figure 3-9. CVs of ultrathin wavy Pt_3Ag alloy nanowires (Pt loading: 10.7 μg/cm^2) and commercial Pt/C (Pt loading: 5.1 μg/cm^2) in 1 M KOH electrolyte at the scan rate of 50 mV/s.

Finally, the chronoamperometry tests (Figure 3-10 (a)) were carried out to evaluate the long-term performance of the Pt_3Ag wavy nanowire electrocatalyst. The Pt_3Ag wavy nanowire can maintain a current of 152 mA/mg at 0.72 V vs. RHE after 6000 s. In sharp contrast, the commercial Pt/C only maintain a mass activity of 16.2 mA/mg at 0.72 V vs. RHE after 6000 s, indicating that Pt_3Ag nanowires has much improved long term performance when compared with

the commercial Pt/C, demonstrating our Pt_3Ag nanowires have much higher stability apart from much higher mass activity, which mainly attributes from the introduction of Ag to enrich the electron density to weaken the chemisorption of the carbonaceous species[22, 43] and the relatively higher stability of the 1D nanowires under harsh electrochemical conditions compared with its 0D counterparts[25]. Meanwhile, we also find that the catalytic activity can be generally recovered after 25 cycles of CV scanning after each CA test. For example, after 10 rounds of repeated CA tests, the nanowires still maintain a high mass activity of 112 mA/mg (Figure 3-10 (b)).

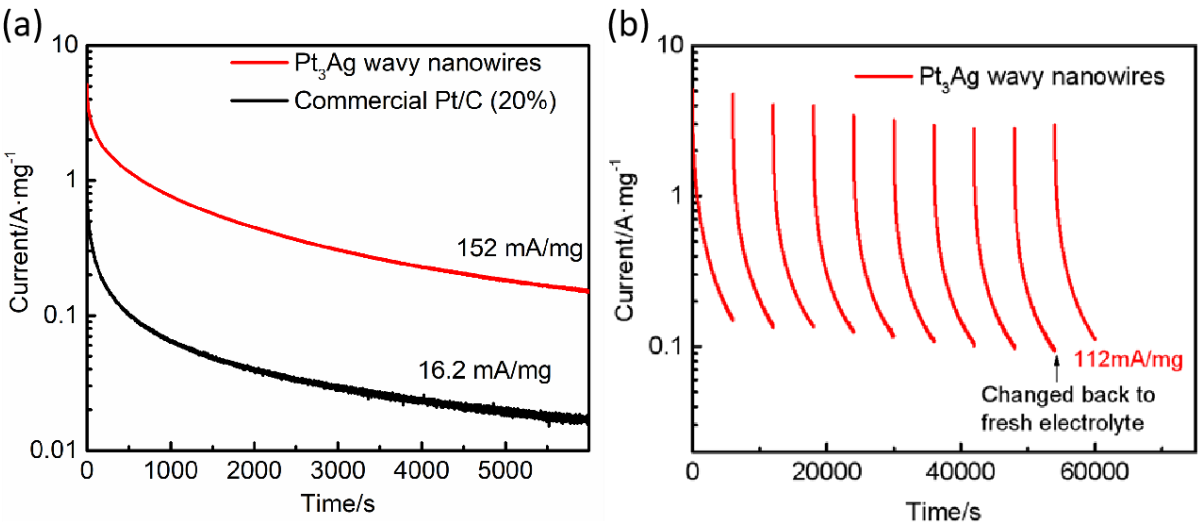

Figure 3-10. Long-term EOR performances of the electrocatalysts. (a) Chronoamperometry results of the ultrathin wavy Pt_3Ag alloy nanowires (Pt loading: 10.7 μg/cm^2) and commercial Pt/C (Pt loading: 10.2 μg/cm^2) electrocatalysts in 1 M KOH + 1 M EtOH electrolyte at 0.72 V vs. RHE. (b) 10 consecutive cycles of chronoamperometry tests of Pt_3Ag wavy nanowires with 25 cycles of CV scanning (50 mV/s) between each two CA tests in the electrolyte of 1 M KOH+ 1 M EtOH. (Electrolyte changed back to the freshly prepared after the 9th cycle).

3.4 Conclusion

In summary, we have successfully synthesized Pt_3Ag wavy nanowires via a particle attachment

mechanism in a facile solvothermal process. The resulting Pt_3Ag wavy nanowires can function as highly effective EOR electrocatalysts with an extraordinary specific activity of 28.0 mA/cm^2 and an ultrahigh mass activity of 6.1 A/mg, considerably higher than most of the previously reported Pt and Pd-based electrocatalysts in alkaline media, which is largely attributed to the formation of Pt-Ag alloy and electron transfer from Ag to Pt. Furthermore, the Pt_3Ag wavy nanowires also show significantly improved stability, and thus can promise a highly effective electrocatalyst for EOR.

3.5 Reference

1. Joghee, P.; Malik, J. N.; Pylypenko, S.; O'Hayre, R., A review on direct methanol fuel cells–In the perspective of energy and sustainability. *MRS Energy Sustain* **2015,** *2*.

2. Antolini, E.; Gonzalez, E. R., Alkaline direct alcohol fuel cells. *J. Power Sources* **2010,** *195* (11), 3431-3450.

3. Yuan, Y.; Wang, J.; Adimi, S.; Shen, H.; Thomas, T.; Ma, R.; Attfield, J. P.; Yang, M., Zirconium nitride catalysts surpass platinum for oxygen reduction. *Nat. Mater.* **2019**, 1-5.

4. Wan, C.; Duan, X.; Huang, Y., Molecular Design of Single-Atom Catalysts for Oxygen Reduction Reaction. *Adv. Energy Mater.* **2020,** *10* (14), 19.

5. Wang, Y.; Li, J.; Wei, Z. D., Transition-metal-oxide-based catalysts for the oxygen reduction reaction. *J. Mater. Chem. A* **2018,** *6* (18), 8194-8209.

6. Wang, D.-W.; Su, D., Heterogeneous nanocarbon materials for oxygen reduction reaction. *Energy Environ. Sci.* **2014,** *7* (2), 576-591.

7. Weng, M. M.; Liu, D. J.; He, X. Q.; Asefa, T., Fe3C nanoparticles-loaded 3D nanoporous N-doped carbon: A highly efficient electrocatalyst for oxygen reduction in alkaline media. *Int. J. Hydrogen Energy* **2019,** *44* (39), 21506-21517.

8. Yu, E. H.; Krewer, U.; Scott, K., Principles and materials aspects of direct alkaline alcohol fuel cells. *Energies* **2010,** *3* (8), 1499-1528.

9. Cifrain, M.; Kordesch, K., Advances, aging mechanism and lifetime in AFCs with circulating electrolytes. *J. Power Sources* **2004,** *127* (1-2), 234-242.

10. Wang, Y.; Li, L.; Hu, L.; Zhuang, L.; Lu, J.; Xu, B., A feasibility analysis for alkaline membrane direct methanol fuel cell: thermodynamic disadvantages versus kinetic advantages. *Electrochem. Commun.* **2003,** *5* (8), 662-666.

11. Zhang, B. W.; Yang, H. L.; Wang, Y. X.; Dou, S. X.; Liu, H. K., A Comprehensive Review on Controlling Surface Composition of Pt-Based Bimetallic Electrocatalysts. *Adv. Energy Mater.* **2018,** *8* (20), 1703597.

12. Zhang, L.; Chang, Q.; Chen, H.; Shao, M., Recent advances in palladium-based electrocatalysts for fuel cell reactions and hydrogen evolution reaction. *Nano Energy* **2016,** *29*, 198-219.

13. Zhao, S.; Yin, H.; Du, L.; Yin, G.; Tang, Z.; Liu, S., Three dimensional N-doped graphene/PtRu nanoparticle hybrids as high performance anode for direct methanol fuel cells. *J. Mater. Chem. A* **2014,** *2* (11), 3719-3724.

14. Lu, S.; Eid, K.; Ge, D.; Guo, J.; Wang, L.; Wang, H.; Gu, H., One-pot synthesis of PtRu nanodendrites as efficient catalysts for methanol oxidation reaction. *Nanoscale* **2017,** *9* (3), 1033-1039.

15. Xu, C. X.; Wang, L.; Mu, X. L.; Ding, Y., Nanoporous PtRu Alloys for Electrocatalysis. *Langmuir* **2010,** *26* (10), 7437-7443.

16. Jiang, Q.; Jiang, L.; Wang, S.; Qi, J.; Sun, G., A highly active PtNi/C electrocatalyst for methanol electro-oxidation in alkaline media. *Catal. Commun.* **2010,** *12* (1), 67-70.

17. Li, M.; Duanmu, K.; Wan, C. Z.; Cheng, T.; Zhang, L.; Dai, S.; Chen, W.; Zhao, Z.; Li, P.; Fei, H.; Zhu, Y.; Yu, R.; Luo; Zang, K.; Lin, Z.; Ding, M.; Huang, J.; Sun, H.; Guo, J.; Pan, X.; Goddard, W. A.; Sautet, P.; Huang, Y.; Duan, X., Single-atom tailoring of platinum nanocatalysts for high-performance multifunctional electrocatalysis. *Nat. Catalysis* **2019,** *2* (6), 495-503.

18. Huang, W.; Wang, H.; Zhou, J.; Wang, J.; Duchesne, P. N.; Muir, D.; Zhang, P.; Han, N.; Zhao, F.; Zeng, M., Highly active and durable methanol oxidation electrocatalyst based on the synergy of platinum–nickel hydroxide–graphene. *Nat. Commun.* **2015,** *6*.

19. Huang, W.; Ma, X. Y.; Wang, H.; Feng, R.; Zhou, J.; Duchesne, P. N.; Zhang, P.; Chen, F.; Han, N.; Zhao, F.; Zhou, J.; Cai, W. B.; Li, Y., Promoting effect of Ni (OH) 2 on palladium nanocrystals leads to greatly improved operation durability for electrocatalytic ethanol oxidation in alkaline solution. *Adv. Mater.* **2017,** *29* (37), 1703057.

20. Zhao, X.; Zhang, H. T.; Yan, Y.; Cao, J. H.; Li, X. Q.; Zhou, S. M.; Peng, Z. M.; Zeng, J., Engineering the Electrical Conductivity of Lamellar Silver-Doped Cobalt(II) Selenide Nanobelts for Enhanced Oxygen Evolution. *Angew. Chem.-Int. Edit.* **2017,** *56* (1), 328-332.

21. Kuhl, K. P.; Hatsukade, T.; Cave, E. R.; Abram, D. N.; Kibsgaard, J.; Jaramillo, T. F., Electrocatalytic conversion of carbon dioxide to methane and methanol on transition metal surfaces. *J. Am. Chem. Soc.* **2014,** *136* (40), 14107-14113.

22. Shang, C.; Guo, Y.; Wang, E., Integration of two-dimensional morphology and porous surfaces to boost methanol electrooxidation performances of PtAg alloy nanomaterials. *Nano Res.* **2018,** *11* (12), 6375-6383.

23. Yang, J.; Ying, J. Y., Nanocomposites of Ag2S and Noble Metals. *Angew. Chem.-Int. Edit.* **2011,** *50* (20), 4637-4643.

24. Monyoncho, E. A.; Steinmann, S. N.; Sautet, P.; Baranova, E. A.; Michel, C., Computational screening for selective catalysts: Cleaving the CC bond during ethanol electro-oxidation reaction. *Electrochim. Acta* **2018,** *274*, 274-278.

25. Li, M.; Zhao, Z.; Cheng, T.; Fortunelli, A.; Chen, C.-Y.; Yu, R.; Zhang, Q.; Gu, L.; Merinov, B. V.; Lin, Z., Ultrafine jagged platinum nanowires enable ultrahigh mass activity for the oxygen reduction reaction. *Science* **2016,** *354* (6318), 1414-1419.

26. Huang, X.; Zhao, Z.; Chen, Y.; Chiu, C.-Y.; Ruan, L.; Liu, Y.; Li, M.; Duan, X.; Huang, Y., High density catalytic hot spots in ultrafine wavy nanowires. *Nano Lett.* **2014,** *14* (7), 3887-3894.

27. Fu, X.; Zhao, Z.; Wan, C.; Wang, Y.; Fan, Z.; Song, F.; Cao, B.; Li, M.; Xue, W.; Huang, Y.; Duan, X., Ultrathin wavy Rh nanowires as highly effective electrocatalysts for methanol oxidation reaction with ultrahigh ECSA. *Nano Res.* **2019,** *12* (1), 211-215.

28. Jiang, X.; Fu, G. T.; Wu, X.; Liu, Y.; Zhang, M. Y.; Sun, D. M.; Xu, L.; Tang, Y. W., Ultrathin AgPt alloy nanowires as a high-performance electrocatalyst for formic acid oxidation. *Nano Res.* **2018,** *11* (1), 499-510.

29. Jiang, X.; Liu, Y.; Wang, J. X.; Wang, Y. F.; Xiong, Y. X.; Liu, Q.; Li, N. X.; Zhou, J. C.; Fu, G. T.; Sun, D. M.; Tang, Y. W., 1-Naphthol induced Pt3Ag nanocorals as

bifunctional cathode and anode catalysts of direct formic acid fuel cells. *Nano Res.* **2019,** *12* (2), 323-329.

30. Khoa, N. T.; Van Thuan, D.; Kim, S. W.; Park, S.; Van Tam, T.; Choi, W. M.; Cho, S.; Kim, E. J.; Hahn, S. H., Facile fabrication of thermally reduced graphene oxide–platinum nanohybrids and their application in catalytic reduction and dye-sensitized solar cells. *RSC Advances* **2016,** *6* (2), 1535-1541.

31. Liu, H.; Ye, F.; Yao, Q. F.; Cao, H. B.; Xie, J. P.; Lee, J. Y.; Yang, J., Stellated Ag-Pt bimetallic nanoparticles: An effective platform for catalytic activity tuning. *Sci. Rep.* **2014,** *4*, 7.

32. Mao, H. B.; Feng, J. Y.; Ma, X.; Wu, C.; Zhao, X. J., One-dimensional silver nanowires synthesized by self-seeding polyol process. *J. Nanopart. Res.* **2012,** *14* (6), 15.

33. Dasdelen, Z.; Yildiz, Y.; Eris, S.; Sen, F., Enhanced electrocatalytic activity and durability of Pt nanoparticles decorated on GO-PVP hybride material for methanol oxidation reaction. *Appl. Catal. B-Environ.* **2017,** *219*, 511-516.

34. Wang, W.; Wang, Z. Y.; Yang, M. M.; Zhong, C. J.; Liu, C. J., Highly active and stable Pt (111) catalysts synthesized by peptide assisted room temperature electron reduction for oxygen reduction reaction. *Nano Energy* **2016,** *25*, 26-33.

35. Huang, J.; Liu, Y.; Xu, M.; Wan, C.; Liu, H.; Li, M.; Huang, Z.; Duan, X.; Pan, X.; Huang, Y., PtCuNi Tetrahedra Catalysts with Tailored Surfaces for Efficient Alcohol Oxidation. *Nano Lett.* **2019,** *19* (8), 5431-5436.

36. Liu, T.; Li, C.; Yuan, Q., Facile synthesis of PtCu alloy/graphene oxide hybrids as improved electrocatalysts for alkaline fuel cells. *ACS Omega* **2018,** *3* (8), 8724-8732.

37. Ren, F. F.; Wang, H. W.; Zhai, C. Y.; Zhu, M. S.; Yue, R. R.; Du, Y. K.; Yang, P.; Xu, J. K.; Lu, W. S., Clean Method for the Synthesis of Reduced Graphene Oxide-Supported PtPd Alloys with High Electrocatalytic Activity for Ethanol Oxidation in Alkaline Medium. *ACS Appl. Mater. Interfaces* **2014,** *6* (5), 3607-3614.

38. Yazdan-Abad, M. Z.; Noroozifar, M.; Alam, A. R. M.; Saravani, H., Palladium aerogel as a high-performance electrocatalyst for ethanol electro-oxidation in alkaline media. *J. Mater. Chem. A* **2017,** *5* (21), 10244-10249.

39. Chung, D. Y.; Lee, K.-J.; Sung, Y.-E., Methanol electro-oxidation on the Pt surface: revisiting the cyclic voltammetry interpretation. *J. Phys. Chem. C* **2016,** *120* (17), 9028-9035.

40. Zhao, Y.; Li, X.; Schechter, J. M.; Yang, Y., Revisiting the oxidation peak in the cathodic scan of the cyclic voltammogram of alcohol oxidation on noble metal electrodes. *RSC Adv.* **2016,** *6* (7), 5384-5390.

41. Hofstead-Duffy, A. M.; Chen, D.-J.; Sun, S.-G.; Tong, Y. J., Origin of the current peak of negative scan in the cyclic voltammetry of methanol electro-oxidation on Pt-based electrocatalysts: a revisit to the current ratio criterion. *J. Mater. Chem.* **2012,** *22* (11), 5205-5208.

42. Sulaiman, J. E.; Zhu, S.; Xing, Z.; Chang, Q.; Shao, M., Pt–Ni octahedra as electrocatalysts for the ethanol electro-oxidation reaction. *ACS Catal.* **2017,** *7* (8), 5134-5141.

43. Zhang, Y. P.; Gao, F.; Song, P. P.; Wang, J.; Guo, J.; Shiraish, Y.; Du, Y. K., Glycine-Assisted Fabrication of N-Doped Graphene-Supported Uniform Multipetal PtAg Nanoflowers for Enhanced Ethanol and Ethylene Glycol Oxidation. *Acs Sustainable Chemistry & Engineering* **2019,** *7* (3), 3176-3184.

Chapter 4. Medium entropy Au-doped PtAgRhCu alloy wavy nanowire as highly effective and durable electrocatalysts for AOR

4.1 Introduction

Compared with compressed hydrogen (@1000 psi, 25^{o}C), alcohols (*e.g.* methanol and ethanol) have over 1-magnitude higher volumetric energy density and over 5-time higher gravimetric energy density (by considering the weight of the hydrogen storage system)[1]. In addition, the storage and transportation have lower cost and higher safety, making them potential candidate fuels for fuel cell applications[1]. The alkaline direct alcohol fuel cell (ADAFC) has also drawn research attention[2]. The alkaline media reverses the direction of the electro-osmotic force and thus helps lower the alcohol crossover from anode compartment to the cathode compartment, leading to less cathode electrocatalyst poisoning by the alcohol and improved efficiency[2, 3]. In addition, the alkaline media also makes many low-cost non noble metal-based cathode oxygen reduction reaction (ORR) electrocatalysts possible and applicable, including ZrN[4], single atom catalysts[5], transition metal oxides[6] and carbon-based nanomaterials[7] to reduce the expense of the fuel cells[8]. However, the alcohol oxidation reaction (AOR) has more sluggish kinetics compared with the hydrogen oxidation reaction (HOR)[1], and normally requires noble metal-based electrocatalysts that are limited by the high cost. Therefore, developing noble metal based electrocatalysts with high mass activity (MA) and good stability is vital for developing cost-effective and durable direct alcohol fuel cells.

Alloying has been a very common strategy in electrocatalyst design to enhance the specific activity (SA) for AOR[9, 10]: Oxophilic metal (*e.g.* Ru[11-13], Ni[14]) can be employed to facilitate the formation of surficial -OH group to benefit the removal of the carbonaceous species, such as CO, on the nearby noble metal sites via the Langmuir-Hinshelwood (L-H) mechanism through

bifunctional effect. Alloying with different metals also leads to ligand effect and strain effect that can tune electronic structure and d-band center, and thus affect and may improve the interactions with different reaction intermediates and adsorbates to potentially enhance the performance[15, 16]. Recently, high entropy alloy and medium entropy alloy nanomaterials have also attracted tremendous research interests as electrocatalyst, since the uniform mixing of the metal atoms can increase the entropy of the system and enhancing the energy barrier for the migration of the atoms[17, 18], which may benefit the stability of the electrocatalyst[19]. In addition, the alloy nanomaterials of various metals may have some unprecedented synergistic effect (cocktail effect) to enhance the SA[17, 18].

Therefore, we decided to design an alloy system with Pt, Rh, Au (doping level), Ag and Cu with medium mixing entropy (~1.45 R), which is close to the entropy level of the high entropy alloy (1.5 R) defined by the previous literatures[17, 18, 20]. Rh, due to its oxophilicity, can facilitate the hydroxyl group formation to facilitate the removal of CO adsorbed onto the nearby sites to benefit AOR via the bifunctional effect[21, 22]. In addition, Rh has also been reported to benefit the C-C bond cleavage to enhance the faradaic efficiency for ethanol oxidation reaction (EOR)[23-25] in both acidic and alkaline media. Au is also reported to benefit the EOR since the higher atomic radius can induce tensile strain to the lattice and the electrocatalyst surface to facilitate the ethanol oxidation by facilitating the adsorption of C1 species and hydroxyl group[26]. While the Ag and Cu are considered to be beneficial because the binding with the carbonaceous species can be weakened[27-30], and their high conductivity may benefit electrocatalysis as well[31]. In addition to the ligand effect, strain effect and bifunctional effect brought by these elements, the unprecedented synergistic effect (cocktail effect) and the sluggish diffusion effect may potentially enhance the SA as well as the stability of the electrocatalyst[17-19].

Ultrathin wavy nanowire is an attractive morphology for electrocatalysts since the ultrathin diameter represents high specific surface area, thus contributing to high electrochemical surface area (ECSA), an equally important factor to enhance MA. The surface defects on the wavy nanowire can contribute to catalytic sites for further enhanced performances[32, 33] and the one-dimensional nanostructure can be helpful for charge transport, which also benefits electrocatalysis[34].

Herein, we report the medium entropy Au-doped PtAgRhCu alloy wavy nanowire with an average diameter of 3.7±1.0 nm via a facile polyol process and can work as a highly effective electrocatalysts for EOR, with ultrahigh MA of 8.43±0.40 $A/mg_{noble\ metal}$ and SA of 22.1±2.3 mA/cm^2 as well as good long-term performance. In addition, good long-term performance for MOR was also achieved, demonstrating great potential when further applied for ADAFCs.

4.2 Experimental

4.2.1 Chemicals

Potassium tetrachloroplatinate (IV) (K_2PtCl_4, 98 %), silver nitrate ($AgNO_3$, >99.0 %, ACS reagent), sodium hexachlororhodate (III) (Na_3RhCl_6, analytical grade), copper sulfate pentahydrate ($CuSO_4 \cdot 5H_2O$, >98 %, ACS reagent), gold (III) chloride trihydrate ($AuCl_3 \cdot 3H_2O$, >99.9% trace metals basis), polyvinylpyrrolidone (PVP, MW. ~55000) and commercial Pt on graphitized carbon (Pt/GC, 20%) were purchased from Sigma Aldrich and the chemicals were used as received without any further purification.

4.2.2 Synthesis of Au-doped PtAgRhCu alloy wavy nanowires

160 mg PVP were dissolved into 4.0 mL of EG after ultrasonication and then the aqueous solution of 0.018 mmol K_2PtCl_4, 0.018 mmol $AgNO_3$, 0.018 mmol Na_3RhCl_6, 0.018 mmol $CuSO_4 \cdot 5H_2O$, 0.0020 mmol $AuCl_3 \cdot 3H_2O$ were added in turn. The vial was then heated at 210 ^oC

for 8h. The products were collected via centrifugation after the addition of acetone and then washed with water for 2 times and ethanol for 2 times and finally dispersed in ethanol.

4.2.3 Structural characterizations

The X-ray diffraction (XRD) was tested on a Panalytical X'Pert Pro X-ray Powder Diffractometer with Cu-Kα radiation with a scan rate of 0.01°/s. The X-ray photoelectron spectroscopy (XPS) was tested on Kratos AXIS Ultra DLD spectrometer, and the samples were prepared by drop casting the ethanol dispersion of the nanowires onto the Si substrate and dried. The transmission electron microscopy (TEM) images were taken on FEI T12 transmission electron microscope at 120 kV with Cu grids as the substrate. The scanning transmission electron microscope (STEM) images and energy dispersive X-ray spectroscopy (EDX) mapping were tested on Joel Jem-300CF (Grand Arm) at 300 kV with Al grids. The noble metal (*e.g.* Pt, Rh, Au) loading and elemental ratio of the nanowires on the electrode were determined from inductively coupled plasma-atomic emission spectroscopy (ICP-AES).

4.2.4 Electrochemical measurements

The electrochemical studies were carried out via three-electrode test system with glassy carbon electrode (GCE) with a geometry area of 0.196 cm^2, Pt coil as counter electrode and Hg/HgO (1.0 M KOH) as the reference electrode for electrochemical test in alkaline media; and graphite rod as counter electrode and Ag/AgCl as the reference electrode in acidic media. The electrocatalysts were homogeneously dispersed in ethanol and 10.0 μL of the ink was drop-cast onto the surface of the electrode surface and dried at room temperature. The noble metal (*e.g.* Pt, Rh, Au) loading of the nanowires on the electrode is determined from ICP-AES, and the loading is ranging in 1.00-1.50 μg (5.10-7.65 μg/cm^2).

Cyclic voltammetry (CV) tests were performed at first in Ar-saturated 0.1 M $HClO_4$ electrolyte

with a scan rate of 50 mV/s ranging from 0.05 V to 1.00 V vs. RHE for electrocatalysts activation and ECSA measurement by integrating hydrogen desorption charge using the constant of 210 μC/cm^2. The electrocatalytic ethanol oxidation reaction (EOR) and methanol oxidation (MOR) were tested via cyclic voltammetry in Ar-saturated 1.0 M KOH + 1.0 M EtOH and 1.0 M KOH + 1.0 M MeOH electrolyte, respectively, at a scan rate of 50 mV/s from 0.05 V to 1.10 V vs. RHE. The chronoamperometry (CA) was tested at 0.67 V vs. RHE for 1h. The commercial Pt/GC (20%) was used as control sample and the catalyst ink was 1.00 mg/mL commercial Pt/GC (20%) with ethanol: Nafion (5 wt%) = 99:1 as the ink solvent. And 10.0 μL of the Pt/C catalyst ink was drop-cast onto the GCE and dried to ensure a platinum loading of 2.00 μg (10.2 μg/cm^2) on the working electrode.

4.3 Results and discussion

4.3.1 Characterization

As shown in Figure 4-1, TEM study reveals the wavy nanowire morphology with diameter mostly ranging in 2.0-5.5 nm and the average diameter is 3.7±1.0 nm, which implies high specific surface area leading to high ECSA. The wavy surface with rich defects may contribute the catalytic sites as a typical characteristic of the wavy nanowire morphology. In Figure 4-2, XRD also demonstrates a single phase of FCC crystal lattice with the peaks corresponding to the (111), (200), (220) and (311) crystal planes positioned amid those corresponding peaks of the FCC Pt (JCPDS No. 04-0802), Ag (JCPDS No. 04-0783), Rh (JCPDS No. 05-0685), Cu (JCPDS No. 04-0836) and Au (JCPDS No. 01-1172) without the existence of any other distinct phase. EDX mapping also shows the uniform distribution of the Pt, Ag, Rh, Cu and Au elements, proving the formation of the medium entropy Au-doped PtAgRhCu alloy (Figure 4-3). ICP-AES also demonstrates an average elemental composition of Pt: Ag: Rh: Cu: Au =1.00: 1.09: 0.97:

0.71: 0.085, which generally agrees with the feed ratio of the precursors. XPS also demonstrates the presence of the Pt, Ag, Rh, Cu, Au elements with the peaks at 71.0 eV (Pt $4f_{7/2}$), 367.9 eV (Ag $3d_{5/2}$), 307.2 eV (Rh $3d_{5/2}$), 932.1 eV (Cu $2p_{5/2}$) and 84.0 eV (Au $4f_{7/2}$), respectively. The negatively shifted binding energies of Pt $4f_{7/2}$ (shifted from ~71.3 eV for commercial Pt/carbon black[28] to 71.0 eV), Rh $3d_{5/2}$ (shifted from ~307.35 eV for Rh wavy nanowire[32, 33] to 307.2 eV) and Au $4f_{7/2}$ (shifted from ~84.3 eV for Au nanowire[35] to 84.0 eV) (EN: 2.54) can be attributed to the electron transfer to them due to their relatively higher electronegativity (Pt: 2.28, Rh: 2.28, Au: 2.54). In contrast, the positively shifted binding energies of Ag $3d_{5/2}$ (from 367.4 eV for Ag nanowire[36] to 367.9 eV) and Cu $2p_{3/2}$ (from 932.7 eV for Cu nanowire[37] to 932.1 eV) can be explained as the electron transfer from them due to their comparably lower electronegativity (Ag: 1.93, Cu: 1.90). Overall, the electron transfer from Ag and Cu to Pt, Rh and Au was demonstrated, and the adjusted electronic structure may be beneficiary to the AOR performance by weakening the binding of the carbonaceous species[28, 30]. In addition, the PtAgRh and PtAgRhCu alloy wavy nanowires were also synthesized with similar nanowire morphology (Figure 4-5), and the introduction of Cu can also lower the average diameter of the nanowire based on the statistical analysis of over 270 measurements, contributing to improved specific surface area and potentially increased ECSA.

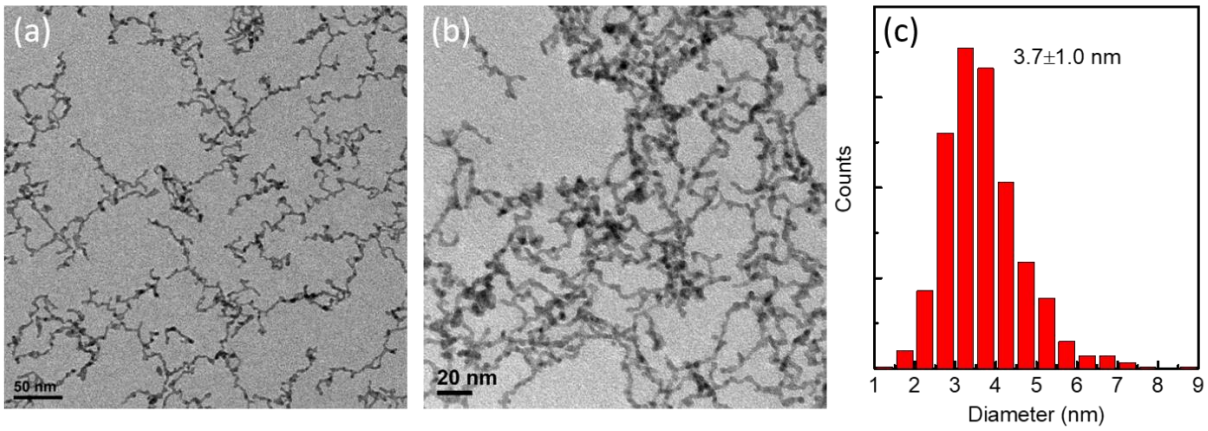

Figure 4-1. (a), (b) TEM pictures of medium entropy Au-doped PtAgRhCu alloy wavy nanowires. (c) Distribution of the diameter of the nanowire obtained from (a).

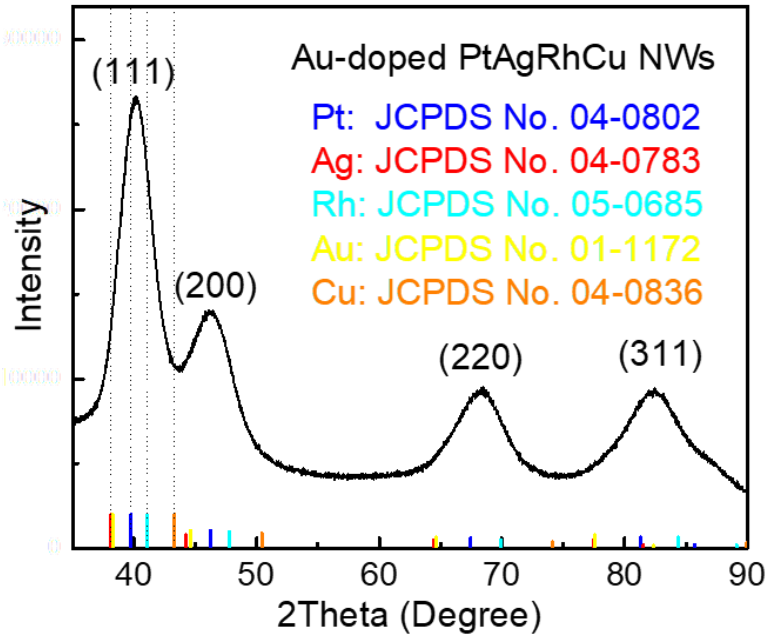

Figure 4-2. XRD pattern of medium entropy Au-doped PtAgRhCu alloy wavy nanowires.

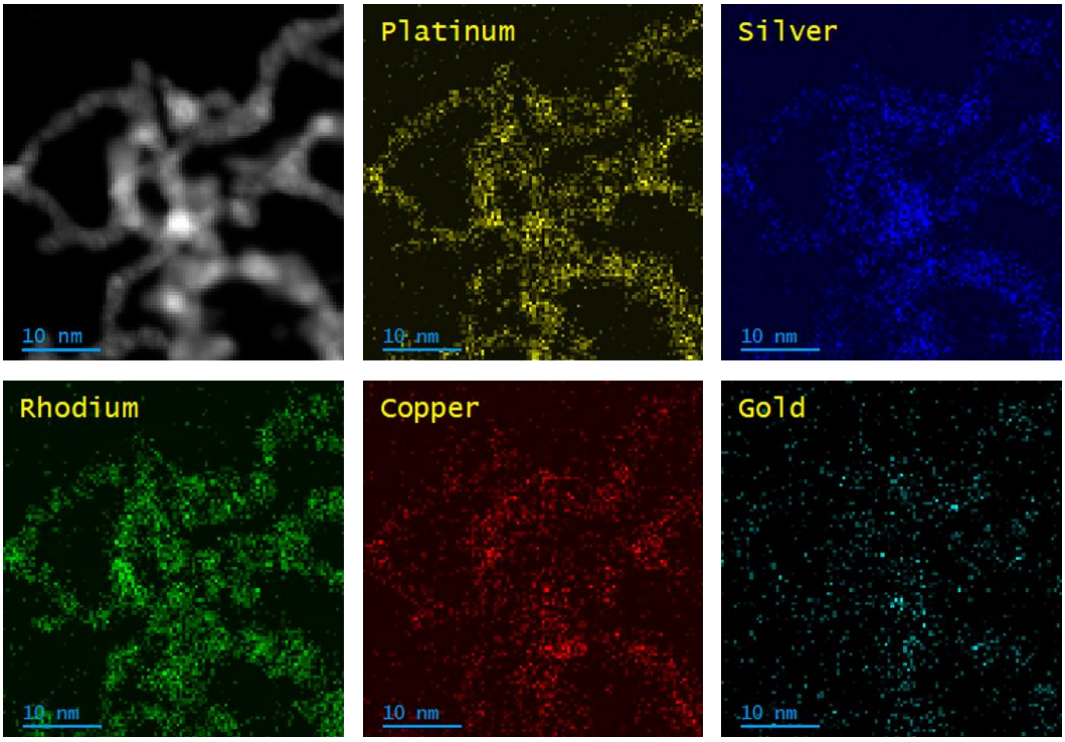

Figure 4-3. EDX mapping medium entropy Au-doped PtAgRhCu alloy wavy nanowires.

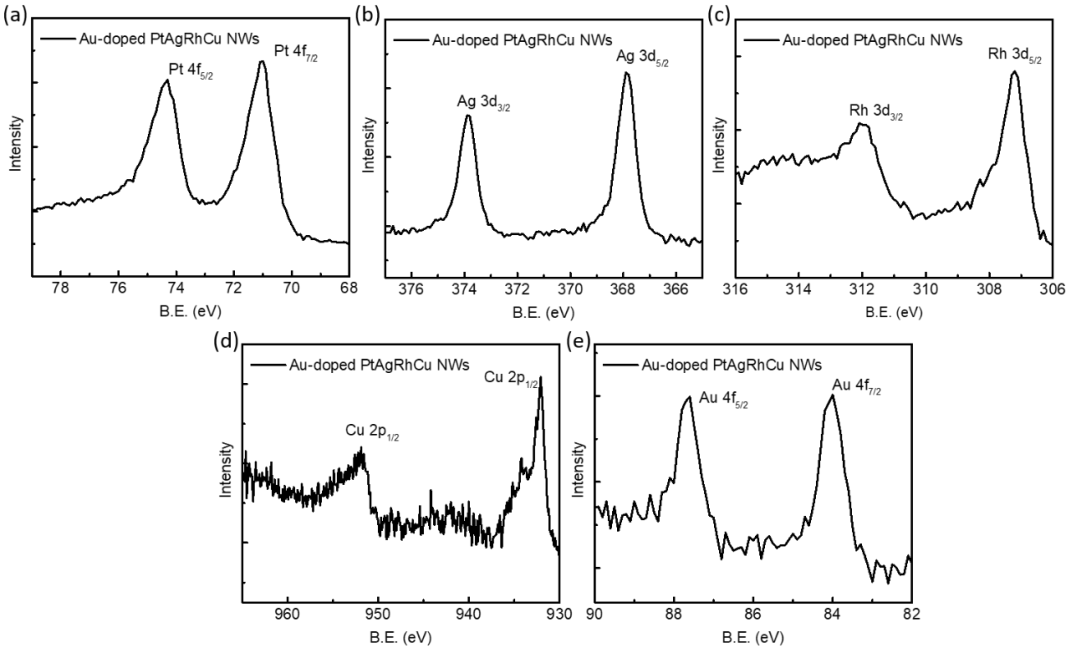

Figure 4-4. XPS characterization of medium entropy Au-doped PtAgRhCu alloy wavy nanowire.

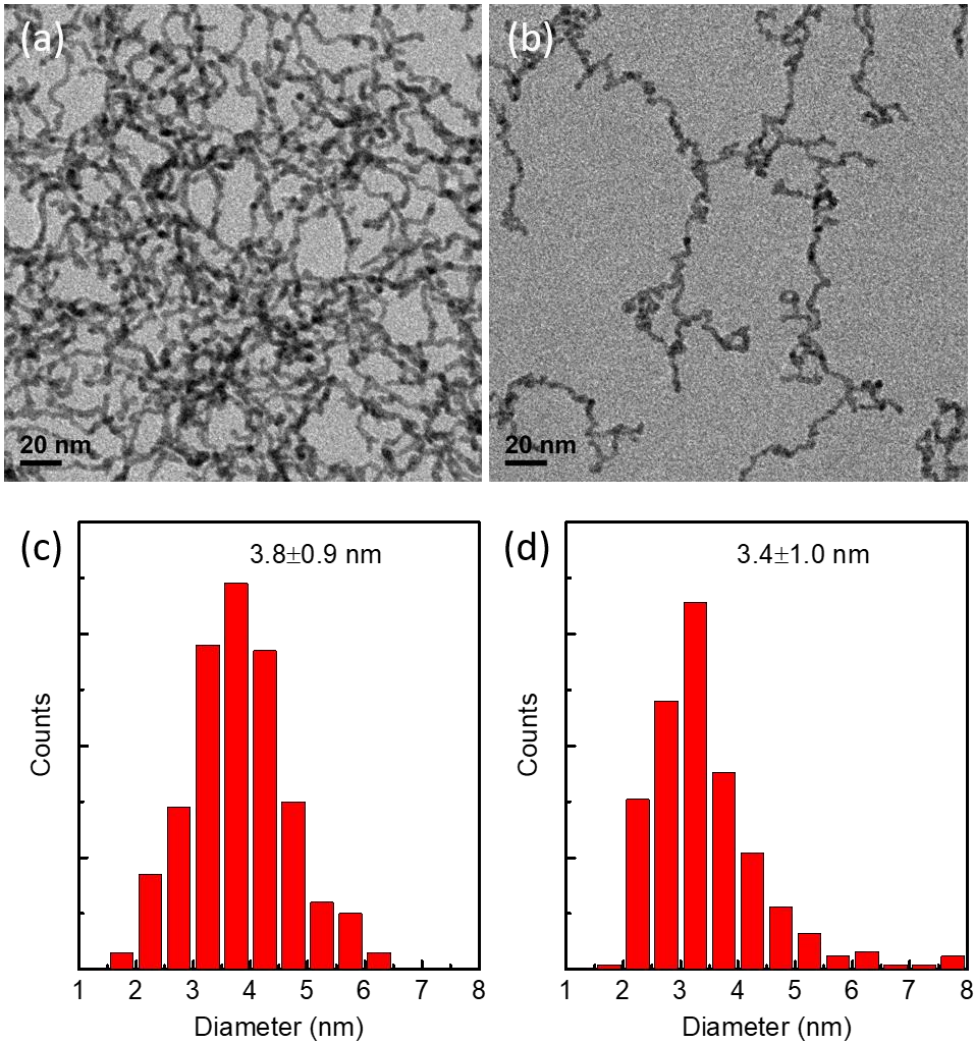

Figure 4-5. TEM pictures of (a) PtAgRh and (b) PtAgRuCu wavy nanowires. Distribution of the diameter of (c) PtAgRh and (d) PtAgRuCu wavy nanowires.

4.3.2 Electrochemical study

The ECSA of the wavy nanowires were determined from the HUPD measurement in 0.1 M $HClO_4$ (Figure 4-6 (a)), and the ECSA of PtAgRh wavy nanowire, PtAgRhCu wavy nanowire and medium entropy Au-doped PtAgRuCu alloy wavy nanowire are 37.0±2.4 $m^2/g_{noble\ metal}$, 41.7±0.9 $m^2/g_{noble\ metal}$ and 38.0±2.1 $m^2/g_{noble\ metal}$, respectively. These wavy nanowires are

demonstrating similar ECSA value largely because they have very similar morphology. Meanwhile the commercial Pt/GC have higher ECSA value of 50.2±1.2 m^2/g.

The EOR performances of the electrocatalysts were studied in 1.0 M KOH + 1.0 M EtOH via CV at a scan rate of 50 mV/s (Figure 4-6 (b)). As shown in the summary Figure 4-6 (c), The medium entropy Au-doped PtAgRhCu alloy wavy nanowire demonstrates the optimized EOR performances with ultrahigh MA of 8.43±0.40 $A/mg_{noble\ metal}$ and SA of 22.1±2.3 mA/cm^2, which is much higher than those of the PtAgRh nanowire and PtAgRhCu nanowire. The Rh can serve as the oxophilic component to facilitate the hydroxyl group adsorption and assist the removal of the carbonaceous species via the L-H mechanism[21, 22] as well as potentially facilitating C1 pathway[23, 24]. The introduction of Cu can also slightly improve the ECSA of the wavy nanowire by slightly lowering the diameter of the nanowire. In addition, Cu may serve as similar role as Ag to weaken the binding of CO and increase the entropy of the system at the same time[27, 38]. The Au doping can also induce tensile strain effect to the nanowire surface, which can also contribute to the oxidation of ethanol and facilitate the hydroxyl group adsorption[26] and there may also be some unexpected synergy (so called "cocktail effect")[18]. In addition, the MA and SA of the Au-doped PtAgRhCu alloy wavy nanowire are also nearly 6-time and 8-time improvements compared with the commercial Pt/GC (MA of 1.46±0.12 A/mg and SA of 2.88±0.27 mA/cm^2), respectively.

The CA tests were employed to study the long-term performances of the electrocatalysts. And significantly, the medium entropy Au-doped PtAgRhCu alloy wavy nanowire also demonstrates good long-term performances, maintaining a current of 674 mA/mg after 1h at 0.67 V vs. RHE, which is nearly 30 times higher compared with the commercial Pt/GC (22.9 mA/mg). Apart from the benefits regarding the ligand effects, bifunctional effects and strain effects from the introduction of Ag, Rh, Cu and Au elements to alleviate the poisoning of carbonaceous species,

this great improvement may also be attributed to the sluggish diffusion effect[18, 19] and thus can greatly improve the long-term performance of the electrocatalysts.

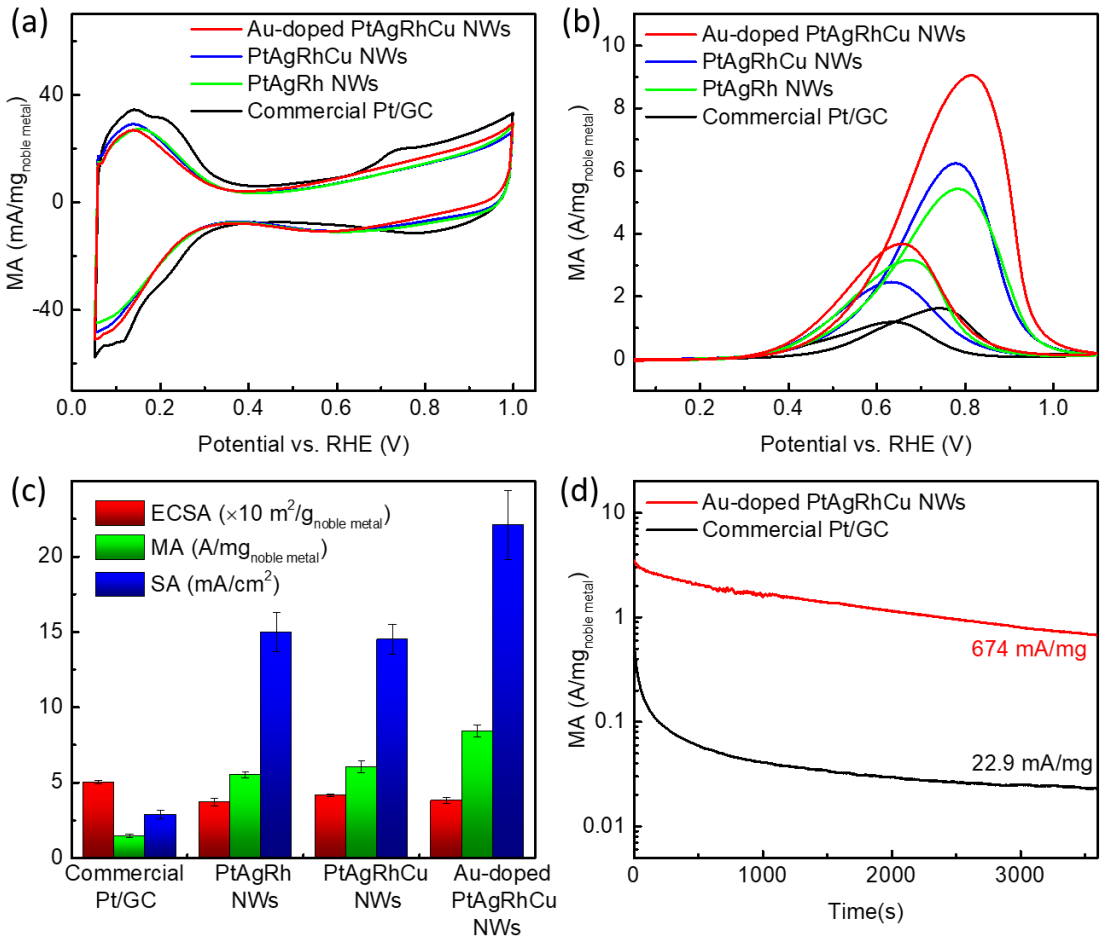

Figure 4-6. Electrochemistry study of the electrocatalysts for EOR. (a) Mass-normalized CV curves of the electrocatalysts in 0.1 M $HClO_4$ electrolyte at scan rate of 50 mV/s. (b) Mass-normalized CV curves of the electrocatalysts in 1.0 M KOH + 1.0 M EtOH electrolyte at scan rate of 50 mV/s. (c) Summary of the EOR performances of the electrocatalysts in terms of ECSA, MA and SA. (d) CA results of the electrocatalysts in 1.0 M KOH + 1.0 M EtOH electrolyte at 0.67 V vs. RHE.

In addition, the MOR performances was also explored in the electrolyte of 1.0 M KOH + 1.0 M

MeOH, and the medium entropy Au-doped PtAgRhCu alloy wavy nanowire demonstrates an MA of 3.27±0.16 A/mg and SA of 8.68±0.81 mA/cm^2, which is also comparably higher than the commercial Pt/GC (MA of 2.59±0.13 A/mg and SA of 5.45±0.16 mA/cm^2) (Figure. 4-7). Despite of the mediocre improvement in MA and SA for MOR, the medium entropy Au-doped PtAgRhCu alloy wavy nanowire demonstrates much improved long-term performances and very high current of 907 mA/mg can be retained after 1 hour of CA test, which is nearly 3-time enhancement compared with the commercial Pt/GC. And this improved long-term performance may be attributed to the sluggish diffusion effect of the medium entropy alloy as well[18, 19].

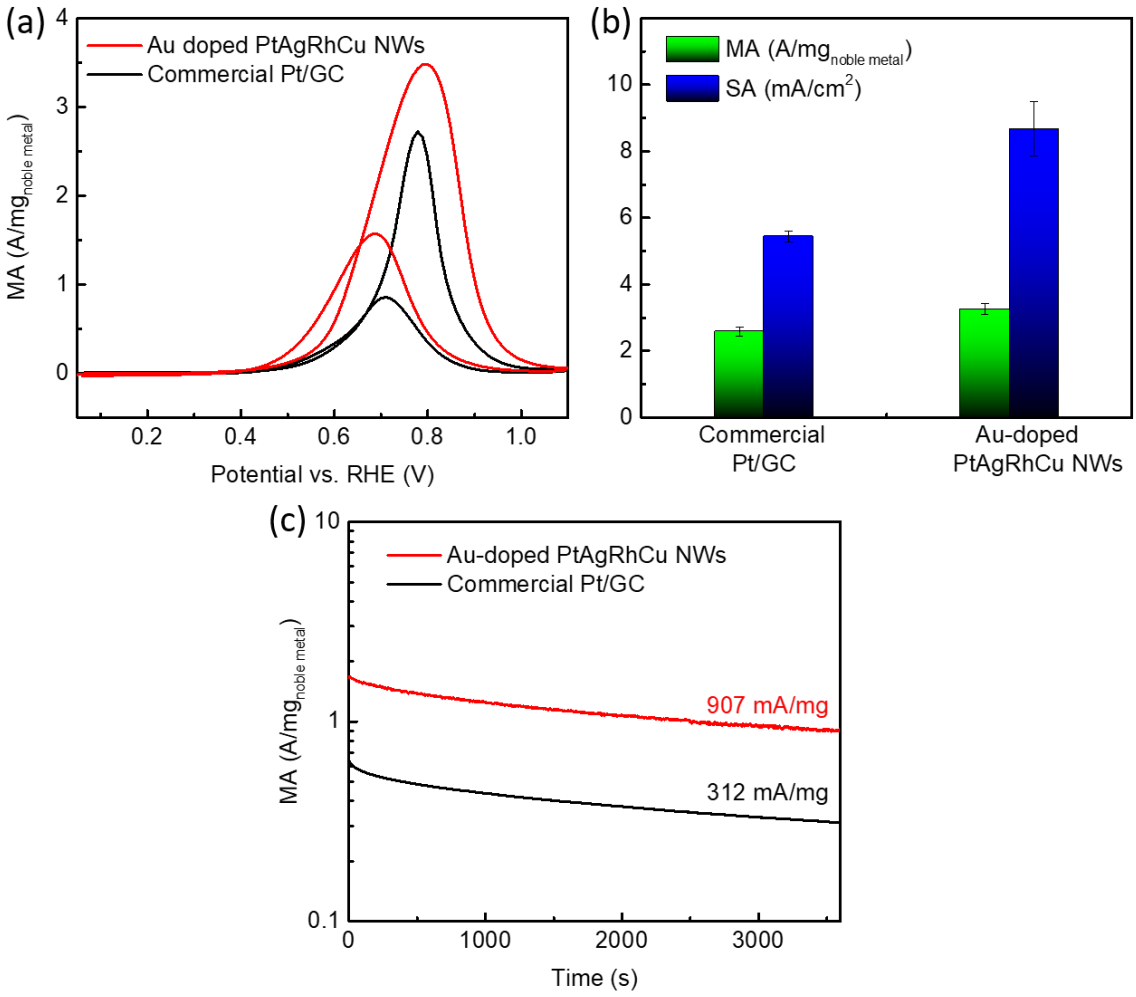

Figure 4-7. Electrochemistry study of the electrocatalysts for MOR. (a) Mass-normalized CV curves of the electrocatalysts in 1.0 M KOH + 1.0 M MeOH electrolyte at scan rate of 50 mV/s. (b) Summary of the MOR performances of the electrocatalysts in terms of MA and SA. (d) CA results of the electrocatalysts in 1.0 M KOH + 1.0 M MeOH electrolyte at 0.67 V vs. RHE.

4.3.3 Comparison with previous literatures

We also compared the EOR performance with the previous literatures and the medium entropy Au-doped PtAgRhCu alloy wavy nanowire has much improved MA compared with many previous literatures[39-44] as shown in Figure 4-8 (a). In addition, the long-term performances from

the CA test is also great improvement (674 mA/mg after 1h) compared with the previous literatures as listed in Table 1.

Although the MOR performances is only a mediocre performance among the previous literatures[33, 39, 40, 45-47] in Figure 4-8 (b). For example, the MA is less than a half of the previously reported single atom Ni decorated Pt nanowire (SANi-PtNWs)[39] and Core-shell (CS)-$Pt_{58}Cu_{28}Ni_{16}$ tetrahedra[40]. However, the medium entropy Au-doped PtAgRhCu alloy wavy nanowire also exhibits comparably better long-term performance from CA test (907 mA/mg after 1h) as shown in Table 1, which may lead to a promising electrocatalyst applied for the anode electrocatalyst of the fuel cells.

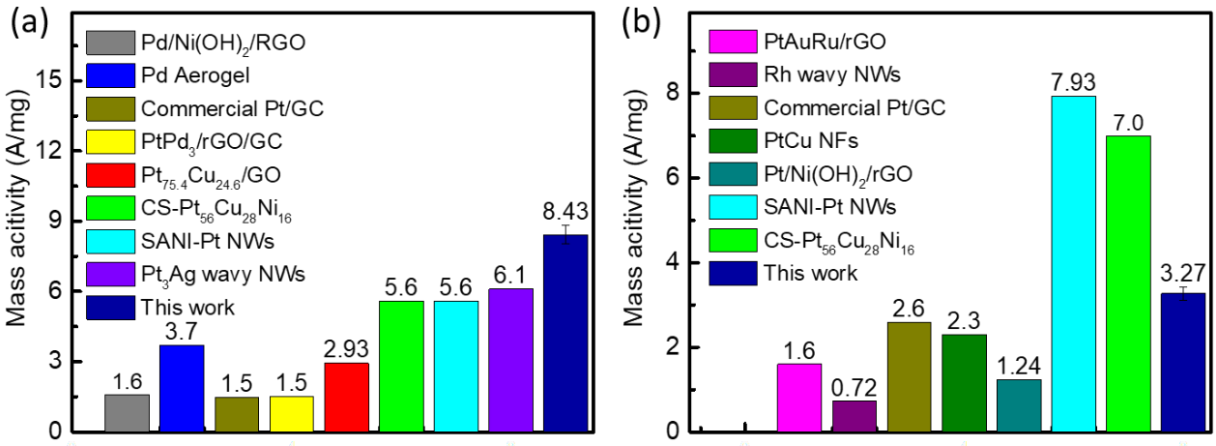

Figure 4-8. Comparison of the EOR performances (a) and MOR performances (b) of our medium entropy Au-doped PtAgRhCu alloy wavy nanowires with the previously reported noble metal-based electrocatalysts tested in alkaline media.

Table 4-1. Comparison with the previous literature in terms of the long-term performances of AOR in alkaline media.

Materials	Electrolyte	Current maintained [A/mg]	Potential vs. RHE [V]	Time [h]	Ref.
Medium entropy Au-doped PtAgRhCu alloy wavy nanowire	1.0 M KOH +1.0 M MeOH	0.91	0.67	1.0	This work
Medium entropy Au-doped PtAgRhCu alloy wavy nanowire	1.0 M KOH +1.0 M EtOH	0.67	0.67	1.0	This work
Commercial Pt/GC	1.0 M KOH +1.0 M MeOH	0.31	0.67	1.0	This work
Commercial Pt/GC	1.0 M KOH +1.0 M EtOH	0.02	0.67	1.0	This work
$Pt/Ni(OH)_2/rGO$	1.0 M KOH +1.0 M MeOH	0.46	0.76	1.0	[45]
$Pt/Ni(OH)_2/rGO$	1.0 M KOH +1.0 M MeOH	0.16	0.76	14	[45]
PtAuRu/rGO	1.0 M KOH +1.0 M MeOH	0.3	0.76	1.1	[46]
SANi-Pt NWs	1.0 M KOH +1.0 M MeOH	0.76	0.65	1.0	[39]
Core-shell $Pt_{56}Cu_{28}Ni_{16}$ tetrahedra	1.0 M KOH +1.0 M MeOH	0.83	0.65	1.0	[40]
Core-shell $Pt_{56}Cu_{28}Ni_{16}$ tetrahedra	1.0 M KOH +1.0 M EtOH	~0.1	0.65	1.0	[40]
Pt_3Ag wavy NWs	1.0 M KOH +1.0 M EtOH	0.15	0.72	1.7	[28]
$Pd/Ni(OH)_2/rGO$	1.0 M KOH +1.0 M EtOH	0.44	0.86	5.6	[41]
Core@shell Au@PtIr	1.0 M KOH +1.0 M EtOH	0.28	0.45	1.7	[26]
Core@skin PtBi@Pt	1.0 M KOH +1.0 M EtOH	0.48	0.62	0.5	[48]
Pd_4Cu_1 nanosheets	1.0 M KOH +1.0 M MeOH	0.2	0.85	1.0	[49]
$PtPd_3/rGO/GC$	1.0 M KOH +1.0 M EtOH	0.08	0.71	1.0	[43]
$Pd_3Ru_1P_{1.5}$	1.0 M KOH +1.0 M MeOH	0.06	0.86	1.0	[50]

Pd/Carbon Black	1.0 M KOH +1.0 M MeOH	0.09	0.7	1.0	[51]

4.4 Conclusion

In this chapter, we reported a straightforward solvothermal synthesis of medium entropy Au-doped PtAgRhCu alloy wavy nanowire as confirmed from the characterizations, demonstrating outstanding MA and SA for EOR, which can be attributed to a combination of ligand effect, strain effect, bifunctional effect and entropy effect from the introduction of the various elements as well as the benefits from the wavy nanowire morphology. Importantly, outstanding long-term performances for EOR and MOR were also exhibited, which may be attributed to the enhanced energy barrier for diffusion (sluggish diffusion effect) in alloying system with increased entropy, making it a highly attractive electrocatalysts to be employed for the anode of the ADAFCs.

4.5 Reference

1. Joghee, P.; Malik, J. N.; Pylypenko, S.; O'Hayre, R., A review on direct methanol fuel cells–In the perspective of energy and sustainability. *MRS Energy Sustain* **2015,** *2*.

2. Antolini, E.; Gonzalez, E. R., Alkaline direct alcohol fuel cells. *J. Power Sources* **2010,** *195* (11), 3431-3450.

3. Yu, E. H.; Krewer, U.; Scott, K., Principles and materials aspects of direct alkaline alcohol fuel cells. *Energies* **2010,** *3* (8), 1499-1528.

4. Yuan, Y.; Wang, J.; Adimi, S.; Shen, H.; Thomas, T.; Ma, R.; Attfield, J. P.; Yang, M., Zirconium nitride catalysts surpass platinum for oxygen reduction. *Nat. Mater.* **2019**, 1-5.

5. Wan, C.; Duan, X.; Huang, Y., Molecular Design of Single-Atom Catalysts for Oxygen Reduction Reaction. *Adv. Energy Mater.* **2020,** *10* (14), 19.

6. Wang, Y.; Li, J.; Wei, Z. D., Transition-metal-oxide-based catalysts for the oxygen reduction reaction. *J. Mater. Chem. A* **2018,** *6* (18), 8194-8209.

7. Wang, D.-W.; Su, D., Heterogeneous nanocarbon materials for oxygen reduction reaction. *Energy Environ. Sci.* **2014,** *7* (2), 576-591.

8. Weng, M. M.; Liu, D. J.; He, X. Q.; Asefa, T., Fe3C nanoparticles-loaded 3D nanoporous N-doped carbon: A highly efficient electrocatalyst for oxygen reduction in alkaline media. *Int. J. Hydrogen Energy* **2019,** *44* (39), 21506-21517.

9. Bai, J.; Liu, D. Y.; Yang, J.; Chen, Y., Nanocatalysts for Electrocatalytic Oxidation of Ethanol. *Chemsuschem* **2019,** *12* (10), 2117-2132.

10. Zhao, X.; Liu, Q. M.; Li, Q. X.; Chen, L. Y.; Mao, L.; Wang, H. Y.; Chen, S. W., Two-dimensional electrocatalysts for alcohol oxidation: A critical review. *Chem. Eng. J.* **2020,** *400*.

11. Zhao, S.; Yin, H.; Du, L.; Yin, G.; Tang, Z.; Liu, S., Three dimensional N-doped graphene/PtRu nanoparticle hybrids as high performance anode for direct methanol fuel cells. *J. Mater. Chem. A* **2014,** *2* (11), 3719-3724.

12. Lu, S.; Eid, K.; Ge, D.; Guo, J.; Wang, L.; Wang, H.; Gu, H., One-pot synthesis of PtRu nanodendrites as efficient catalysts for methanol oxidation reaction. *Nanoscale* **2017,** *9* (3), 1033-1039.

13. Xu, C. X.; Wang, L.; Mu, X. L.; Ding, Y., Nanoporous PtRu Alloys for Electrocatalysis. *Langmuir* **2010,** *26* (10), 7437-7443.

14. Jiang, Q.; Jiang, L.; Wang, S.; Qi, J.; Sun, G., A highly active PtNi/C electrocatalyst for methanol electro-oxidation in alkaline media. *Catal. Commun.* **2010,** *12* (1), 67-70.

15. Hammer, B.; Norskov, J. K., Theoretical surface science and catalysis - Calculations and concepts. In *Advances in Catalysis, Vol 45: Impact of Surface Science on Catalysis*, Gates, B. C.; Knozinger, H., Eds. Elsevier Academic Press Inc: San Diego, 2000; Vol. 45, pp 71-129.

16. Mavrikakis, M.; Hammer, B.; Norskov, J. K., Effect of strain on the reactivity of metal surfaces. *Phys. Rev. Lett.* **1998,** *81* (13), 2819-2822.

17. Wang, X.; Guo, W.; Fu, Y. Z., High-entropy alloys: emerging materials for advanced functional applications. *J. Mater. Chem. A* **2021,** *9* (2).

18. Xin, Y.; Li, S. H.; Qian, Y. Y.; Zhu, W. K.; Yuan, H. B.; Jiang, P. Y.; Guo, R. H.; Wang, L. B., High-Entropy Alloys as a Platform for Catalysis: Progress, Challenges, and Opportunities. *ACS Catal.* **2020,** *10* (19), 11280-11306.

19. Jin, Z. Y.; Lv, J.; Jia, H. L.; Liu, W. H.; Li, H. L.; Chen, Z. H.; Lin, X.; Xie, G. Q.; Liu, X. J.; Sun, S. H.; Qiu, H. J., Nanoporous Al-Ni-Co-Ir-Mo High-Entropy Alloy for Record-High Water Splitting Activity in Acidic Environments. *Small* **2019,** *15* (47).

20. Yeh, J. W., Alloy Design Strategies and Future Trends in High-Entropy Alloys. *JOM* **2013,** *65* (12), 1759-1771.

21. Shen, S. Y.; Zhao, T. S.; Xu, J. B., Carbon supported PtRh catalysts for ethanol oxidation in alkaline direct ethanol fuel cell. *Int. J. Hydrogen Energy* **2010,** *35* (23), 12911-12917.

22. Moreira, T. F. M.; Neto, S. A.; Lemoine, C.; Kokoh, K. B.; Morais, C.; Napporn, T. W.; Olivi, P., Rhodium effects on Pt anode materials in a direct alkaline ethanol fuel cell. *Rsc Advances* **2020,** *10* (58), 35310-35317.

23. Erini, N.; Beermann, V.; Gocyla, M.; Gliech, M.; Heggen, M.; Dunin-Borkowski, R. E.; Strasser, P., The Effect of Surface Site Ensembles on the Activity and Selectivity of

Ethanol Electrooxidation by Octahedral PtNiRh Nanoparticles. *Angew. Chem.-Int. Edit.* **2017,** *56* (23), 6533-6538.

24. Zhang, J. W.; Ye, J. Y.; Fan, Q. Y.; Jiang, Y. T.; Zhu, Y. F.; Li, H. Q.; Cao, Z. M.; Kuang, Q.; Cheng, J.; Zheng, J.; Xie, Z. X., Cyclic Penta-Twinned Rhodium Nanobranches as Superior Catalysts for Ethanol Electro-oxidation. *J. Am. Chem. Soc.* **2018,** *140* (36), 11232-11240.

25. Kowal, A.; Li, M.; Shao, M.; Sasaki, K.; Vukmirovic, M. B.; Zhang, J.; Marinkovic, N. S.; Liu, P.; Frenkel, A. I.; Adzic, R. R., Ternary Pt/Rh/SnO2 electrocatalysts for oxidizing ethanol to CO2. *Nat. Mater.* **2009,** *8* (4), 325-330.

26. Liang, Z.; Song, L.; Deng, S.; Zhu, Y.; Stavitski, E.; Adzic, R. R.; Chen, J.; Wang, J., Direct 12-electron oxidation of ethanol on a ternary Au (core)-PtIr (shell) electrocatalyst. *J. Am. Chem. Soc.* **2019,** *141* (24), 9629-9636.

27. Liu, T. Y.; Wang, K.; Yuan, Q.; Shen, Z. B.; Wang, Y.; Zhang, Q. H.; Wang, X., Monodispersed sub-5.0 nm PtCu nanoalloys as enhanced bifunctional electrocatalysts for oxygen reduction reaction and ethanol oxidation reaction. *Nanoscale* **2017,** *9* (9), 2963-2968.

28. Fu, X.; Wan, C.; Zhang, A.; Zhao, Z.; Huyan, H.; Pan, X.; Du, S.; Duan, X.; Huang, Y., Pt3Ag alloy wavy nanowires as highly effective electrocatalysts for ethanol oxidation reaction. *Nano Res.* **2020,** *13* (5), 1472-1478.

29. Jiang, X.; Liu, Y.; Wang, J. X.; Wang, Y. F.; Xiong, Y. X.; Liu, Q.; Li, N. X.; Zhou, J. C.; Fu, G. T.; Sun, D. M.; Tang, Y. W., 1-Naphthol induced Pt3Ag nanocorals as bifunctional cathode and anode catalysts of direct formic acid fuel cells. *Nano Res.* **2019,** *12* (2), 323-329.

30. Jiang, X.; Fu, G. T.; Wu, X.; Liu, Y.; Zhang, M. Y.; Sun, D. M.; Xu, L.; Tang, Y. W., Ultrathin AgPt alloy nanowires as a high-performance electrocatalyst for formic acid oxidation. *Nano Res.* **2018,** *11* (1), 499-510.

31. Zhao, X.; Zhang, H. T.; Yan, Y.; Cao, J. H.; Li, X. Q.; Zhou, S. M.; Peng, Z. M.; Zeng, J., Engineering the Electrical Conductivity of Lamellar Silver-Doped Cobalt(II) Selenide Nanobelts for Enhanced Oxygen Evolution. *Angew. Chem.-Int. Edit.* **2017,** *56* (1), 328-332.

32. Huang, X.; Zhao, Z.; Chen, Y.; Chiu, C.-Y.; Ruan, L.; Liu, Y.; Li, M.; Duan, X.; Huang, Y., High density catalytic hot spots in ultrafine wavy nanowires. *Nano Lett.* **2014,** *14* (7), 3887-3894.

33. Fu, X.; Zhao, Z.; Wan, C.; Wang, Y.; Fan, Z.; Song, F.; Cao, B.; Li, M.; Xue, W.; Huang, Y.; Duan, X., Ultrathin wavy Rh nanowires as highly effective electrocatalysts for methanol oxidation reaction with ultrahigh ECSA. *Nano Res.* **2019,** *12* (1), 211-215.

34. Li, M.; Zhao, Z.; Cheng, T.; Fortunelli, A.; Chen, C.; Yu, R.; Zhang, Q.; Gu, L.; Merinov, B. V.; Lin, Z.; Zhu, E.; Yu, T.; Jia, Q.; Guo, J.; Zhang, L.; Goddard, W. A.; Huang, Y.; Duan, X., Ultrafine jagged platinum nanowires enable ultrahigh mass activity for the oxygen reduction reaction. *Science* **2016,** *354* (6318), 1414-1419.

35. Jiang, X.; Qiu, X. Y.; Fu, G. T.; Sun, J. Z.; Huang, Z. N.; Sun, D. M.; Xu, L.; Zhou, J. C.; Tang, Y. W., Highly simple and rapid synthesis of ultrathin gold nanowires with (111)-dominant facets and enhanced electrocatalytic properties. *J. Mater. Chem. A* **2018,** *6* (36), 17682-17687.

36. Mao, H. B.; Feng, J. Y.; Ma, X.; Wu, C.; Zhao, X. J., One-dimensional silver nanowires synthesized by self-seeding polyol process. *J. Nanopart. Res.* **2012,** *14* (6), 15.

37. Kim, H.; Choi, S. H.; Kim, M.; Park, J. U.; Bae, J.; Park, J., Seed-mediated synthesis of ultra-long copper nanowires and their application as transparent conducting electrodes. *Appl. Surf. Sci.* **2017,** *422*, 731-737.

38. Li, H.-H.; Fu, Q.-Q.; Xu, L.; Ma, S.-Y.; Zheng, Y.-R.; Liu, X.-J.; Yu, S.-H., Highly crystalline PtCu nanotubes with three dimensional molecular accessible and restructured surface for efficient catalysis. *Energy Environ. Sci.* **2017**.

39. Li, M.; Duanmu, K.; Wan, C. Z.; Cheng, T.; Zhang, L.; Dai, S.; Chen, W.; Zhao, Z.; Li, P.; Fei, H.; Zhu, Y.; Yu, R.; Luo; Zang, K.; Lin, Z.; Ding, M.; Huang, J.; Sun, H.; Guo, J.; Pan, X.; Goddard, W. A.; Sautet, P.; Huang, Y.; Duan, X., Single-atom tailoring of platinum nanocatalysts for high-performance multifunctional electrocatalysis. *Nat. Catalysis* **2019,** *2* (6), 495-503.

40. Huang, J.; Liu, Y.; Xu, M.; Wan, C.; Liu, H.; Li, M.; Huang, Z.; Duan, X.; Pan, X.; Huang, Y., PtCuNi Tetrahedra Catalysts with Tailored Surfaces for Efficient Alcohol Oxidation. *Nano Lett.* **2019,** *19* (8), 5431-5436.

41. Huang, W.; Ma, X. Y.; Wang, H.; Feng, R.; Zhou, J.; Duchesne, P. N.; Zhang, P.; Chen, F.; Han, N.; Zhao, F.; Zhou, J.; Cai, W. B.; Li, Y., Promoting effect of Ni (OH) 2 on palladium nanocrystals leads to greatly improved operation durability for electrocatalytic ethanol oxidation in alkaline solution. *Adv. Mater.* **2017,** *29* (37), 1703057.

42. Yazdan-Abad, M. Z.; Noroozifar, M.; Alam, A. R. M.; Saravani, H., Palladium aerogel as a high-performance electrocatalyst for ethanol electro-oxidation in alkaline media. *J. Mater. Chem. A* **2017,** *5* (21), 10244-10249.

43. Ren, F. F.; Wang, H. W.; Zhai, C. Y.; Zhu, M. S.; Yue, R. R.; Du, Y. K.; Yang, P.; Xu, J. K.; Lu, W. S., Clean Method for the Synthesis of Reduced Graphene

Oxide-Supported PtPd Alloys with High Electrocatalytic Activity for Ethanol Oxidation in Alkaline Medium. *ACS Appl. Mater. Interfaces* **2014,** *6* (5), 3607-3614.

44. Liu, T.; Li, C.; Yuan, Q., Facile synthesis of PtCu alloy/graphene oxide hybrids as improved electrocatalysts for alkaline fuel cells. *ACS Omega* **2018,** *3* (8), 8724-8732.

45. Huang, W.; Wang, H.; Zhou, J.; Wang, J.; Duchesne, P. N.; Muir, D.; Zhang, P.; Han, N.; Zhao, F.; Zeng, M., Highly active and durable methanol oxidation electrocatalyst based on the synergy of platinum–nickel hydroxide–graphene. *Nat. Commun.* **2015,** *6*.

46. Ren, F.; Wang, C.; Zhai, C.; Jiang, F.; Yue, R.; Du, Y.; Yang, P.; Xu, J., One-pot synthesis of a RGO-supported ultrafine ternary PtAuRu catalyst with high electrocatalytic activity towards methanol oxidation in alkaline medium. *J. Mater. Chem. A* **2013,** *1* (24), 7255-7261.

47. Zhang, Z.; Luo, Z.; Chen, B.; Wei, C.; Zhao, J.; Chen, J.; Zhang, X.; Lai, Z.; Fan, Z.; Tan, C., One-Pot Synthesis of Highly Anisotropic Five-Fold-Twinned PtCu Nanoframes Used as a Bifunctional Electrocatalyst for Oxygen Reduction and Methanol Oxidation. *Adv. Mater.* **2016,** *28* (39), 8712-8717.

48. Zhang, B.-W.; Lai, W.-H.; Sheng, T.; Qu, X.-M.; Wang, Y.-X.; Ren, L.; Zhang, L.; Du, Y.; Jiang, Y.-X.; Sun, S.-G., Ordered platinum–bismuth intermetallic clusters with Pt-skin for a highly efficient electrochemical ethanol oxidation reaction. *J. Mater. Chem. A* **2019,** *7* (10), 5214-5220.

49. Fan, J.; Yu, S.; Qi, K.; Liu, C.; Zhang, L.; Zhang, H.; Cui, X.; Zheng, W., Synthesis of ultrathin wrinkle-free PdCu alloy nanosheets for modulating d-band electrons for efficient methanol oxidation. *J. Mater. Chem. A* **2018,** *6* (18), 8531-8536.

50. Xu, H.; Yan, B.; Zhang, K.; Wang, C. Q.; Zhong, J. T.; Li, S. M.; Yang, P.; Du, Y. K., Facile synthesis of Pd-Ru-P ternary nanoparticle networks with enhanced electrocatalytic performance for methanol oxidation. *Int. J. Hydrogen Energy* **2017,** *42* (16), 11229-11238.

51. Hu, C.; Wang, X., Highly dispersed palladium nanoparticles on commercial carbon black with significantly high electro-catalytic activity for methanol and ethanol oxidation. *Int. J. Hydrogen Energy* **2015,** *40* (36), 12382-12391.

Chapter 5. Ultrathin $RhRu_{0.5}$ alloy nanowire for as highly efficient hydrazine total electrooxidation with ultrahigh mass activity

5.1 Introduction

Hydrazine has been studied as a media for hydrogen storage and its decomposition produces hydrogen gas which can then be applied for hydrogen fuel cells[1]. As an alternative, it may be more convenient to directly convert the chemical energy stored in hydrazine into electricity via direct hydrazine fuel cells (DHFCs) to save up the decomposition procedure for hydrogen generation. In addition, hydrazine also has high gravimetric and volumetric energy density, which is comparable with the alcohols and much higher than the compressed hydrogen (by considering the hydrogen storage system for the gravimetric energy density calculation)[2, 3]. Only nitrogen gas and water will be produced from the total electrooxidation of hydrazine, which means zero carbon emission compared with alcohols. In addition, when applied for the alkaline direct hydrazine fuel cells (ADHFCs) with the advantages of enabling cheaper cathode electrocatalysts for oxygen reduction reaction (*e.g.* Single atom Fe and Co electrocatalysts[4, 5], ZrN[6], AlN[7], etc.) and less fuel crossover from anode to cathode due to the reversed direction of osmotic force in alkaline environment[8], there will be no evident pH drop during operation compared with the alkaline direct alcohol fuel cells (ADAFCs) which generate carbonate during operation. Although anhydrous hydrazine is a toxic chemical, the carcinogenicity of its aqueous solution is lower and placed in the class 2B, which is at the same level as gasoline[9, 10]. Therefore, hydrazine oxidation reaction (HzOR) has also attracted research interests due to its potential application for fuel cells[11].

Despite of many non-noble metal based electrocatalysts (*e.g.* Ni[12], Co[13, 14], Ru[15, 16], etc.) for hydrazine oxidation reaction (HzOR) reported to date, previous systematic study with metal

rotating disk electrode (RDE) has demonstrated these non-noble metals are unable to achieve the total electrooxidation of hydrazine[17], which negates their advantage for having much lower costs since the total electrooxidation is also important, not only for the efficient utilization of hydrazine as a fuel, but also to prevent the potential generation of harmful byproducts (*e.g.* NH_3) rather than the environmentally friendly N_2. The production of NH_3 was also confirmed via differential electrochemical mass spectrometry (DEMS) in the previous study about single atom catalyst (SAC)-Fe, Co and Ni[18]. And noble metal (*e.g.* Rh, Pt and Pd) are still required to achieve the total oxidation of hydrazine with a charge transfer number of four[17]. Among them, Rh has the lowest half wave potential for HzOR[17], therefore, becomes our primary choice of electrocatalyst. However, the noble metal based electrocatalysts are greatly suffering from the scarcity and high cost, which will limit the widespread application of the fuel cells, therefore, it is essential to develop highly effective electrocatalyst with high mass activity (MA) to lower the required mass loading. Hydrazine oxidation reaction can be considered as an analogue of hydrogen oxidation reaction to some extent, which involves the removal of surficially adsorbed hydrogen species[19], and this dehydrogenation step can be boosted by the introduction of Ru species as well. Similar examples of PtRu electrocatalysts have been reported before to boost the HOR performances[20, 21]. In addition, Ru also has lower onset and half wave potential for HzOR based on the previous RDE study so the alloying may bring synergistic effect to benefit the Rh based electrocatalysts to lower the overpotential while maintaining the capability of achieving the total oxidation of hydrazine[17]. RhRu-based alloy has been studied recently and explored as electrocatalysts for the hydrogen evolution reaction (HER)[22, 23], oxygen evolution reaction (OER)[24, 25] and nitrogen reduction reaction (NRR)[26], however, its potential application for HzOR has not been explored before to our best knowledge.

ECSA is also an important factor to improve MA and typically enhancing ECSA requires ultrafine nanostructures, such as ultrathin wavy nanowires, which have high specific surface area because of the ultrathin diameter, rich surficial defects and potentially catalytic sites thanks to the wavy surface and good charge transport due to the one-dimensional nanostructure[27-29]. Therefore, in this study we designed ultrathin $RhRu_{0.5}$ alloy wavy nanowire as the electrocatalyst for HzOR via a facile solvothermal synthesis. The introduction of Ru can greatly lower the overpotential of the HzOR and thus greatly enhances the performances with an ultrahigh MA of 60.4±6.2 A/mg at 0.20 V vs. RHE from the tests on carbon paper, which is much higher than the Rh wavy nanowires and over one magnitude higher than that of the commercial Pt on graphitized carbon (Pt/GC). The chronoamperometry (CA) tests also demonstrate great long-term performances for the $RhRu_{0.5}$ alloy wavy nanowires compared with Rh wavy nanowires and commercial Pt/GC. RDE tests also demonstrate the total oxidation with an electron transfer number of four, proving the total oxidation of hydrazine to environmentally friendly nitrogen gas. Therefore, we believe the $RhRu_{0.5}$ alloy wavy nanowire will be a highly promising anode electrocatalyst for the ADHFCs applications.

5.2 Experimental

5.2.1 Chemicals

Sodium hexachlororhodate (III) (Na_3RhCl_6, analytical grade), Ruthenium chloride hydrate ($RuCl_3 \cdot xH_2O$, 38.0% - 42.0% Ru basis), sodium iodide (NaI, ACS reagent, ≥ 99.5%), polyvinylpyrrolidone (PVP, MW ~55,000), sodium ascorbate (NaAA, crystalline, ≥ 98%), hydrazine solution (35 wt% in water) and commercial Pt on graphitized carbon (Pt/GC, 20%) were all purchased from Sigma-Aldrich.

5.2.2 Synthesis of $RhRu_{0.5}$ alloy wavy nanowires

The synthesis was carried out via a polyol method following the previous research. 40 mg NaAA, 160 mg PVP and 75 mg NaI were mixed with 1.00 mL aqueous solution of Na_3RhCl_6 (10.0 mg/mL), 0.333 mL aqueous solution of $RuCl_3 \cdot xH_2O$ (10.0 mg/mL, 40-42% metal basis) and dissolved after ultra-sonication followed by adding 5.0 mL of ethylene glycol (EG). Then the vial was heated at 210 ^oC for 4h and the post-synthetic treatment were carried out by washing/centrifuging with ethanol/acetone and ethanol/hexane. The final products were re-dispersed in ethanol. For comparison, the Rh wavy nanowire and Ru nanoparticles are synthesized at the same conditions with the addition of individual noble metal precursor only.

5.2.3 Structural characterizations

The transmission electron microscopy (TEM) was carried out on FEI T12 transmission electron microscope operated at 120 kV. The X-ray diffraction (XRD) was carried out on a Panalytical X'Pert Pro X-ray Powder Diffractometer with Cu-Kα radiation. X-ray photoelectron spectroscopy (XPS) was carried out with Kratos AXIS Ultra DLD spectrometer. The scanning transmission electron microscope (STEM) image and energy dispersive x-ray spectroscopy (EDX) mapping were carried out on Joel Jem-300CF (Grand Arm) operated at 300 kV. The inductively coupled plasma-atomic emission spectroscopy (ICP-AES) was carried out to determine the elemental ratio and loading of the electrocatalysts.

5.2.4 Electrochemical measurements

The electrochemical tests were carried out in a three-electrode cell system. The working electrode was an RDE with a geometric area of 0.196 cm^2 and the counter electrode was a Pt coil. The reference electrode was Hg/HgO (1.0 M KOH) and the potentials are converted against reversible hydrogen electrode (RHE). The homogeneous ethanol dispersion of the electrocatalysts was dropcasted onto the GCE surface and dried under room temperature with

Rh loading of 1.00 μg (5.07 μg/cm^2) for the $RhRu_{0.5}$ and Rh wavy nanowire, and Ru loading of 1.00 μg (5.07 μg/cm^2) for the Ru nanoparticle. Cyclic voltammetry (CV) was performed in Ar-saturated 1.0 M KOH electrolyte with a scan rate of 50 mV/s ranging from 0.05 to 1.10 V vs. RHE to determine the electrochemically active surface area ($ECSA_{HUPD}$). HzOR tests were carried out in Ar-saturated electrolyte of 1.0 M KOH, 0.010 M hydrazine via linear sweep voltammetry (LSV) at varying rotation rate of 225, 400, 625, 900, 1225 and 1600 rppm, with potential scan rate of 20 mV/s to study the electron transfer number. To probe the potential for real world applications, the HzOR tests were also carried out on the carbon paper electrode with the loading of the electrocatalysts (1.00 μg Rh or Pt on 1 cm^2 carbon paper area) in the electrolyte of 1.0 M KOH, 0.10 M hydrazine via LSV. The chronoamperometry (CA) tests were carried out at 0.20 V vs. RHE for 1 h.

5.3 Results and discussion

5.3.1 Characterization

The TEM images demonstrate wavy nanowire morphologies for the $RhRu_{0.5}$ and Rh nanomaterials with ultrathin diameter (2-3 nm) and wavy surface (Figure 5-1 (a) and (b)). The ultrathin diameter will lead to ultrahigh ECSA and the wavy surface of the electrocatalyst can also contribute to the surficial catalytic sites, and the one-dimensional nanostructure can benefit the charge transport as well. In contrast, the monometallic Ru will be synthesized as nanoparticle morphology under this condition (Figure 5-1 (c)).

The XRD study demonstrates very similar pattern for the $RhRu_{0.5}$ wavy nanowire compared with Rh wavy nanowire with FCC (JCPDS No. 05-0685) crystal structure with peaks corresponding to the characteristic (111), (200), (220) and (311) crystal planes. While the Ru nanoparticle synthesized under the same condition demonstrates HCP (JCPDS No. 06-0663)

crystal structure, indicating the formation of the alloy phase and the Ru was facilitated to be grown into the FCC lattice. And similar phenomenon has also been reported in the previous literatures regarding RhRu alloys as well[22]. The EDX mapping demonstrates uniform distribution of Rh and Ru elements with an atomic ratio of Ru:Rh=50.4%, which agrees with the ICP-AES (Ru:Rh=52.9±3.3%) results. XPS also demonstrates peaks for Rh $3d_{5/2}$, Rh $3d_{3/2}$, Ru $3p_{3/2}$ and Ru $3p_{1/2}$ (Figure 5-5), and the similar value of electronegativity for Rh (2.28) and Ru (2.2) explains that there is no evident shift in binding energy.

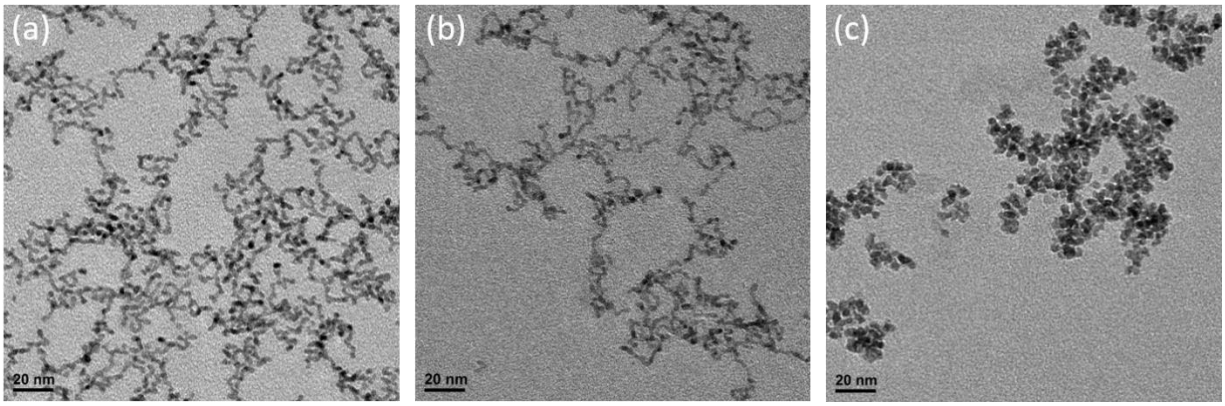

Figure 5-1. TEM pictures (a) $RhRu_{0.5}$ wavy nanowires, (b) Rh wavy nanowires and (c) Ru nanoparticles.

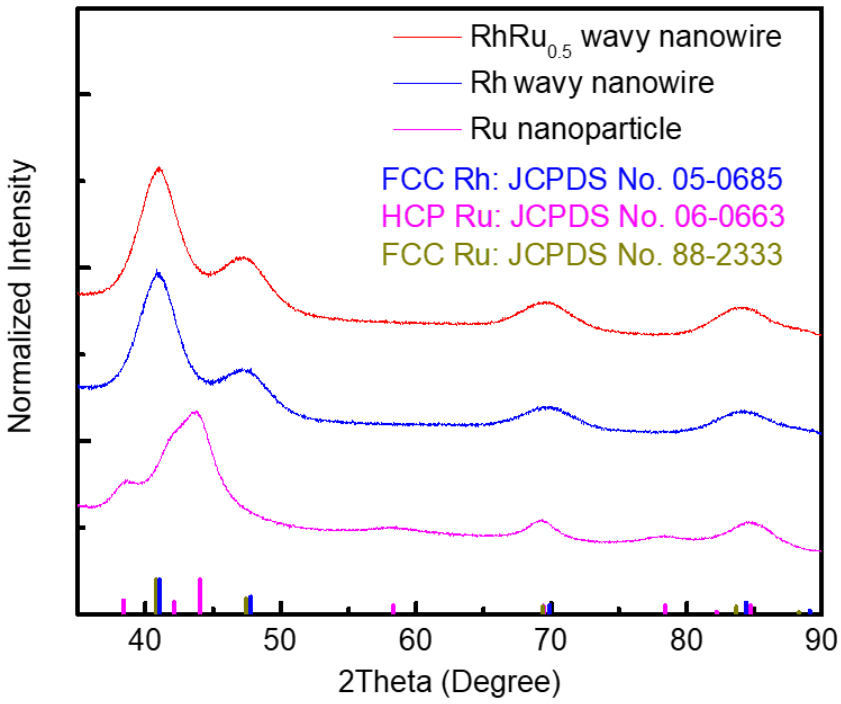

Figure 5-2. XRD patterns of $RhRu_{0.5}$ wavy nanowires, Rh wavy nanowires and Ru nanoparticles.

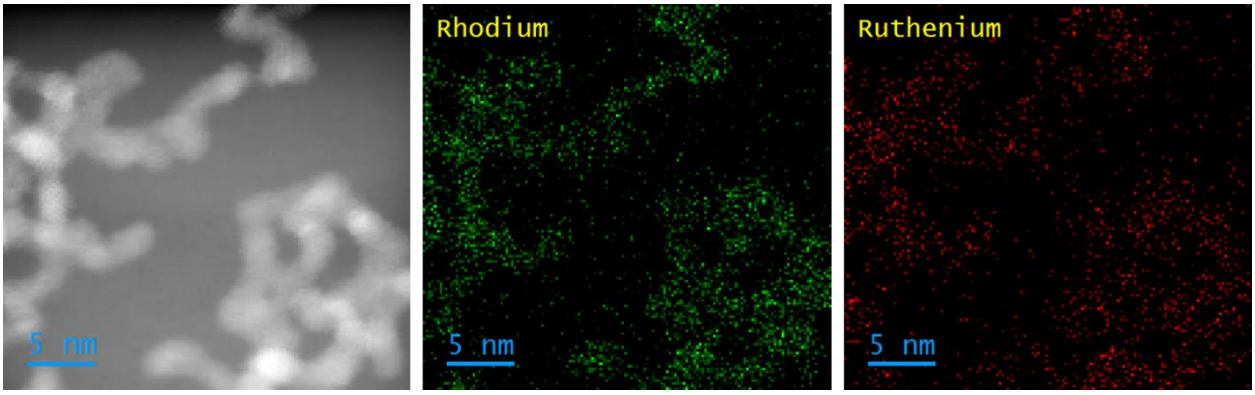

Figure 5-3. EDX mapping of the $RhRu_{0.5}$ alloy wavy nanowires.

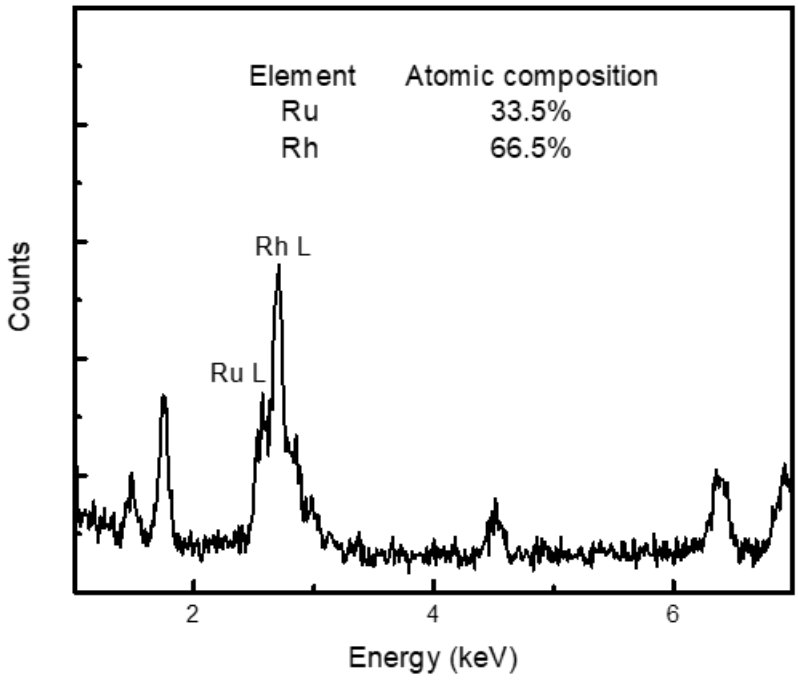

Figure 5-4. EDX spectrum of the $RhRu_{0.5}$ alloy wavy nanowires.

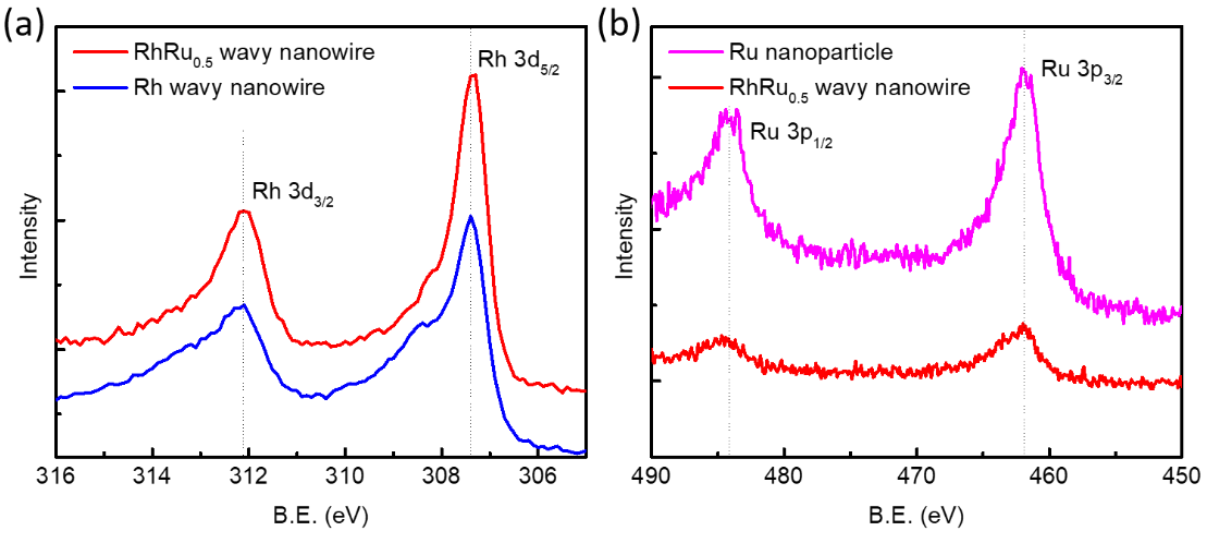

Figure 5-5. (a) XPS characterization of $RhRu_{0.5}$ wavy nanowires and Rh wavy nanowires for Rh element. (b) XPS characterization of $RhRu_{0.5}$ wavy nanowires and Ru nanoparticles for Ru element.

5.3.2 Electrochemical study

The electrochemical performances of the nanowire catalysts were first studied via CV to determine the $ECSA_{HUPD}$ as shown in Figure. 5-6 (a). Significantly, the ECSA of the $RhRu_{0.5}$ and Rh wavy nanowires are 101.3±3.1 m^2/g and 101.0±1.3 m^2/g, respectively, which are ultrahigh ECSA due to the ultrathin diameter of these nanowires and high specific surface area. The ECSA values are similar since the morphology of the $RhRu_{0.5}$ alloy wavy nanowire is not greatly changed upon the alloying with the Ru.

In addition, for the $RhRu_{0.5}$ alloy wavy nanowires, the peaks for hydrogen adsorption and desorption also shifted to lower potential, which demonstrates the more facilitated removal of the adsorbed hydrogen species on the electrocatalysts surface upon the introduction of Ru and similar phenomenon has also been reported before for the PtRu based nanomaterials upon Ru introduction to boost HOR[20] despite no consensus has reached about whether this facilitated hydrogen removal is attributed to electronic effect[20] or bifunctional effect (facilitated hydroxyl group formation on Ru sites)[21]. In addition, Ru also has the intrinsic capability to lower the overpotential of the HzOR[17], therefore, we believe the $RhRu_{0.5}$ alloy wavy nanowire will serve as a highly effective electrocatalyst for HzOR.

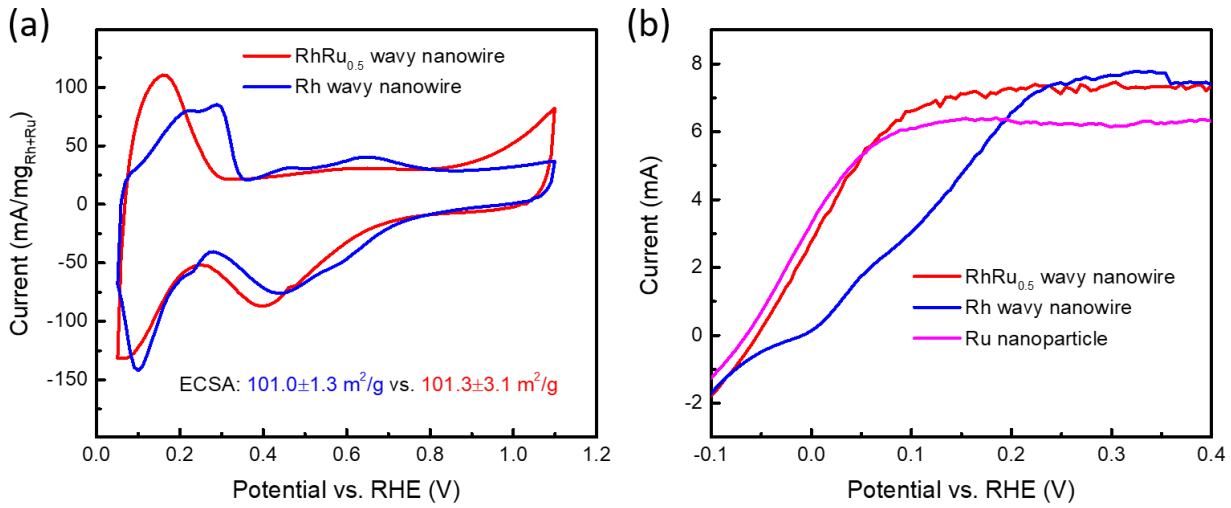

Figure 5-6. Electrochemical study on RDE. (a) CV curves of the $RhRu_{0.5}$ alloy wavy nanowire and Rh wavy nanowire in 1.0 M KOH electrolyte for ECSA determination. (b) LSV curves of $RhRu_{0.5}$ alloy wavy nanowire, Rh wavy nanowire and Ru nanoparticle in 1.0 M KOH + 10 mM N_2H_4 electrolyte at rotation rate of 1600 rppm and scan rate of 20 mV/s.

The preliminary catalytic activity was carried out in the electrolyte of 1 M KOH and 0.010 M hydrazine as shown in Figure 5-6 (b). The LSV demonstrates a current plateau, indicating a diffusion limited current ~7.4 mA for the $RhRu_{0.5}$ alloy wavy nanowire, which is similar to that of the Rh wavy nanowire. The current plateau also has lots of trembles due to the generation of N_2 gas during the reaction blocking the surface of the electrocatalyst and electrode. Importantly, compared with the Rh wavy nanowires, the $RhRu_{0.5}$ alloy wavy nanowires demonstrate improved performances for HzOR with much lower halfwave potential (~105 mV) and open circuit potential (~45 mV), which can be attributed to the synergistic effect upon alloy formation with Ru to enhance the HzOR performance with lowered overpotential. In contrast, although the Ru nanoparticle has low halfwave potential and open circuit potential as well, the evidently lowered diffusion limited current implies its disadvantage to achieve the total

electrooxidation of hydrazine, which is further proved by the study on the RDE as shown in Figure 5-7: The linear fitting between the diffusion limited current and the square root of the corresponding rotation rate according to the Levich equation was carried out as shown below[17]:

$$I_{DL} = 0.201nFAD_R^{2/3}\nu^{-1/6}C\omega^{1/2}$$

The values of the coefficients from the previous literatures[17]: ν=1.07×10^{-2} cm^2/s, F=96500 C/mol, A=0.196 cm^2, D_R=1.40×10^{-5} cm^2/s and C=0.010 mol/L. The linear fitting demonstrates good linear correlation (R^2>0.99) and the electron transfer number is calculated as 4.02±0.12 for $RhRu_{0.5}$ wavy nanowire, 4.08±0.08 for Rh wavy nanowire and 3.37±0.11 for Ru nanoparticle, respectively, indicating the capability of total electrooxidation of hydrazine on Rh based electrocatalysts.[17] In sharp contrast, the Ru nanoparticle cannot achieve the total electrooxidation with a similar charge transfer number according to the previous literature on RDE study[17]. The lowered electron transfer number maybe caused by the production of ammonia[18], which not only leads to the lowered efficiency in fuel utilization but also results in the production of harmful byproducts despite of the lower overpotential and lower cost of Ru. Therefore, we consider the $RhRu_{0.5}$ alloy wavy nanowire as the optimized electrocatalysts with much lowered overpotential attributed to the alloying with Ru while maintaining the capability to achieve the total electrooxidation.

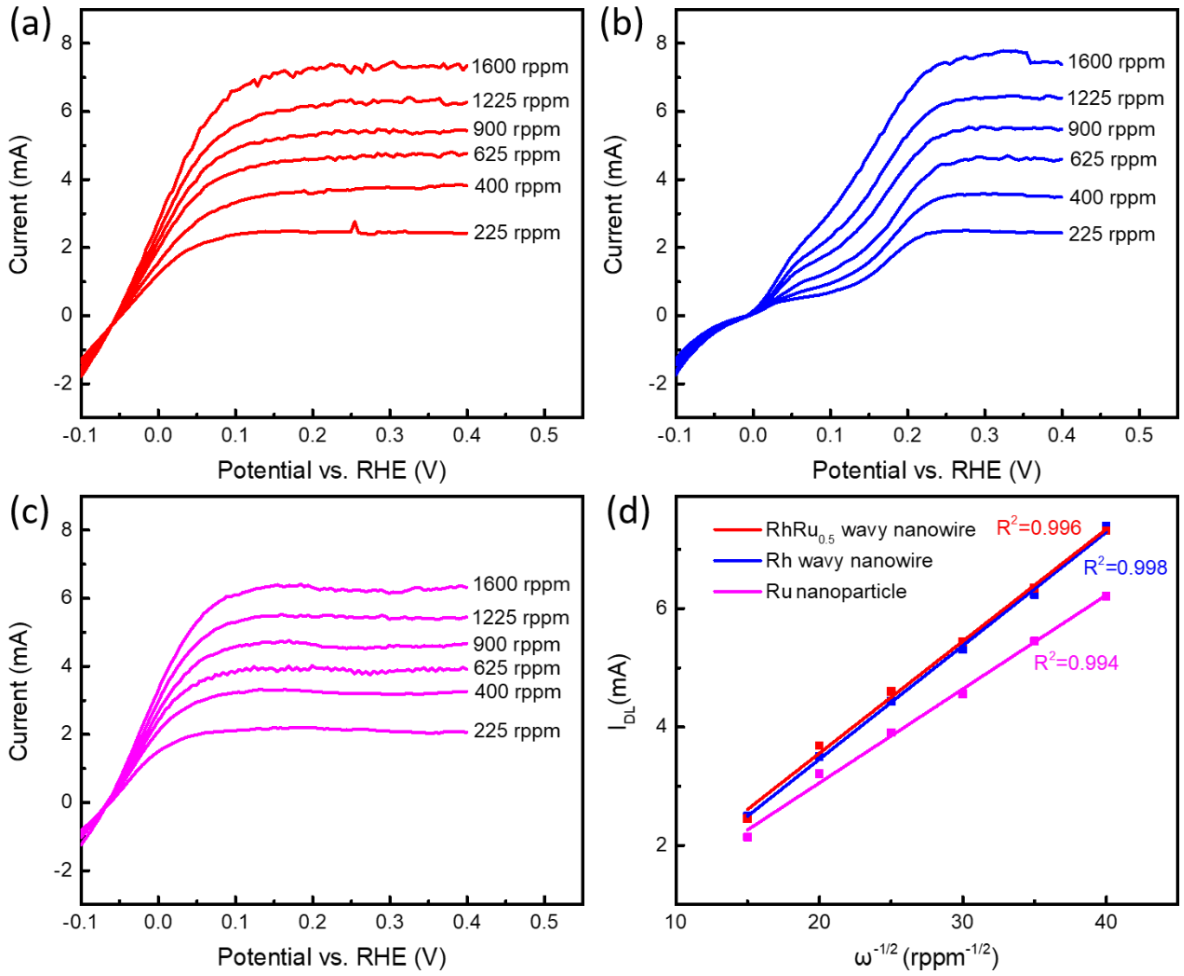

Figure 5-7. RDE study of HzOR at different rotation rate. (a) $RhRu_{0.5}$ alloy wavy nanowire. (b) Rh wavy nanowire. (c) Ru nanoparticle. (d) Linear fitting of the diffusion limited current at different rotation rate.

In the next stage, we carried out the electrochemical study on the carbon paper electrode since this will be closer to the real-world application scenarios. The carbon paper is considered as an ideal supporter for the electrocatalysts because it has highly porous nanostructures to greatly facilitate the nitrogen gas removal during the hydrazine electrooxidation process. We find out extremely high performances of 60.4±6.2 A/mg at 0.20 V vs. RHE, which is much higher compared with the Rh nanowires (37.6±2.1 A/mg) as well as lower overpotential. In addition,

the performance of commercial Pt/GC was also studied as a very common electrocatalysts, demonstrating much lower MA (5.42±0.24 A/mg).

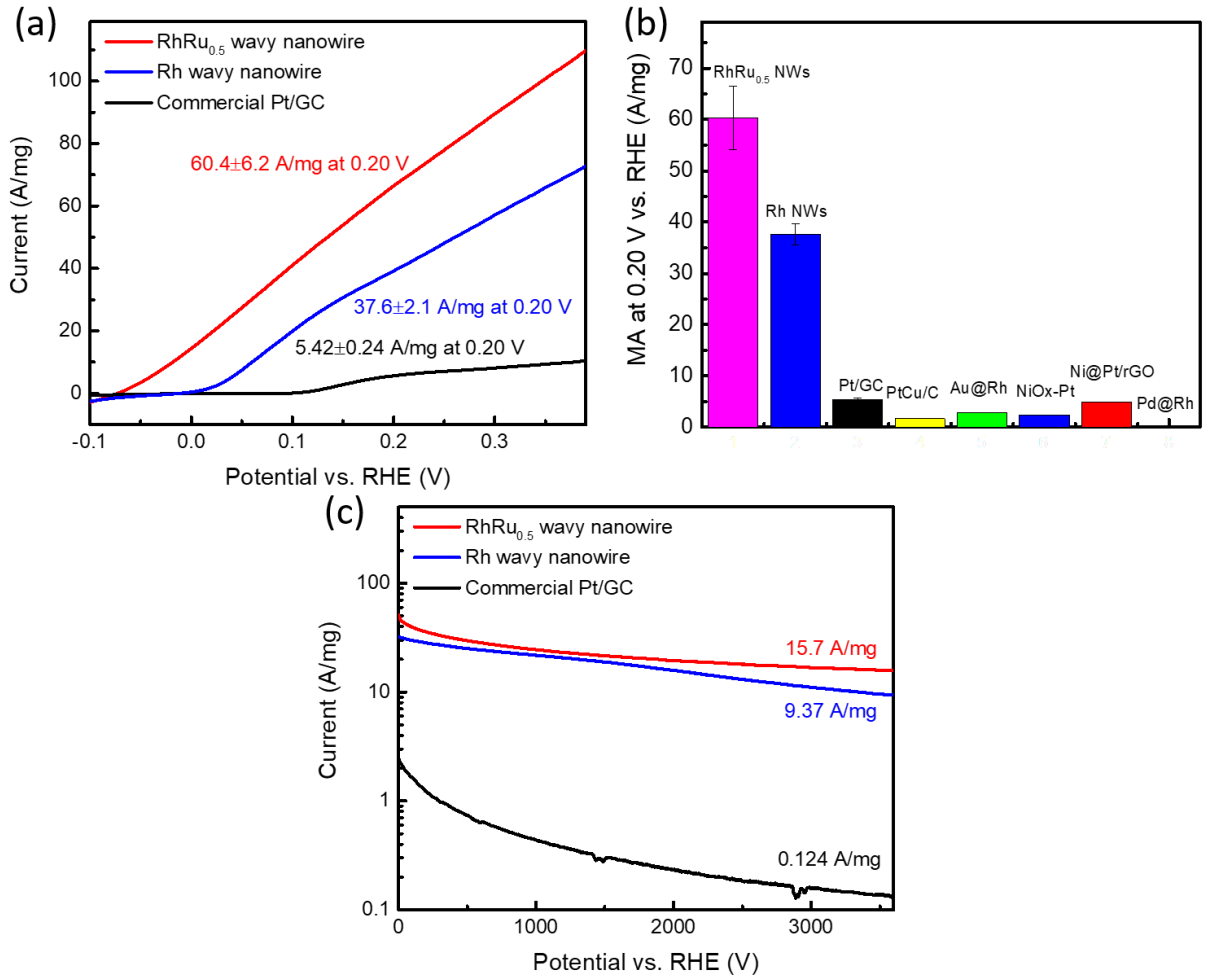

Figure 5-8. HzOR tested on carbon paper. (a) LSV curves of $RhRu_{0.5}$ alloy wavy nanowire (1.0 μg/cm^2 Rh loading), Rh wavy nanowire (1.0 μg/cm^2 Rh loading) and commercial Pt/GC (1.0 μg/cm^2 Pt loading) in the 1.0 M KOH+ 0.10 M N_2H_4 electrolyte at scan rate of 5 mV/s. (b) Comparison of the MA at 0.20 V vs. RHE with the previously reported HzOR electrocatalysts. (c) CA results of the of $RhRu_{0.5}$ alloy wavy nanowire, Rh wavy nanowire and commercial Pt/GC in the 1.0 M KOH+ 0.10 M N_2H_4 electrolyte at 0.20 V vs. RHE.

To compare with the previously reported noble metal based electrocatalysts, we can figure out that the $RhRu_{0.5}$ alloy wavy nanowires demonstrate much improved performances with one-magnitude higher mass activity compared with the previously reported electrocatalysts, including PtCu/C[30], Au@Rh core-shell nanowire[31], NiO_x-Pt[19], Ni@Pt/RGO[32], Pd@Rh[33] electrocatalysts as shown in Figure 5-7 (b) and these electrocatalysts were all tested in the alkaline media (1.0 M KOH) with same concentration of hydrazine (0.10 M, except for PtCu/C tested in 1.0 M KOH + 1.0 M hydrazine and Au@Rh nanowires tested in 0.1 M KOH+0.1 M hydrazine). In addition, very high geometric current density (60.4±6.2 mA/cm^2) is also achieved for the $RhRu_{0.5}$ alloy wavy nanowires at 0.20 V vs. RHE, which is also comparable with the results from the previous literatures[19, 30-33], which will be highly beneficial and demonstrating great potential for fuel cells applications due to the similar geometric current density with one magnitude lower noble metal loading on the electrode to greatly lower the overall cost of the fuel cells.

To study the long-term performance, the CA tests were carried out as shown in Figure 5-8 (c) and the $RhRu_{0.5}$ alloy wavy nanowires can maintain very high current of 15.7 A/mg at 0.20 V vs. RHE after 1 h of test, which is much higher than the Rh nanowires (9.37 A/mg) and two magnitudes higher than commercial Pt/GC (0.124 A/mg), indicating great potential when ultimately applied for ADHFCs for long time operation.

5.4 Conclusion

In conclusion, we developed $RhRu_{0.5}$ alloy wavy nanowire with a facile solvothermal method, demonstrating great performances for electrocatalytic HzOR with ultrahigh MA and lower overpotential, which far outperforms the previously reported noble metal based electrocatalysts as well as the controlled samples, because of the ultrahigh ECSA as well as the synergistic

effect between Rh and Ru. In addition, the capability to achieve the total electrooxidation of the hydrazine was also achieved as proved from the RDE study. Greatly improved long-term performances were also achieved and very high geometric current density can be accomplished with ultralow noble metal loading as well. Together, these will make $RhRu_{0.5}$ alloy nanowires a highly potential electrocatalysts for the ADHFCs anodes.

5.5 Reference

1. Zhao, B. T.; Song, J.; Ran, R.; Shao, Z. P., Catalytic decomposition of hydrous hydrazine to hydrogen over oxide catalysts at ambient conditions for PEMFCs. *Int. J. Hydrogen Energy* **2012,** *37* (1), 1133-1139.

2. Joghee, P.; Malik, J. N.; Pylypenko, S.; O'Hayre, R., A review on direct methanol fuel cells–In the perspective of energy and sustainability. *MRS Energy Sustain* **2015,** *2*.

3. Kobayashi, H.; Hayakawa, A.; Somarathne, K.; Okafor, E. C., Science and technology of ammonia combustion. *Proceedings of the Combustion Institute* **2019,** *37* (1), 109-133.

4. Fei, H. L.; Dong, J. C.; Chen, D. L.; Hu, T. D.; Duan, X. D.; Shakir, I. R.; Huang, Y.; Duan, X. F., Single atom electrocatalysts supported on graphene or graphene-like carbons. *Chem. Soc. Rev.* **2019,** *48* (20), 5207-5241.

5. Wan, C.; Duan, X.; Huang, Y., Molecular Design of Single-Atom Catalysts for Oxygen Reduction Reaction. *Adv. Energy Mater.* **2020,** *10* (14), 19.

6. Yuan, Y.; Wang, J.; Adimi, S.; Shen, H.; Thomas, T.; Ma, R.; Attfield, J. P.; Yang, M., Zirconium nitride catalysts surpass platinum for oxygen reduction. *Nat. Mater.* **2019**, 1-5.

7. Lei, M.; Wang, J.; Li, J.; Wang, Y.; Tang, H.; Wang, W., Emerging methanol-tolerant AlN nanowire oxygen reduction electrocatalyst for alkaline direct methanol fuel cell. *Sci. Rep.* **2014,** *4*, 6013.

8. Antolini, E.; Gonzalez, E. R., Alkaline direct alcohol fuel cells. *J. Power Sources* **2010,** *195* (11), 3431-3450.

9. Sakamoto, T.; Serov, A.; Masuda, T.; Kamakura, M.; Yoshimoto, K.; Omata, T.; Kishi, H.; Yamaguchi, S.; Hori, A.; Horiuchi, Y.; Terada, T.; Artyushkova, K.; Atanassov, P.; Tanaka, H., Highly durable direct hydrazine hydrate anion exchange membrane fuel cell. *J. Power Sources* **2018,** *375*, 291-299.

10. Who In *IARC MONOGRAPHS ON THE EVALUATION OF CARCINOGENIC RISKS TO HUMANS*, Conference of the IARC Monographs on the Evaluation of Carcinogenic Risks to Humans, Lyon, FRANCE, Oct 10-17; Lyon, FRANCE, 2006; pp 9-38.

11. Serov, A.; Kwak, C., Direct hydrazine fuel cells: A review. *Appl. Catal. B-Environ.* **2010,** *98* (1-2), 1-9.

12. Tang, P. P.; Lin, X.; Yin, H.; Zhang, D. X.; Wen, H.; Wang, J. J.; Wang, P., Hierarchically Nanostructured Nickel-Cobalt Alloy Supported on Nickel Foam as a Highly Efficient Electrocatalyst for Hydrazine Oxidation. *Acs Sustainable Chemistry & Engineering* **2020,** *8* (44), 16583-16590.

13. Feng, G.; An, L.; Li, B.; Zuo, Y. X.; Song, J.; Ning, F. H.; Jiang, N.; Cheng, X. P.; Zhang, Y. F.; Xia, D. G., Atomically ordered non-precious Co3Ta intermetallic nanoparticles as high-performance catalysts for hydrazine electrooxidation. *Nat. Commun.* **2019,** *10*.

14. Liu, Y.; Zhang, J. H.; Li, Y. P.; Qian, Q. Z.; Li, Z. Y.; Zhu, Y.; Zhang, G. Q., Manipulating dehydrogenation kinetics through dual-doping Co3N electrode enables highly efficient hydrazine oxidation assisting self-powered H-2 production. *Nat. Commun.* **2020,** *11* (1).

15. Li, Y. P.; Zhang, J. H.; Liu, Y.; Qian, Q. Z.; Li, Z. Y.; Zhu, Y.; Zhang, G. Q., Partially exposed RuP2 surface in hybrid structure endows its bifunctionality for hydrazine oxidation and hydrogen evolution catalysis. *Sci. Adv.* **2020,** *6* (44).

16. He, F.; Xia, N. N.; Zheng, Y.; Zhang, Y. X.; Fan, H. L.; Ma, D. L.; Liu, Q. H.; Hu, X., In Situ Electrochemical Fabrication of Ultrasmall Ru-Based Nanoparticles for Robust N2H4 Oxidation. *ACS Appl. Mater. Interfaces* **2021,** *13* (7), 8488-8496.

17. Finkelstein, D. A.; Imbeault, R.; Garbarino, S.; Roue, L.; Guay, D., Trends in Catalysis and Catalyst Cost Effectiveness for N2H4 Fuel Cells and Sensors: a Rotating Disk Electrode (RDE) Study. *Journal of Physical Chemistry C* **2016,** *120* (9), 4717-4738.

18. Zhang, J.; Wang, Y. X.; Yang, C. J.; Chen, S.; Li, Z. J.; Cheng, Y.; Wang, H. N.; Xiang, Y.; Lu, S. F.; Wang, S. Y., Elucidating the electro-catalytic oxidation of hydrazine over carbon nanotube-based transition metal single atom catalysts. *Nano Res.* **2021**.

19. de Oliveira, D. C.; Silva, W. O.; Chatenet, M.; Lima, F. H. B., NiOX-Pt/C nanocomposites: Highly active electrocatalysts for the electrochemical oxidation of hydrazine. *Appl. Catal. B-Environ.* **2017,** *201*, 22-28.

20. Wang, Y.; Wang, G.; Li, G.; Huang, B.; Pan, J.; Liu, Q.; Han, J.; Xiao, L.; Lu, J.; Zhuang, L., Pt–Ru catalyzed hydrogen oxidation in alkaline media: oxophilic effect or electronic effect? *Energy Environ. Sci.* **2015,** *8* (1), 177-181.

21. Li, J. K.; Ghoshal, S.; Bates, M. K.; Miller, T. E.; Davies, V.; Stavitski, E.; Attenkofer, K.; Mukerjee, S.; Ma, Z. F.; Jia, Q. Y., Experimental Proof of the Bifunctional Mechanism for the Hydrogen Oxidation in Alkaline Media. *Angew. Chem.-Int. Edit.* **2017,** *56* (49), 15594-15598.

22. Li, Y.; Guo, Y.; Yang, S. F.; Li, Q. B.; Chen, S.; Lu, B. Y.; Zou, H. B.; Liu, X. C.; Tong, X. L.; Yang, H. Q., Mesoporous RhRu Nanosponges with Enhanced Water Dissociation toward Efficient Alkaline Hydrogen Evolution. *ACS Appl. Mater. Interfaces* **2021,** *13* (4), 5052-5060.

23. Ding, Z. Q.; Wang, K.; Mai, Z. Q.; He, G. Q.; Liu, Z.; Tang, Z. H., RhRu alloyed nanoparticles confined within metal organic frameworks for electrochemical hydrogen evolution at all pH values. *Int. J. Hydrogen Energy* **2019,** *44* (45), 24680-24689.

24. Park, S.; Yoon, D.; Bang, S.; Kim, J.; Baik, H.; Yang, H.; Lee, K., Formation of a Cu@RhRu core-shell concave nanooctahedron via Ru-assisted extraction of Rh from the Cu matrix and its excellent electrocatalytic activity toward the oxygen evolution reaction. *Nanoscale* **2015,** *7* (37), 15065-15069.

25. Wang, K.; Huang, B. L.; Zhang, W. Y.; Lv, F.; Xing, Y.; Zhang, W. S.; Zhou, J. H.; Yang, W. X.; Lin, F. X.; Zhou, P.; Li, M. Q.; Gao, P.; Guo, S. J., Ultrathin RuRh@(RuRh)O(2)core@shell nanosheets as stable oxygen evolution electrocatalysts. *J. Mater. Chem. A* **2020,** *8* (31), 15746-15751.

26. Zhao, L.; Liu, X. J.; Zhang, S.; Zhao, J.; Xu, X. L.; Du, Y.; Sun, X.; Zhang, N. U.; Zhang, Y.; Ren, X.; Wei, Q., Rational design of bimetallic Rh0.6Ru0.4 nanoalloys for enhanced nitrogen reduction electrocatalysis under mild conditions. *J. Mater. Chem. A* **2021,** *9* (1), 259-263.

27. Fu, X.; Zhao, Z.; Wan, C.; Wang, Y.; Fan, Z.; Song, F.; Cao, B.; Li, M.; Xue, W.; Huang, Y.; Duan, X., Ultrathin wavy Rh nanowires as highly effective electrocatalysts for methanol oxidation reaction with ultrahigh ECSA. *Nano Res.* **2019,** *12* (1), 211-215.

28. Huang, X.; Zhao, Z.; Chen, Y.; Chiu, C.-Y.; Ruan, L.; Liu, Y.; Li, M.; Duan, X.; Huang, Y., High density catalytic hot spots in ultrafine wavy nanowires. *Nano Lett.* **2014,** *14* (7), 3887-3894.

29. Li, M.; Zhao, Z.; Cheng, T.; Fortunelli, A.; Chen, C.; Yu, R.; Zhang, Q.; Gu, L.; Merinov, B. V.; Lin, Z.; Zhu, E.; Yu, T.; Jia, Q.; Guo, J.; Zhang, L.; Goddard, W. A.; Huang, Y.; Duan, X., Ultrafine jagged platinum nanowires enable ultrahigh mass activity for the oxygen reduction reaction. *Science* **2016,** *354* (6318), 1414-1419.

30. Crisafulli, R.; de Barros, V. V. S.; de Oliveira, F. E. R.; Rocha, T. D.; Zignani, S.; Spadaro, L.; Palella, A.; Dias, J. A.; Linares, J. J., On the promotional effect of Cu on Pt for hydrazine electrooxidation in alkaline medium. *Appl. Catal. B-Environ.* **2018,** *236*, 36-44.

31. Xue, Q.; Huang, H.; Zhu, J. Y.; Zhao, Y.; Li, F. M.; Chen, P.; Chen, Y., Au@Rh core-shell nanowires for hydrazine electrooxidation. *Appl. Catal. B-Environ.* **2020,** *278*, 10.

32. Hosseini, M. G.; Mahmoodi, R.; Abdolmaleki, M., High performance direct hydrazine-hydrogen peroxide fuel cell using reduced graphene oxide supported Ni@M (M = Pt, Pd, Ru) nanoparticles as novel anodic electrocatalysts. *New J. Chem.* **2018,** *42* (14), 12222-12233.

33. Wang, G. J.; Jing, S. C.; Tan, Y. W., Branched Pd@Rh core@shell nanocrystals with exposed Rh {100} facets: an effective electrocatalyst for hydrazine electro-oxidation. *Sci. Rep.* **2017,** *7*, 10.